THE JOURNAL
OF
CHEMICAL PHYSICS

VOLUME 10 JUNE, 1942 NUMBER 6

The Crystal Structure of Hydrazinium Difluoride*

MARRITT L. KRONBERG† AND DAVID HARKER‡
The Remsen Chemical Laboratories, The Johns Hopkins University, Baltimore, Maryland
(Received March 28, 1942)

An x-ray analysis shows that crystalline hydrazinium difluoride is built upon a rhombohedral unit cell having $a_0=5.43$A, $\alpha=38°10'$, containing one molecular formula. The positions of the atoms have been determined and correspond to *trans*-hydrazinium ions which form linear hydrogen bonds to fluoride ions at the corners of an elongated octahedron. Each fluoride ion forms three hydrogen bonds to different hydrazinium ions, and condenses the octahedra into continuous layers. As a result of the packing of these layers to build up the structure, each nitrogen atom comes in contact with an "extra" fluoride ion and thereby assumes a coordination number of 5. Analysis of the N–N and N–H . . . F distances of 1.42A and 2.62A, respectively, shows that each atom in the hydrazinium ion bears approximately $\frac{1}{4}$ of a unit of positive charge. The bearing of the structure of the ion on the adjacent charge rule is discussed. Some of the properties of the ion are interpreted in terms of the structure.

INTRODUCTION

A COMPLETE structural analysis of crystalline hydrazinium difluoride, $N_2H_6F_2$, should afford considerable information concerning the distribution of the two positive charges within the hydrazinium ion, $N_2H_6^{++}$. This ion is unusual in that it is one of the rare stable substances whose accepted Lewis structure,

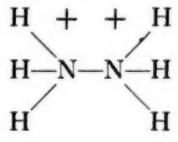

places like formal charges on adjacent atoms. However, many of the physical and chemical properties of the ion generally resemble those of the ammonium ion, NH_4^+; and since it is known that the positive charge is not localized upon the nitrogen atom in this ion,[1] it can be expected that the charges are not localized upon the adjacent nitrogen atoms in the hydrazinium ion, but rather are distributed among all the atoms. Pauling's adjacent charge rule, which states that unperturbed structures with similar adjacent charges do not contribute appreciably to the normal state of a molecule, leads one to an essentially similar expectation. Moreover, it leads one to anticipate even more ionic character in the N−H bonds of the hydrazinium ion than in the same bonds in the ammonium ion. Analyses of the N−N distance and of the lengths of the hydrogen bonds to be expected in $N_2H_6F_2$ should afford the required information for determining the true structure of the ion. This detailed structural analysis has been accomplished; it will be described below.

* The experimental work involved was done at the Johns Hopkins University, but a large part of the paper was prepared at the California Institute of Technology.

† Charles A. Coffin Fellow at the Johns Hopkins University (1939–40), at the California Institute of Technology (1940–41); present address: General Electric Company, Pittsfield Works Laboratory, Pittsfield, Massachusetts.

‡ Present address: General Electric Company, Research Laboratory, Schenectady, New York.

[1] L. Pauling, *The Nature of the Chemical Bond* (Cornell University Press, Ithaca, New York, 1939).

EXPERIMENTAL

Preparation of Crystals

A water solution containing hydrazine and hydrofluoric acid in a 1 : 2 molar ratio was allowed to evaporate slowly over sulfuric acid in a vacuum desiccator. Well-formed transparent hexagonal plates crystallized after several days. They were found to be quite stable in air and easily handled. Examination of several crystals showed them to be hard, and brought out the existence of an excellent basal cleavage. More rapid evaporation produced truncated hexahedra closely resembling regular octahedra. Both types of crystals were examined under the polarizing microscope and were seen to be optically anisotropic. The final evidence indicating that both types were of the same crystal class was the identical nature of the Laue photographs taken of both species.

These data are not in accord with the observations of Curtius and Schulz,[2] who reported that the crystals they prepared by a similar procedure were optically isotropic. Since no trace of an isotropic modification was found in this work, a chemical analysis for fluorine was performed on both types of crystals grown for this investigation. The results, based on the method of Swift,[3] are: Observed percent of fluorine:

Hexagonal sample No. 1 = 52.0 percent
Hexagonal sample No. 2 = 52.3 percent
Truncated hexahedra No. 1 = 52.5 percent.

Calculated percent of fluorine in $N_2H_6F_2$ = 52.8 percent.

It is seen that the results check the chemical composition corresponding to the formula $N_2H_6F_2$. In view of these facts, it must be concluded that the crystals used in this investigation are of a different species from those obtained by Curtius and Schulz; or that their crystals were similar to the ones used in the experiments to be described, but that in their optical analysis the crystals rested on faces perpendicular to the optic axis. Under such circumstances the crystals would appear to be isotropic in polarized light.

[2] T. Curtius and S. Schulz, Ber. **23**, 3023 (1890).
[3] E. H. Swift, *A System of Chemical Analysis* (Prentice-Hall, Inc., New York, 1938).

Determination of Unit Cell and Space Group

A Laue photograph taken perpendicular to a large hexagonal face of one of the crystals showed a threefold axis and three planes of symmetry perpendicular to this face, showing the Laue symmetry to be D_{3d}. Oscillation photographs using CuK radiation filtered through nickel foil were taken about the [10.1], [00.1], and [11.0] axes of sections of some crystals that were shaped into laths whose dimensions were about $0.2\times0.2\times1.5$ mm. Analysis of these films showed that the hexagonal unit cell has the dimensions $a_0 = 4.43\text{A}\pm0.01\text{A}$, $c_0 = 14.37\text{A}\pm0.02\text{A}$. No reflections were found on any of the films that did not obey the criterion $2\text{H}+\text{K}+L=3n$, and so, in the absence of any other evidence to the contrary, it can be assumed that the lattice is rhombohedral, $a_0 = 5.43\text{A}$, $\alpha = 18°\ 10'$.

A pyroelectric experiment was performed in order to determine whether the crystals possess a center of symmetry. A crystal suspended from a fine silk thread was lowered into a Dewar flask containing liquid nitrogen. When the crystal was slowly withdrawn from the liquid, it showed no tendency to be attracted to the wall of the flask even when caused to swing toward the wall. This result permits a symmetry center within the crystal. Many reflections of the type $OK\cdot L$ with L odd were observed, which eliminates the possibility that a glide plane is present. These data are in accord with the space group $D_{3d}{}^5-R\bar{3}m$. Since it is found possible to assign a structure to hydrazinium difluoride which is based on this space group and which is in accord with all the data, it can be accepted as being correct.

Calculations using the hexagonal unit cell dimensions and the density, determined by flotation to be about 1.46 g/cc, indicate that there are three molecular formulae per hexagonal unit cell. There is accordingly one molecular formula in the rhombohedral unit cell. The positions of $2N$, $2F$, and $6H$ define the structure. The space group $D_{3d}{}^5-R\bar{3}m$ provides positions for two atoms of fluorine at $\pm(v, v, v)$, for two atoms of nitrogen at $\pm(u, u, u)$, and for six atoms of hydrogen at $\pm(xxy)$, $\pm(x\bar{x}o)$, and $\pm(x\bar{x}\frac{1}{2})$. The exact positions of the hydrogen atoms cannot be determined since their contributions to

the intensities of x-ray reflections is vanishingly small, but their locations can be inferred from the directions of the expected hydrogen bonds. There are accordingly two parameters to be determined from the data: u and v.

Evaluation of Parameters and Determination of Structure

The intensities of the reflections observed on the oscillation photographs were readily estimated by means of a visual comparison scale. Absorption corrections were omitted in view of the small volume and semi-ideal shape of each crystal used. All observed intensities were corrected to the same relative exposure time by the use of the factor $1/\sin\beta$ (as defined in the *Internationale Tabellen*). The data obtained in this manner are listed according to forms in Table I, and are probably accurate to about ± 25 percent.

TABLE I. Intensities for $[HK\cdot L]$ reflections.* Calculated and observed intensities.

Indices of form	Calculated	Observed
32.7	6.9	6.0
02.16	15.4	13.3
22.12	0.8	~0.5
01.17	12.7	13.4
31.11	14.6	12.0
12.14	14.0	13.9
14.0	31.7	21.5
13.10	24.0	18.3
32.4	13.7	10.0
40.7	4.3	2.0
10.16	8.5	8.3
30.12	0.6	~1
23.2	1.4	1.2
11.15	3.1	3.1
21.13	0.02	~0
32.1	4.6	4.5
22.9	1.0	2.0
20.14	10.2	7.5
31.8	1.1	~1
40.4	11.1	9.5
13.7	4.6	3.6
00.15	3.6	2.7
02.13	0.01	~0
04.2	1.5	1.2
40.1	3.8	3.5
12.11	9.4	12.1
01.14	10.2	10.2
31.5	0.3	~0.5
22.6	11.0	9.2
30.9	0.8	~1
21.10	21.4	16.4
13.4	12.2	8.6
11.12	0.8	1.4
31.2	1.6	1.6
10.13	0.01	~0
13.1	2.3	2.9
22.3	1.1	1.2
20.11	11.5	13.0
30.6	13.0	9.7
12.8	1.6	1.9
02.10	25.2	20.0
21.7	4.7	4.9
00.12	1.2	2.6
30.3	1.3	1.5
01.11	15.1	16.0
30.0	33.0	27.0
11.9	1.0	2.8
12.5	0.6	~1
20.8	2.6	2.5

* The former are listed in order of increasing $HK\cdot L$.

For the purpose of calculating intensities, scattering factors were taken from the table of James and Brindley as listed in the *Internationale Tabellen*. As is usual when working with hard substances composed of relatively light atoms, no attempt was made to correct the intensities for the effect of thermal motion. The calculated intensities were all weighted by the Lorentz and polarization factor $(1+\cos^2 2\theta)/2\sin 2\theta$ to make them comparable with the observed intensities. Although it is customary to calculate intensities using rhombohedral indices, it was decided to perform these calculations using hexagonal indices for the sake of convenience. The formula used is:

$$I_{HK\cdot L}=K\times\frac{1+\cos^2 2\theta}{2\sin 2\theta}\times(f_N\cos 2\pi Lu+f_F\cos 2\pi Lv)^2.$$

It is to be noted that the intensity of a reflection from a plane of the type $(HK\cdot L)$ depends only on the L index, corresponding in rhombohedral coordinates to the sum of the indices of a plane of the type (hkl).

Qualitative intensity comparisons readily excluded all parameter values except those in the region of $u\leqq 0.05$ and $v\leqq 0.25$. For the refinement of these values the parameters were made to satisfy the following qualitatively observed intensity relationship.

$$I_L=I_{10}\gg I_{11}\gtrsim I_{14}\gtrsim I_{17}\gtrsim I_{16}>I_{15}>I_{12}\gg I_{13}\leqq 0.$$

Intensities of planes for which $L<10$ were not used in these calculations, because the sensitivity to fine parameter variations of the intensities of such reflections is too low to be of any value. The value of this sequence is greatly enhanced by the observation that reflections from planes of the type $(HK\cdot 13)$ were so weak as to be almost unobservable—of the dozen times that such planes were in position to reflect only twice were such reflections observed, and then just barely so, on photographs of long exposure and

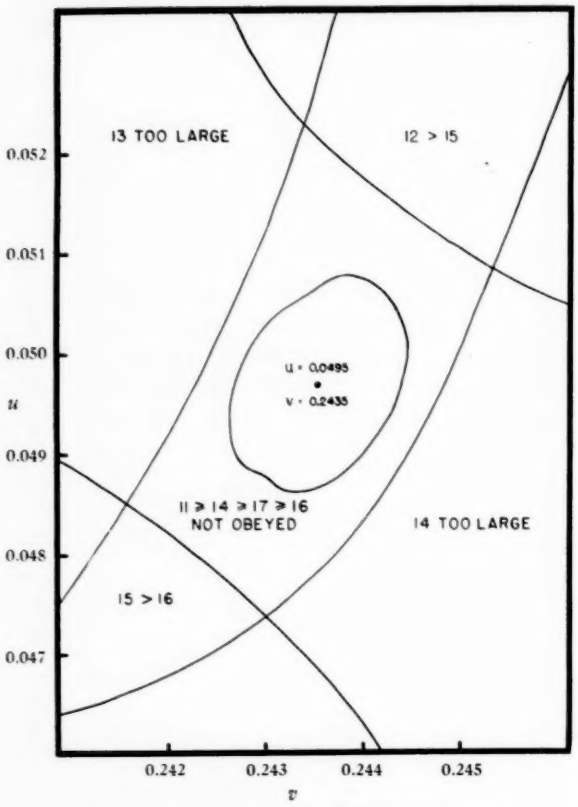

FIG. 1. Plot illustrating parameter variations.

in positions where the Lorentz and polarization factor was most favorable for increasing the intensity.

Figure 1 illustrates in graphical fashion the results of this treatment. The final parameters chosen are:

$$u = 0.0495 \pm 0.0010,$$
$$v = 0.2435 \pm 0.0010.$$

Using these parameters, the intensities of all the observed reflections for which $\sin\theta > 0.55$ were calculated. It was felt that the simplicity of the problem justified the neglect of planes reflecting at small angles. The intensities observed for planes of the same form were about the same, to within the limits of the estimated experimental error, and so, for simplicity, these values were averaged to give the intensity of each form. This process probably helped to average out the effects of absorption for the various planes of any one form. These values are tabulated with the calculated values in Table I, and it is seen that the agreement is very satisfactory.

DISCUSSION OF THE STRUCTURE

Figures 2 and 3 show photographs of a model of a portion of the structure which illustrate the atomic arrangement in the crystal and bring out the rhombohedral cell. The structure may be considered to be related to the cadmium chloride $CdCl_2$ layer type, in which fluoride ions have replaced the chloride ions and hydrazinium ions the cadmium ions. It is seen that each hydrazinium ion is forming six linear hydrogen bonds to fluoride ions at the corners of an octahedron elongated in the direction of the N−N axis. Therefore, the hydrogen atoms in the ion must have the *trans-*, or staggered, configuration. Each fluoride ion forms three hydrogen bonds to different hydrazinium ions and thereby condenses the octahedra into layers. Figure 4 is a photograph of a model of a portion of one of these layers viewed slightly off the normal to the base plane. These layers then stack together according to a definite pattern (that will be discussed) to build up the structure in the *C* direction.

The positions of the atoms in the cadmium chloride structure are those obtained from a closest packing of the anions; and therefore the distances between neighboring anions correspond to the Van der Waals contact distances. However, such a close packing of anions does not exist in the hydrazinium difluoride structure. The observed distance of 4.43A between adjacent fluoride ions within an octahedral layer is much larger than the expected Van der Waals contact distance of 2.70A.

The positions of the fluoride ions within an octahedral layer are determined by the hydrogen bonds formed with the hydrazinium ions. Because of the directed nature of these bonds, the adjacent fluoride ions are unable to come in close contact with each other, but rather are spread out so that the distance between each pair is about 64 percent larger than that corresponding to closest packing. In excellent accord with the postulate of linear hydrogen bonds is

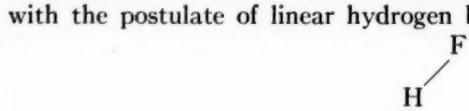

the observation that the N—N angle is the tetrahedral angle expected for such bonds.

Each octahedral layer is thus a very open type of structure. Particularly interesting are the unusually large tetrahedral holes formed adjacent to each nitrogen atom by each set of 3 fluoride ions that are hydrogen bonded to the nitrogen atom. These holes are very convenient for packing purposes and are filled during the stacking process by fluoride ions from neighboring layers. The holes are so large that an incoming fluoride ion comes into contact with the exposed nitrogen atom rather than in contact with the surrounding fluoride ions. Inspection of the packing diagram 6 shows several hydrazinium ions and associated hydrogen bonded fluoride ions, and shows in addition some of the packing holes—some of the holes are occupied to show the very economical type of packing that exists. This type of packing brings the fluoride ion in the hole within the sphere of influence of the hydrogen atoms bound to the nitrogen atom. (It will be shown that there is roughly a quarter of a unit of positive charge on each of the atoms in the ion.) Thus the coulombic attraction between the negative charge on the fluoride ion and the positive charge on these neighboring atoms serves to hold the fluoride ions in the pockets and thereby binds the layers together. This type of binding is the weakest in the crystal, and the observed basal cleavage breaks only these weakest bonds.

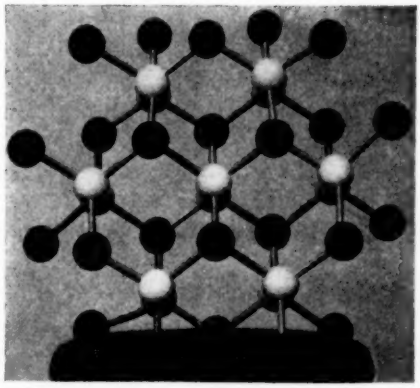

FIG. 4. Photograph of a model showing a portion of an octahedral layer, viewed somewhat off the normal to the plane of the layer. White balls represent nitrogen atoms; black balls represent fluorine atoms; all links indicate hydrogen bonds.

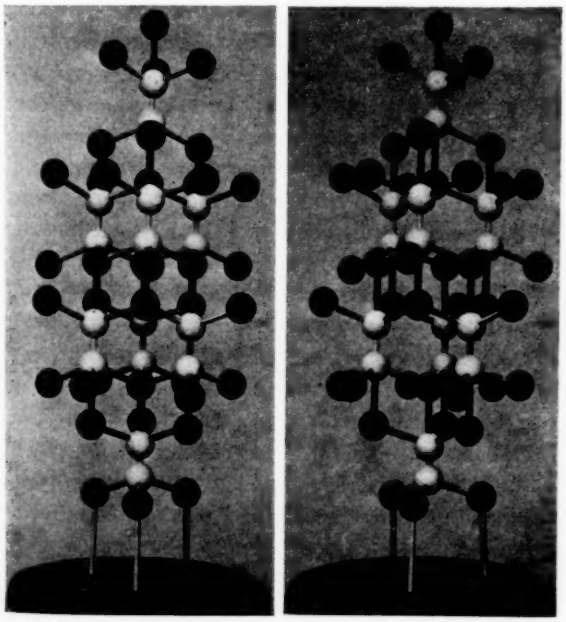

FIGS. 2 AND 3. Photographs of a model showing the rhombohedral unit cell. The midpoints of each of the eight hydrazinium ions in each figure correspond to the corners of the unit rhomb. The white balls indicate nitrogen atoms; the black balls indicate fluorine atoms; all non-vertical links represent linear hydrogen bonds; all vertical links between white and black balls indicate van der Waals contacts.

The observed distance of 3.38A from a fluoride ion in a hole to a neighboring fluoride ion helping to form the hole is accordingly about 25 percent larger than the normal contact distance of about 2.70A, whereas the observed distance of 2.80A between a nitrogen atom and the fluoride ion in the adjacent hole is even slightly less than an expected contact distance of about 2.85A. This is a reasonable N ··· F contact distance, for the coulombic force which holds the atoms together might be expected to pull the atoms somewhat closer than expected for pure Van der Waals packing. The appreciable interpenetration of adjacent fluoride layers is indicated by the distance of 2.21A between median planes passed through two such layers—the distance expected between non-interpenetrating layers being around 3.60A.

It is interesting to note that there are no Van der Waals contacts between the fluoride ions in the structure. Thus the macro structure is determined completely by the geometry of the hydrazinium ion and the lengths and directions of the hydrogen bonds.

The unique packing of layers gives rise to a new and unexpected yet very satisfactory type

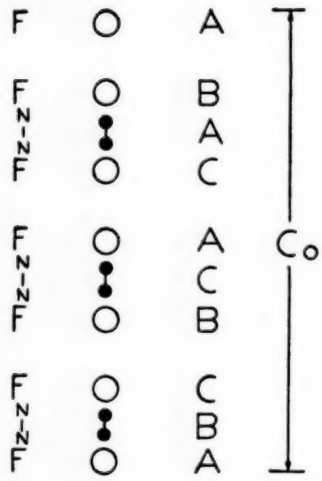

FIG. 5. Diagram illustrating packing of atoms and layers of atoms.

of coordination around the hydrazinium ion. Examination of the packing diagram 6 shows the environment of a hydrazinium ion, and shows the presence of the five atoms around each $(-NH_3)^+$ group. The binding between the nitrogen atoms is, of course, purely covalent; whereas the binding with the four fluoride ions is electrostatic—atoms 1, 2, and 3 are held by the electrostatic attraction of the somewhat positively charged hydrogen atoms; and atom four is held by the electrostatic attraction of the positively charged $(-NH_3)^+$ group of atoms.

It is convenient to discuss the packing of the octahedral layers in terms of the packing positions *A*, *B*, and *C*.[1] Using this convention and considering the hydrazinium ion as a packing unit, the structure may be described by the following sequence (Fig. 5):

It is seen that the identity distance in the *C* direction (hexagonal cell) is achieved through the packing of three octahedral layers. The fluoride ions follow the sequence *ABC* corresponding to the positions of cubic packing; whereas the environment of a fluoride ion is that of hexagonal packing, the sequence being of the type *ABA*. On the other hand, the hydrazinium ions are not only in the positions of cubic packing with respect to each other, but are also in the environment of cubic packing. It is to be noted that the packing of the octahedral layers considered as packing units corresponds to cubic closest packing.

The hydrazinium difluoride structure bears an interesting relationship to the structure of the face-centered cubic crystal fluorite, CaF_2. This structure consists of a cubic closest packing of fluoride ions with the cations occupying all of the octahedral holes, the same general type of packing as exists in the hydrazinium difluoride structure. However, because of the anisotropy of the shape and charge distribution of the hydrazinium ion, the hydrazinium difluoride structure can assume only rhombohedral symmetry.

The interesting distances within the crystal are summarized as follows:

$N_1-N_2=1.42$A,

$F_1F_2=4.43$A,

$F_1F_4=3.38$A,

N—H F = 2.62A,

$N_1F_4=2.80$A

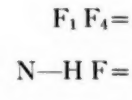

angle = 110°.

Distance between median planes through adjacent layers of fluoride ions = 2.21A (numbers refer to atoms in Fig. 6).

It is estimated that the probable error of these values (taking into account all of the possible sources of error) is within ±0.02A.

The implications of the N−N and N−H ··· F distances allow an insight to be gained into the charge distribution within the hydrazinium ion. The N−N distance of 1.42A represents a shortening of about 0.05A from the normal distance of 1.47A found to exist in gaseous hydrazine.[4] This shortening is caused by the formal charge effect resulting from the coulombic attraction between a formal nuclear charge and the charge on the surrounding electron cloud. The magnitude of the effect[1] indicates an appreciable contribution of the like adjacent charge structure to the normal state of the ion. It seems unlikely that there is any appreciable change in the N−N bond length because of the repulsions of the fractional charges placed on the adjacent nuclei by any contributions of the adjacent charge structure to the ground state of the ion. Any appreciable increase due to such a cause should be most favorably exhibited in the case of the doubly charged helium molecule ion, He_2^{++}. The calculated distance for this species is actually less by about 0.02A than the

[4] Private communication, V. Shomaker and P. Giguére, California Institute of Technology.

distance calculated in the same manner for the hydrogen molecule.

The $N-H \cdots F$ distance of 2.62A is the shortest hydrogen bond distance observed between nitrogen and fluorine atoms. The corresponding distance in crystalline ammonium bifluoride, NH_4HF_2, is 2.76A[1] and in ammonium fluoride is 2.68A[1]—the latter distance being the next shortest one known. Because of the ionic character of the hydrogen bond, the unusually short $N-H \cdots F$ distance in hydrazinium difluoride indicates that ionic structures of the type:

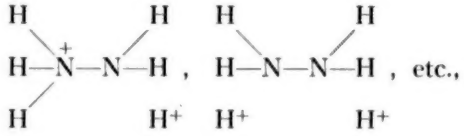

contribute quite heavily to the normal state of the ion.

In order to get an estimate of the sizes of the contributions of these various structures it is useful to compare the hydrazinium difluoride structure with the Wurtzite-like ammonium fluoride structure. In this hexagonal crystal there are ammonium ions surrounded by fluoride ions at the corners of a regular tetrahedron. Each fluoride ion forms four linear hydrogen bonds to different ammonium ions and thereby builds up a three-dimensional structure. As is the case for the hydrazinium difluoride structure there are no contacts between the fluoride ions, the structure being completely determined by the geometry of the ammonium ion and the lengths and directions of the hydrogen bonds.

Since the structural principles upon which the two crystals are based are the same, the shorter hydrogen bond distance in hydrazinium difluoride indicates that there is more ionic character in the $N-H$ bonds in the hydrazinium ion than in the same bonds in the ammonium ion. In ammonium fluoride each nitrogen atom forms four hydrogen bonds, whereas in hydrazinium difluoride each nitrogen forms only three. Other things being equal, there should be a slight shortening of the $N-H \cdots F$ bond in hydrazinium difluoride because of this decrease in the number of hydrogen bonds. On the other hand, the presence of a fluoride ion in the hole adjacent to a nitrogen atom in the hydrazinium difluoride structure might be expected to affect the distance in the opposite direction, since the electrostatic interaction between the negative charge on the fluoride ion and the positive charge distributed among the neighboring nitrogen and hydrogen atoms should usurp part of the positive charge responsible for the linear hydrogen bonding.

The magnitudes of these effects are rather small; and since they are working in opposite directions any deviations from equality can be expected to give rise only to a negligible second-order effect. Thus for practical purposes, each nitrogen atom can be considered to be forming four hydrogen bonds.

Pauling[1] estimates that in the ammonium ion each $N-H$ bond has about 20 percent ionic character and that as a result, each atom in the ion bears a positive charge of about one-fifth of a unit. Thus in the hydrazinium ion there must be more than $\frac{1}{5}$ of a unit of charge on each hydrogen atom. On the other hand, the magnitude of the formal charge effect indicates that there cannot be much more charge on the hydrogen atoms, since a value as large as $\frac{1}{3}$ would leave the nitrogen atoms uncharged. It seems that a reasonable value is about $\frac{1}{4}$, or that the charges are approximately equally divided amongst all the atoms in the hydrazinium ion.

The ion may be described appropriately as resonating between forms of these principal

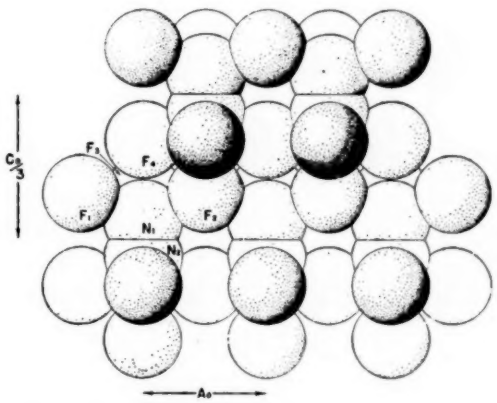

FIG. 6. Packing drawing and projection of portion of structure, illustrating environment of hydrazinium ions, packing holes, packing of layers, etc. Hydrogen atoms are not shown but the overlapping of the nitrogen and fluoride atoms indicates the hydrogen bonds.

types:

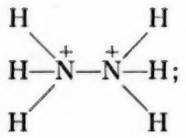

~25 percent

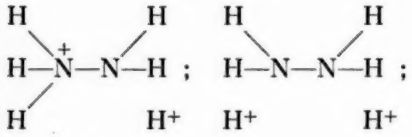

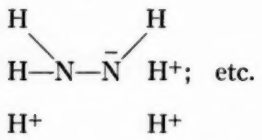

Σ ionic≦75 percent

The existence of a 25 percent contribution of the adjacent charge structure constitutes a deviation from the adjacent charge rule; the reason for this contradiction is rather clear.

The adjacent charge rule resulted from considerations of resonating molecules whose ground states are achieved through resonance among purely covalent structures. For this type of molecule, the non-contributing adjacent charge structure differs from the contributing structures only by the distribution of covalent bonds. Thus the internal energy due to the like adjacent charges on this structure increases the energy of the species to a point where it can no longer resonate with the other structures.

In the case of the hydrazinium ion, however, the only completely covalent structure is the adjacent charge one. The structures which do not have adjacent charges are ionic ones, and since these contain fewer covalent bonds than the completely covalent structure they will be less stable by an energy difference corresponding to the diminution of covalent bonds. Thus the factor which governs the sizes of the contributions of the two types of structures is the balance between the destabilizing effect of the adjacent charges in the case of the covalent structure, and the destabilizing effect resulting from the loss of covalent bond energy in the case of the ionic structures.

Thus it may be concluded that the adjacent charge rule as originally enunciated is strictly applicable to molecules whose unperturbed structures differ only in the distribution of covalent bonds.

However, the implications of the rule are well demonstrated in the chemical behavior of the hydrazinium ion. This ion is the strongest known nitrogen acid, having an acid constant of $K=11$ in comparison with $K=5.6\times10^{-10}$ for the ammonium ion, NH_4^+, and $K=1.2\times10^{-8}$ for the singly charged hydrazinium ion, $N_2H_5^+$. This property is forcefully exemplified by the completeness of the reaction of the ion with water or aqueous fluoride ions:

$$N_2H_6^{++}+H_2O\rightarrow N_2H_5^+ + H_3O^+,$$
$$N_2H_6^{++}+2F^-\rightarrow N_2H_5^+ + HF_2^-.$$

Thus upon solution in either of these media the ion reacts to eliminate completely one of the fractional charges on the adjacent nitrogen atoms; and the decrease in internal energy accompanying the loss of the adjacent charges is the unusually strong driving force for the reaction.

It is interesting at this point to review the state of affairs concerning the structure of nitrogen tetroxide, N_2O_4.[1] Because of experimental difficulties it has been impossible to determine the structure of this molecule in any unambiguous fashion. However, the symmetrical structure

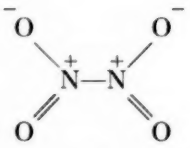

containing like adjacent charges on the nitrogen atoms is suggested by entropy measurements[5] and x-ray data.[6] Indirect evidence against this structure comes from the adjacent charge rule, as originally conceived, which indicates that an unsymmetrical structure such as

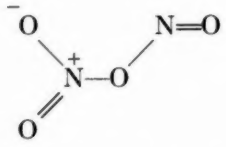

[5] W. F. Giauque and J. D. Kemp, J. Chem. Phys. **6**, 40 (1938).
[6] S. B. Hendrichs, E. F. Phys. **70**, 699 (1931).

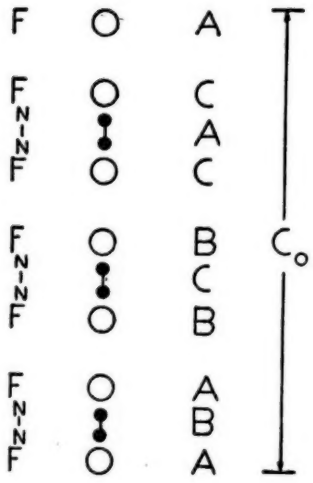

FIG. 7. Diagram illustrating hypothetical packing of atoms and layers of atoms in hypothetical *cis*-structure.

should be more stable and should thus be the preferred one. It is to be noted that the symmetrical structure is better from the viewpoint of resonance stabilization. It is clear, however, that the indicated symmetrical structure is in the class of substances, like the hydrazinium ion, to which the adjacent charge rule is not strictly applicable. Rather, the symmetrical structure is in agreement with the rule as modified in this paper. It is to be expected, because of the greater electronegativity of the oxygen atoms in nitrogen tetroxide in comparison with the electronegativity of the hydrogen atoms in the hydrazinium ion, that there should be much more formal charge on the nitrogen atoms in nitrogen tetroxide than in the hydrazinium ion. As a result the molecule should exhibit an even stronger tendency than does the hydrazinium ion to react so as to remove the adjacent charges. Thus the marked physical instability of gaseous nitrogen tetroxide even at low temperatures is readily understood in this light. The conclusion to be drawn from this qualitative discussion is only that the existence of the symmetrical structure for nitrogen tetroxide is in agreement with the modified adjacent charge rule.

It has been pointed out that the hydrogen atoms on the hydrazinium ion (and also the fluoride ions which are hydrogen bonded to such an ion) are in the *trans*-configuration. There is another conceivable structure for hydrazinium difluoride which differs from the true structure in that it is based upon *cis*-hydrazinium ions. Such a structure is rigidly excluded because the intensities calculated for it show no agreement with those observed. The packing sequence for such a hypothetical structure is (Fig. 7):

It might be assumed from the non-existence of this structure that the *trans*-configuration of the hydrogen and fluorine atoms is inherently a more stable configuration than the *cis*. However, Professor Pauling[7] has suggested another factor which is probably of more importance in the selection of the *trans*-structure as the preferred one. During the hypothetical packing of layers to form the *cis*-structure, only half of the holes adjacent to the nitrogen atoms would be occupied by fluoride ions from neighboring layers. The other half would be left vacant, and the fluoride ions which in the case of the true structure fill these holes would have to fit into holes which are bounded only by other fluoride ions. Thus such a structure would have only one-half as many ionic bonds holding the layers together, and furthermore would contain aggregates of fluoride ions. It is clear that these disadvantages make the *cis*-structure much less stable than the *trans*-structure, and therefore it does not exist in the crystal.

ACKNOWLEDGMENT

One of us (M. L. K.) takes this opportunity to express his gratitude to the Charles A. Coffin Foundation for the fellowships supporting him in his researches.

The research reported on in this paper was partially supported by a grant from the Johns Hopkins' Dunning Fund, and we thank Dr. H. A. B. Dunning for this aid.

It is a pleasure for M. L. K. to acknowledge his indebtedness to Professor Linus Pauling for several helpful discussions, for many criticisms and suggestions, and for his general encouragement.

The invaluable assistance of Dr. Henri Levi and Mr. Bernard Kronberg in the preparation of some of the figures is likewise acknowledged.

[7] L. Pauling, private discussion.

Ferromagnetic Gold-Iron Alloys

S. T. PAN, A. R. KAUFMANN, AND F. BITTER
Massachusetts Institute of Technology, Cambridge, Massachusetts
(Received March 23, 1942)

Magnetic measurements were made on a gold-iron alloy containing 37 atomic percent iron, both in the quenched and successively annealed states. It was found that the quenched supersaturated solid solution is ferromagnetic. When this supersaturated solid solution was gradually heated up, perceptible precipitation took place at about 450°C. Both the final gold-rich and iron-rich phases precipitated at 450°C were found to be magnetic at room temperatures. Magnetic measurements, checked by Debye-Scherrer patterns, indicate that the mechanism of precipitation in this alloy is mainly of the non-uniform type.

SEVERAL investigations on the gold-iron alloys are available in the literature. These results have been summarized by Hansen[1] in a phase diagram which is reproduced in Fig. 1. While this diagram does not show whether the gold-rich alloys are magnetic, Shih[2] and Jette and collaborators[3] found that gold-rich alloys containing 10 and 15 percent iron are definitely ferromagnetic at room temperatures. In the course of experiments on the aging of supersaturated solid solutions, we have had occasion to prepare an alloy of gold containing 37 atomic percent iron. Our main purpose was to investigate the mechanism of precipitation in this alloy and the change of magnetic properties with composition and other effects.

The alloy was made by melting pure gold and iron, covered by borax, in a porcelain crucible in a gas furnace and casting in an iron mold in the form of a $\frac{7}{16}$-inch rod. The ingot was then swagged into a $\frac{1}{4}$-inch rod. All the specimens subsequently used were cut from this quarter-inch rod and cold worked and heat treated. Chemical analysis gave the accurate composition as 13.74 weight percent iron.

The apparatus and the method of high temperature measurements were the same as those described in a previous work on copper-iron alloys reported by two of the authors.[4] With this apparatus, we were able to separate the paramagnetic susceptibility superposed on the ferromagnetic saturation magnetization. As the alloy was magnetic in this case, the force exerted by the field on a sample was so large that very small specimens had to be used. In each case, the specimen was about 1 mm in diameter and 3 mm long. The specimen was placed in a copper holder which was suspended from the balance arm. The force exerted by the field on the holder and suspensions was found to be negligible.

For liquid nitrogen measurements, the tube furnace was replaced by a long Dewar flask of about the same size. Inside the Dewar flask was a long Pyrex tube which was closed at the bottom and in which the specimen was suspended. Liquid nitrogen was introduced into the

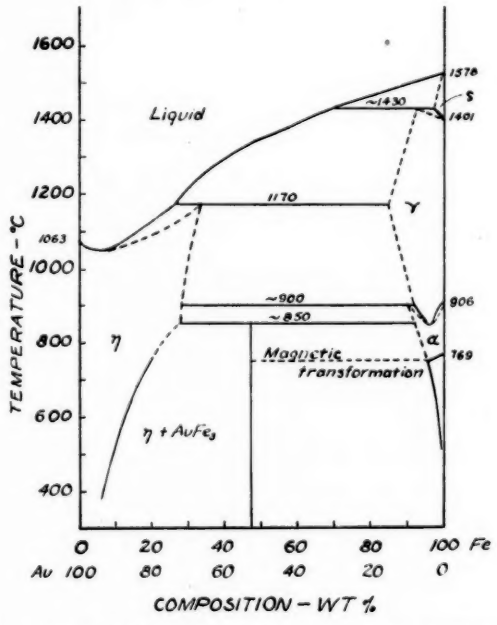

FIG. 1. The gold-iron phase diagram according to Hansen.

[1] M. Hansen, *Der Aufbau der Zweistofflegierungen* (Springer, Berlin, 1936).
[2] J. W. Shih, Phys. Rev. **38**, 2051 (1931).
[3] E. R. Jette, W. L. Bruner, and F. Foote, Trans. A. I. M. E. **111**, 354 (1394).
[4] F. Bitter and A. R. Kaufmann, Phys. Rev. **56**, 1044 (1939).

space between the tube and the Dewar flask. Through a side opening at the top of the Pyrex tube, hydrogen could be blown into the latter in order to prevent condensation of air or water vapor inside the tube. The temperature was measured by a copper-constantan thermocouple made of fine wires, which was soldered to the specimen holder. Thus, the couple wires served as suspension for the holder at the same time. Low temperature measurements were also made by previously cooling the Dewar flask and the specimen with liquid nitrogen and measuring in steps as the temperature gradually rose. The drifting of the temperature was sufficiently slow so that during each set of measurements it was constant within a few degrees. At low temperatures, the force arising from the saturation magnetization became so large that the sensitivity of the balance had to be reduced. Hence, these measurements are not accurate enough for calculating the superposed paramagnetic susceptibilities.

By a simple arrangement, specimens could be annealed in hydrogen and quenched into water without being exposed to air. A piece of the sample thus quenched from 870°C was found to be still magnetic. Polishing and etching by aqua regia revealed under the microscope a polygonal structure with twins characteristic of a single phase. No trace of precipitate could be detected, thus proving the magnetic nature of the supersaturated solid solution.

Preliminary measurements on a quenched specimen showed that the supersaturated solid solution had a Curie temperature of about 230°C. Pronounced precipitation took place at 450°C on heating and at 500°C on cooling. The progress of precipitation could be watched by noticing the increase in the force exerted by the field on the specimen with time. In the temperature range 650°C–950°C in which the solid solution was paramagnetic, the susceptibility was found to obey the Curie-Weiss law. When precipitation was allowed to be fairly completed at 500°C, it was found that the specimen contained two phases both of which were ferromagnetic. The main phase had a Curie temperature near room temperature, while the precipitated phase had a Curie temperature above the equilibrium temperature of the solid solution.

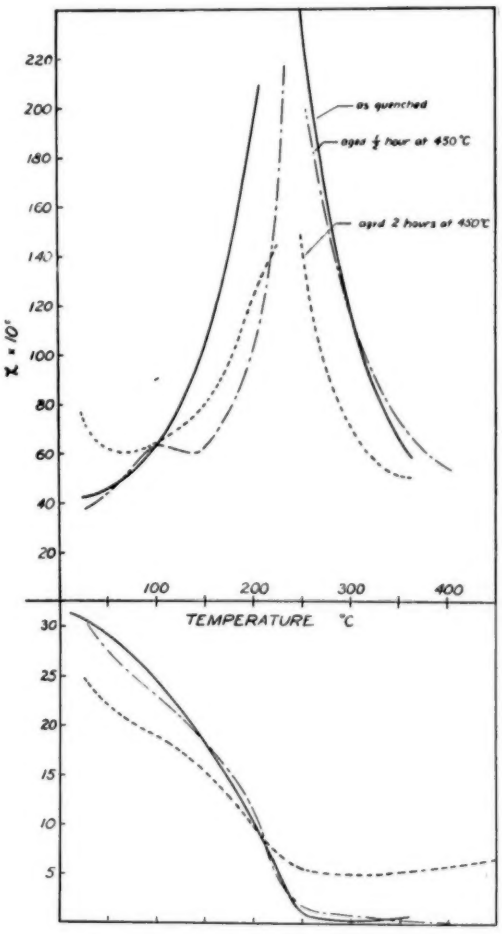

FIG. 2. Magnetic measurements on quenched and aged specimens of same alloy.

The results on three specimens with different treatments are shown in Fig. 2 in which Σ and χ are the mass saturation magnetization and the mass susceptibility, respectively. It is evident that all three specimens contain a phase with a Curie temperature of 230°C, which is better determined by the peak of the $\chi - T$ curve. This phase is easily identified as the undecomposed supersaturated solid solution. However, in the curves of the aged specimens, two additional phases show up, one of which is identified by the peaks of the $\chi - T$ curves near room temperature. The other phase, owing to its high Curie temperature and its small quantity, can only be detected in the $\Sigma - T$ curve of the specimen annealed for 2 hours at 450°C. These phases are evidently the products of precipitation. The

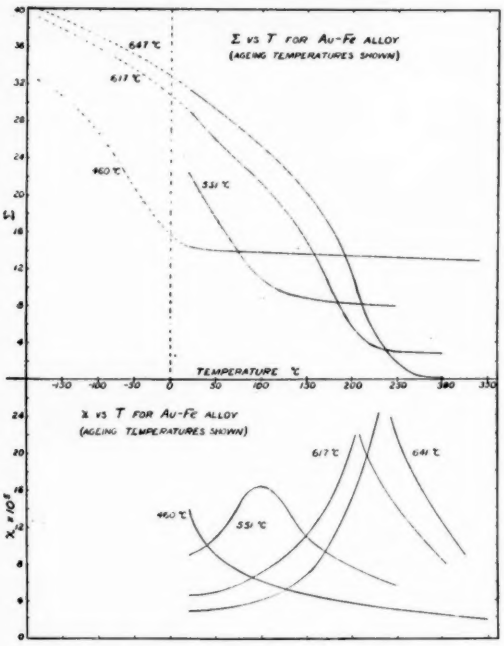

FIG. 3. Magnetic measurements on specimens which are approximately in equilibrium conditions at indicated temperatures.

presence of the precipitated phases with the original supersaturated solid solution in the same specimen characterizes the non-uniform nature of the precipitation process. In other words, precipitation in this alloy does not start at every point of the specimen at the same time and when precipitation occurs at any point the supersaturated solution breaks into the final phases with little intermediate change of composition.

Figure 3 shows the results on four specimens each annealed at a particular temperature for four days. These curves, however, should be interpreted differently. As the time of annealing was very long, equilibrium must have been approached in each specimen. Therefore, these curves show the variation of the Curie temperature of the gold-rich phase with composition rather than the mechanism of precipitation. The specimen annealed at 641°C still has a Curie temperature of 230°C, hence 641°C must be very near to the solubility limit temperature of the solid solution. One can approximately determine the variation of the Curie temperature of the gold-rich phase with composition by combining our results with Jette's[3] solubility limit curve. It is thus estimated that the Curie temperature becomes 0°C when the iron content is 8 percent by weight.

A portion of the sample was further swagged and drawn into a 0.006-inch wire. A piece of this wire was annealed and quenched from 970°C. The other was slowly cooled from 950°C with a duration of four hours in the range 500–400°C. Figures 4 and 5 show Debye-Scherrer patterns for the quenched and annealed wires, respectively. The quenched specimen gives spotted rings corresponding to an f.c.c. structure of lattice constant 3.967A. The annealed specimen, however, gives two sets of rings, one spotted and one fine, both corresponding to f.c.c. structures. The spotted set gives the same lattice constant as that of the quenched specimen while the fine rings give a lattice constant of 4.043A.

FIG. 4.

FIG. 5.

FIG. 4. Debye-Scherrer pattern of a specimen quenched from 970°C, showing a single phase of lattice constant 3.967A.

FIG. 5. Debye-Scherrer pattern of a specimen slowly cooled from 970°C, showing the original coarse-grained phase and a fine precipitated phase of lattice constant 4.043A.

These values are believed to be accurate to about 0.001A. According to Jette[3] and co-workers, the lattice constant of 4.043A corresponds to a gold-iron solid solution containing 3 percent of iron by weight. This seems to disagree with our results hitherto described, as we always found in an annealed specimen a phase with a Curie temperature near room temperature which, presumably, contained more than 8 percent of iron. The explanation is that, during cooling, the annealed specimen in this case was left at 340°C overnight so that the precipitated gold-rich phase should almost be in equilibrium at that temperature. If we check up with Jette's[3] solubility limit curve again, we find that the solubility of iron in gold at 340°C is just about 3 percent. The annealed specimen for x-ray investigation was later checked by magnetic measurements. The results are about the same as shown by the curves in Fig. 2. The only difference is that, in this case, we no longer find any Curie point near room temperature.

Thus, both magnetic and x-ray measurements prove the non-uniform nature of the precipitation process in the gold-iron alloys. The absence of the precipitated iron-rich phase in the Debye-Scherrer pattern of the annealed specimen shows that its quantity must be very small. This supports the conclusion obtained by Jette[3] and co-workers that the intermetallic compound $AuFe_3$ in Hansen's[1] phase diagram does not exist and that the solubility of gold in α-iron is very small. The fact that the lines of the precipitated gold-rich phase are fine in contrast with the spotted lines of the original supersaturated phase also substantiates the conclusion arrived at by previous investigators[5] that in non-uniform precipitation, the original grains in the sample are not preserved.

In conclusion, the authors wish to express their appreciation to Dr. B. M. Loring for taking the x-ray pictures.

[5] R. Becker and W. Döring, *Ferromagnetismus*, Sections 26 and 27 (Springer, Berlin, 1939).

JUNE, 1942 JOURNAL OF CHEMICAL PHYSICS VOLUME 10

Exchange of Radioactive Silver with Silver Chloride Suspensions

A. LANGER
Westinghouse Research Laboratories, East Pittsburgh, Pennsylvania
(Received February 27, 1942)

From exchange experiments on radioactive silver in solution with silver chloride in suspension, it can be shown that the silver ions in solution are constantly exchanging with the silver ions in the precipitate. This exchange is not limited to the surface of the crystals, but, probably by means of self-diffusion, is propagated into the precipitate. A steady radioactive state obtains when a homogeneous distribution of the radioactive silver throughout the whole system is reached. The time necessary to obtain a given fraction of complete exchange for a given amount of precipitate depends strongly on the area of the crystal surface.

THE exchange of silver ions in solution with silver chloride in suspension was studied, using radioactive silver as an exchange indicator. It was observed that the radioactive silver undergoes quite a rapid exchange with the precipitate, indicating that in all cases after sufficient time, a homogeneous distribution of the radioactive silver throughout the whole system can be obtained. The phenomenon was studied in detail with respect to the concentration of the silver in solution and the amount of precipitate used, with respect to the previous treatment of the silver chloride leading to different crystal sizes and consequently to different surfaces as determined by the dye adsorption method, and with respect to the effect of temperature. The influence of dyes previously adsorbed on the precipitates was also investigated. A possible interpretation of the observed curves in terms of diffusion and crystal size is given.

APPARATUS AND PROCEDURE

The arrangement of the apparatus is shown in Fig. 1. The shaking beaker was constricted to prevent splashing of the precipitate throughout the whole vessel. As can be seen, it was suspended on a rubber tube and shaken by an eccentric pulley and could be immersed in a small bath into which water was pumped continuously from a large thermostat. The temperature was 25°±1°C.

For the radioactivity measurements a counter system was used. The counter tube was of the liquid jacket pipette type already described.[1] For each experiment a clean Corning fritted glass dipping filter was used. The counter tube was connected to a Neher-Harper self-quenching arrangement in connection with a Reich scale of four scaling circuit and a Cenco counter. A timer accurate to $\frac{1}{10}$ second was used for automatically timing the counting interval. The counting system was tested in regard to reliability. The radioactive silver was produced by proton bombardment of palladium in the University of Rochester cyclotron. The palladium was dissolved in nitric acid, silver added as carrier, and precipitated as silver chloride. The precipitate was washed and the silver electroplated from ammonia solution. A stock solution of radioactive silver nitrate was prepared by dissolving a weighed amount of this electrolytic silver in nitric acid. After evaporation to dryness the silver nitrate was dissolved in a known amount of water. Non-radioactive silver nitrate was prepared from the purest available silver according to the standard procedure. The sodium chloride solution was prepared from pure sodium chloride.

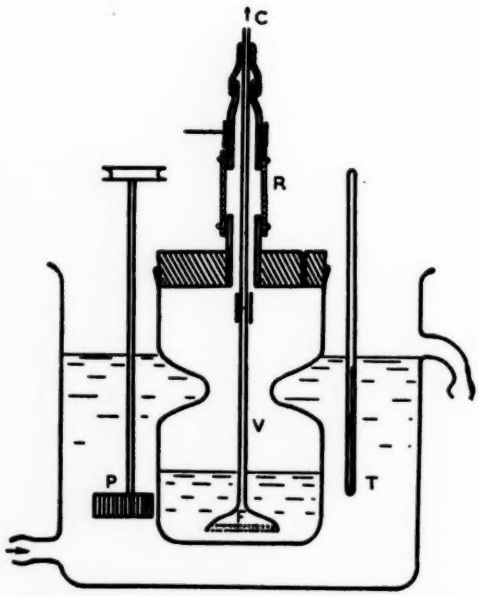

FIG. 1. Shaking arrangement for the exchange experiments. (*F*) Fritted glass filter; (*P*) eccentric pulley for shaking the vessel (*V*); (*R*) rubber tube holding the vessel; (*C*) connection to a liquid jacket counter tube.

The silver chloride for the experiments was always prepared in the same way, but was given different subsequent treatments. To measured amounts of 0.10 *M* sodium chloride, 1 ml of 0.1 *M* nitric acid was added and to this solution a 1-percent excess of 0.10 *M* silver nitrate was added with stirring in about 20 seconds. All the manipulations with the precipitate were done in photographically inactive red light. After the treatments to be described below, the coagulated precipitate was centrifuged at low speed for 3 minutes, then the liquid was decanted, the precipitate shaken for 1 minute with 30 ml of 10^{-3} *N* nitric acid, centrifuged, and the shaking repeated with water. The suspension was centrifuged again and the precipitate drained and partly dried in vacuum for a short time. To the damp precipitate (containing about 0.1 g water) 40 ml of the radioactive silver solution of a previously determined radioactive strength and known silver content was added and shaken in the apparatus described. After an arbitrary time, five to twenty minutes, liquid was drawn into the counter (filling time about 30 seconds) and the counts recorded during four minutes. The liquid was then returned to the original solution by applying pressure. The time was measured from the addition of the radioactive solution to the time when the counter tube was half filled with the liquid. The uncertainty in this measurement is about 30 seconds. Somewhat higher activities can be expected with this method of determining the radioactivity, because 6 ml solution removed from the bulk of the solution each time for about 5 minutes while its activity was being measured, took no part in the exchange. This error becomes small after long shaking periods. The error introduced by the

[1] A. Langer, J. Phys. Chem. **45**, 639 (1941).

statistical fluctuations in the counting rate was also a few percent because of the relatively low number of counts taken. Since the 45-day silver isotope was predominant, no corrections for decay during a single experiment were necessary.[2] The measured activities were corrected for the background.

EXPERIMENTAL RESULTS

The first experiments were done with precipitates prepared by shaking them for 5 minutes with the mother liquid after precipitation. Figure 2 shows activity-time curves obtained with the indicated amounts of silver in solution and silver in the precipitate. It can be seen that the original activity (C_0) of the solution rapidly decreases from the beginning of the shaking and becomes almost constant after about one hour. It was found that this final activity (C_∞) as measured by the counting rate and taken proportional to the concentration of the radioactive silver in the solution, corresponds closely to a homogeneous distribution of the radioactive silver through the whole system given by:

$$C_\infty = C_0(M_s/M_t). \quad (1)$$

Where (M_s) is the amount of silver in the solution and (M_t) the total amount of silver present:

$$M_t = M_s + M_p, \quad (2)$$

where (M_p) is the amount of silver in the precipitate. The computed (C_∞)'s are indicated in Fig. 2 with arrows and it can be seen that these values are reached within the limits of the experimental errors. The similarity of the curves shows that the process of exchange is not markedly affected by the ratio of the silver in solution to that in the precipitate if the precipitates are prepared in the same manner and the curves taken under similar conditions.

That one deals here with only an exchange reaction is indicated by the fact that the total concentration of the silver in solution after the shaking with the precipitate is practically unchanged. This was shown by comparison of the titers of the filtered solutions before and after shaking. It was also found that the exchange is reversible in the sense that if the precipitate is made radioactive and the solution used is

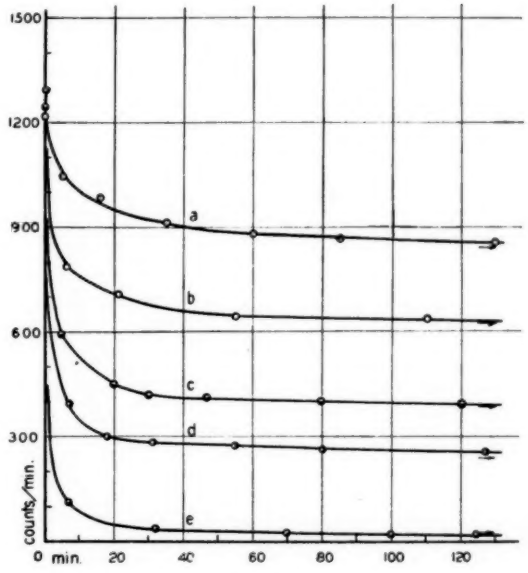

FIG. 2. Radioactive silver exchange—time curves for fresh silver chloride with different amounts of total silver in the precipitate (M_p) and in solution (M_s) at 25°C.

Curve	*a*	*b*	*c*	*d*	*e*
M_p mg Ag	10.8	107.9	53.9	107.9	215.8
M_s mg Ag	24.4	104.0	24.4	24.4	3.6

inactive, the activity of the solution increases to a value corresponding to a homogeneous distribution of the radioactive silver.

That the exchange of the silver ions in the solution with the silver in the precipitate must be continuous was indicated by experiments in which a new radioactive solution was added to the solution which was already in exchange equilibrium with the precipitate. It was found that after about the same time as before a new equilibrium was established. Repeated addition of the radioactive silver solution gave again an homogeneous distribution.

Experiments were made to determine whether different treatments of the precipitates, which could change the crystal size by way of recrystallization, have any influence on the exchange rate. Precipitates obtained from 10 ml 0.1 *M* sodium chloride with 10.1 ml of 0.1 *M* silver nitrate had the following treatments: (a) shaken in the mother liquid for five minutes; (b) shaken for one hour; (c) shaken for one day; (d) after addition of 10 ml concentrated nitric acid to the mother liquid, boiled for five minutes; (e) boiled for one hour; (f) boiled in concentrated nitric acid for three hours; (g) recrystallized from

[2] T. Enns, Phys. Rev. **56**, 872 (1939).

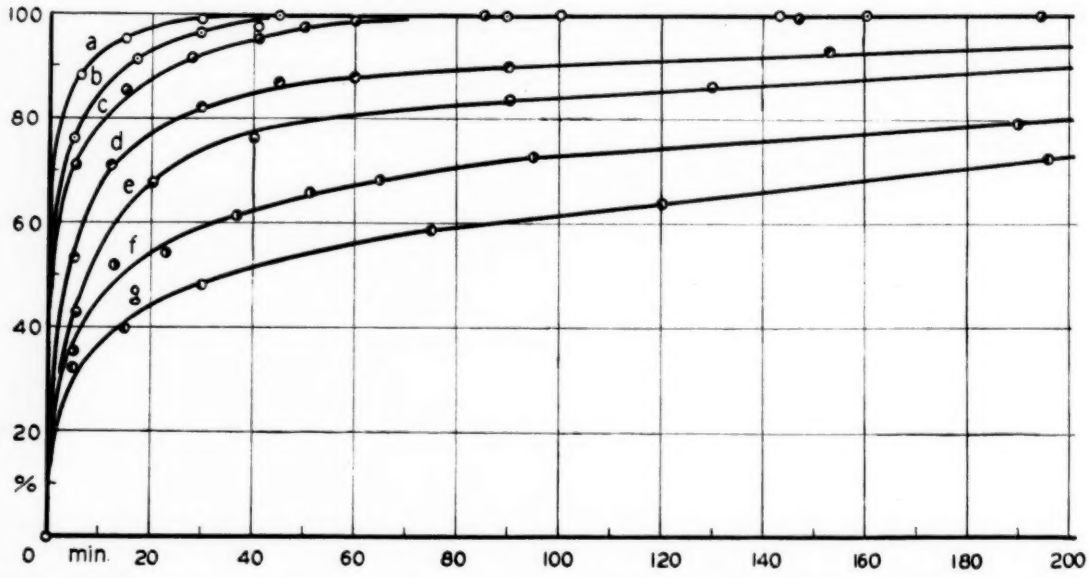

FIG. 3. Radioactive silver exchange—time curves for silver chloride of different origin; $M_p = 107.9$ mg Ag, $M_s = 24.4$ mg Ag, temperature = 25°C, curves *a*, *b*, *c*, shaken with the mother liquid, *d*, *e*, *f*, boiled with nitric acid, *g* recrystalized from ammonia.

ammonia by slowly heating and stirring. The results obtained with these different precipitates are given in Fig. 3. In order to eliminate differences in the exchange-time curves, resulting from different initial strength of the radioactive solution, all the activity measurements are expressed by the fraction

$$\alpha = \frac{C_0 - C_t}{C_0 - C_\infty} \times 100, \qquad (3)$$

where (C_t) is the radioactivity after the time (t) and (C_∞) as computed from Eq. (1). It can be seen that (α) expresses in percent the completeness of exchange. These time-exchange curves indicate that there is a difference in exchange rate for silver chloride precipitates having different treatment. The fresh silver chloride and even that shaken in the mother liquid for one day was in complete equilibrium after about 1 hour, whereas the precipitate recrystallized from ammonia was only 50 percent exchanged in the same time. Microscopic measurements showed that the mean crystal diameter of the fresh precipitates was of the order of 10^{-4} cm and that the crystallites are of a fairly uniform size and a round appearance. The crystals recrystallized from ammonia were much larger, more plate-like in shape, and not as uniform in size. Because it was difficult to estimate the average size of all the precipitates used, dye absorption measurements on the crystal surface were made in order to determine the surface area which is related to the crystal size. For this reason the precipitates shaken with the radioactive silver were centrifuged, washed twice with 20 ml water, and partly dried. After that, 10 ml of 0.01 percent methylene blue chloride solution were added and the precipitate shaken with the dye for two hours, then the solution was centrifuged and the clear solution compared with the original one by means of a visual photometer. At the same time a similar experiment was done with a precipitate which had not been shaken with the radioactive silver solution. The two methods checked to within 10 percent. Because only small amounts of dye were adsorbed on aged precipitates, the accuracy of measurements is about of that order of magnitude. This indicates that no substantial surface change took place during the experiments. It was found in general that with decreasing amounts of adsorbed dyes the time to reach a given percentage of exchange increases rapidly (see Fig. 4).

To see whether the coating of the precipitate surface with an adsorbed dye prevents the silver

in solution from exchanging with the precipitate, the five-minute old silver chlorides were shaken with one percent solutions of the following dyes in water: fluorescein, eosin, methylene blue, and wool violet. After 30 minutes of shaking the precipitate was centrifuged and then shaken with the radioactive silver solution as described before. Figure 5 indicates that the coatings with the dyes used had almost no effect on the rate of exchange and could not prevent an homogeneous distribution of the radioactive silver. The points obtained give also an indication of the reproducibility of the precipitates and of the measurements.

In Fig. 6 the influence of the temperature on the speed of exchange is given. All the precipitates were prepared from 10 ml 0.1 *M* sodium chloride with 1 ml concentrated nitric acid and 10.1 ml 0.10 *M* silver nitrate boiled with the mother liquid for 30 minutes and shaken for 3 days at room temperature. This treatment was used to minimize the influence of temperature on the crystal size during the shaking with the radioactive silver nitrate. From this figure it can be seen that the speed of exchange increases markedly with the temperature. Previous experiments with a standard radioactive silver solution showed that the effect of temperature on the counting rate is negligible.

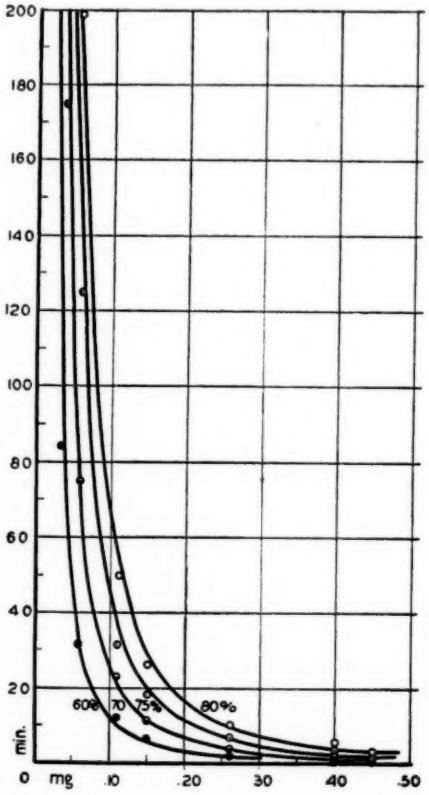

FIG. 4. Curves indicating the relation between the amount of adsorbed methylene blue in mg of dye per millimole of silver chloride and the time to obtain an indicated fraction of radioactive exchange.

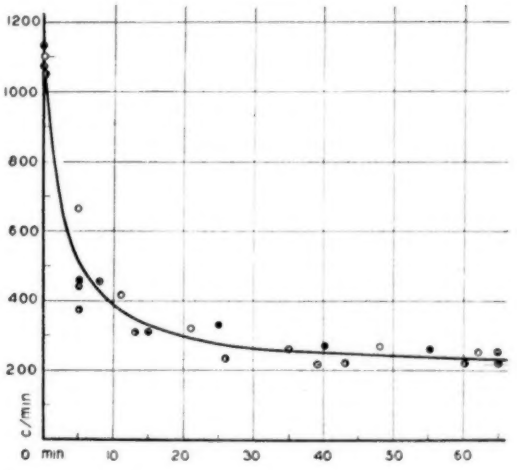

FIG. 5. Radioactive silver exchange-time curves for fresh silver chloride with dye coated surface. ⊙ = methylene blue; ○ = fluorescein; ◑ = wool violet 5*BN*; ◒ = Eosin; ●—without dye.
M_p = 109.7 mg Ag; M_s = 24.4 mg Ag at 25°C.

DISCUSSION

To explain the exchange of the silver ions in solution with the silver in the precipitate quantitatively, let us assume that the crystals are spherical and that in addition to a rapid surface exchange, the distribution of the radioactive silver inside the crystal lattice will take place by diffusion. Although the surface exchange is governed also by a diffusion process through the adsorbed layer of solution, this process will probably be very rapid because of the vigorous shaking of the liquid and will be neglected in further considerations. If, therefore, only diffusion into the solid is the main factor governing the exchange process, then the problem of the radioactive exchange in such a simple case is exactly analogous to the cooling of a hot stirred liquid, insulated from outside, in which is immersed a given mass of cold spheres. Experiments done jointly with Dr. Kauzmann have

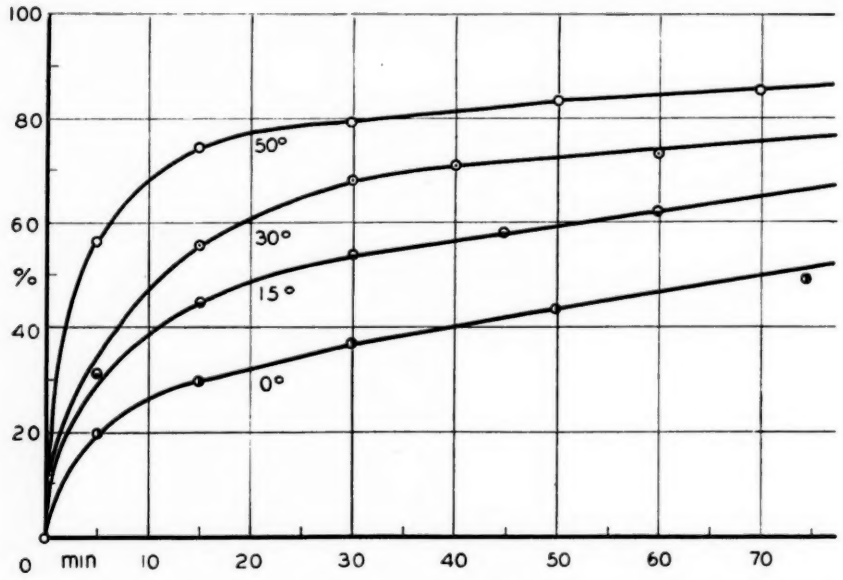

FIG. 6. Radioactive silver exchange curves for silver chloride at 0°, 15°, 30°, and 50°C; $M_p = 107.9$ mg Ag, $M_s = 24.4$ mg Ag.

shown that the cooling-time curve of stirred carbon tetrachloride in a Dewar flask containing a steel ball previously cooled in ice water resembles very closely the radioactive exchange curve. For a given mass of solid and liquid, different rates of cooling can be obtained by subdividing the solids into spheres of different sizes.

Assuming such a diffusion, that concentric surfaces have the same concentration, then this problem may be treated quantitatively by solving the differential equation for Fick's law for a sphere

$$\frac{\partial(rc)}{\partial t} = D_T \frac{\partial^2(rc)}{\partial r^2}. \tag{4}$$

The solutions of this differential equation are known to be of the form[3]

$$rc = [A \sin \mu r + B \cos \mu r] \exp(-\mu^2 D_T t). \tag{5}$$

Since at the start of the experiment we have no radioactive atoms in the solid, and assuming that the distribution of the radioactive atoms at the surface of the solid is the same as that in the stirred liquid (C_l),

$$C_s(a, t) = C_l(t)$$

as a boundary condition, where (a) is the radius of the sphere it can be shown[4] that $C_l(t)$ can be expressed as:

$$C_l(t) = \sum_{n=0}^{\infty} A_n \exp\left[-k_n \frac{D_T t}{a^2}\right], \tag{6}$$

where D_T is the diffusion coefficient at the temperature T of the experiment and A_n and k_n are constants. In general, the concentration of the radioactive material in the liquid at any time (t) after the start of the diffusion process can therefore be expressed as:

$$C_l(t) = f(D_T t/a^2). \tag{6a}$$

The exchange fraction (α) is given in terms of (C_t) by Eq. (3). This means that for a given mass of solid and a given value of (α) the quantity

$$D_T t/a^2 = \text{const.} \tag{7}$$

for uniform spheres of any size.

The radii of the spherical particles in any precipitate are correlated to the surface as found from the dye absorption measurements as follows. Since in all of these measurements the same amount of solid silver chloride was used,

[3] H. S. Carslaw, *The Conduction of Heat* (Macmillan, 1921), p. 135; R. M. Barrer, *Diffusion in and Through Solids* (Macmillan, 1941), p. 11.

[4] For more details: H. W. March and W. Weaver, Phys. Rev. **31**, 1072 (1928); R. E. Langer, Tohoku Math. J. **35**, 260 (1932).

a change in the area of surface must be accompanied by a change in the size and in the number of the spheres. It is easily shown, assuming the crystal to be uniform, that the surface (S) which we can assume to be proportional to the amount of dye adsorbed is related to the radius (a) by:

$$S = K/a. \tag{8}$$

Thus we have for a given value of (α) at a given temperature substituting (8) into (7) the quantity

$$S^2 t = \text{const.} \tag{9}$$

That is, for a given amount of precipitate, the product of the square of the surface (expressed, for example, in the amount of large dye molecules adsorbed uniformly only on the surface) and the time required for the same precipitate to arrive at a given fraction of complete exchange with the "tagged" atoms should be constant. In Fig. 4 are indicated the points obtained by plotting the time to reach a given (α) taken from Fig. 3 against the amount of dye adsorbed on the precipitate used. These points fall close to the solid curves which were calculated for $S^2t = \text{constant}$. This quite close agreement, in spite of the necessary assumptions, indicates that simple considerations of crystal size and diffusion rate are sufficient to account for the large variations in the exchange rates with aged silver chloride.

The influence of temperature can also be easily explained. Since the diffusion coefficient for silver ions moving through the silver chloride lattice doubtless changes with changing temperature according to the known relation

$$D_T = D_0 \exp(-Q/RT), \tag{10}$$

where (Q) is the activation energy for the ionic movement, (R) the gas constant, and (T) the absolute temperature. A plot of (ln D) *versus* ($1/T$) should give a straight line with a slope of ($-Q/R$). But from Eq. (7) we can see that as long as the particle size is constant, the time (t) for a given fraction of exchange (α) to be reached should be inversely proportional to the diffusion constant. Dye absorption measurements indicate

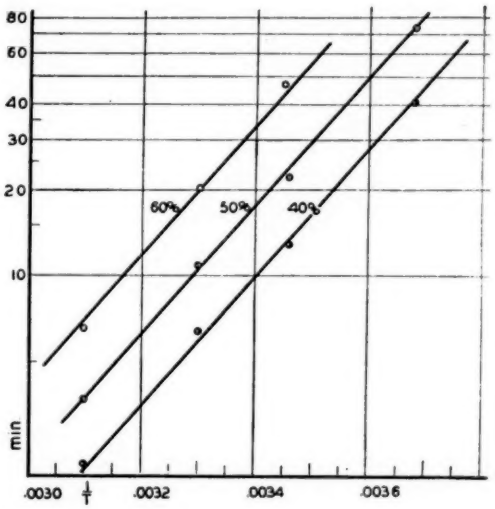

FIG. 7. Time of exchange plots, for a given exchange, *versus* the reciprocal of the absolute temperature on a semi-logarithmic scale.

that for the precipitates used in the exchange measurements at different temperatures, the surface and hence the particle size is roughly constant. In Fig. 7 are given semi-logarithmic plots of the times to reach various fractions of exchange against ($1/T$). The fact that the slopes of these straight lines are the same is also an evidence for the interpretation proposed here. The slopes of these lines indicate a rather low activation energy for the movement of silver ions through the silver chloride lattice.

The value thus obtained, approximately 10 kcal., seems to be at least of the right order of magnitude as compared with 18.5 kcal. derived from conductivity measurements of Koch and Wagner.[5] However, much more carefully planned experiments with radioactive silver must be made before any definite value of Q for the flow of the silver ions only can be given.

It is a pleasure to thank Dr. E. U. Condon for his interest in this work and for help in deriving the mathematical expression for the diffusion equation.

[5] E. Koch and C. Wagner, Zeits. f. physik. Chemie, **B38**, 295 (1937); N. F. Mott and R. W. Gurney, *Electronic Process in Ionic Crystals* (Oxford, 1940) p. 47.

The Vibrational Spectra of Pyrrole and Some of Its Deuterium Derivatives

R. C. LORD, JR. AND FOIL A. MILLER*
Department of Chemistry, The Johns Hopkins University, Baltimore, Maryland
(Received March 23, 1942)

The Raman spectra of pyrrole, pyrrole-*N*-*d*, symmetrical pyrrole-d_4, and pyrrole-d_5 have been studied with a high speed grating spectrograph. The infra-red absorption spectra of the same compounds have been investigated in the liquid state in the region 750–1900 cm^{-1}. With the help of the selection principles and Teller's product rule, these spectra have been analyzed for a molecule of C_{2v} symmetry. The analysis yields values for all but one of the twenty-four fundamental frequencies, and this one has been estimated. The spectra indicate clearly a C_{2v} structure for pyrrole, although a C_s (non-planar) structure cannot yet be rigorously excluded.

INTRODUCTION

THE pyrrole ring is of interest because it is found in many chemical substances of biological importance. In such compounds as hemoglobin, chlorophyll, the porphyrins, and several of the oxidative enzymes it is one of the chief constituents of the molecule. Our knowledge of the pyrrole molecule itself, however, is far from complete. In particular its vibrational spectra have never been analyzed, and therefore it has been impossible to establish the symmetry of pyrrole through such an analysis. The molecular symmetry must be low at best, which means that the selection rules for the vibrational spectra will not be very restrictive. Because of this lack of restriction and because of the large number of fundamental frequencies, the analysis of the vibrational spectra has not been carried very far, despite the fact that spectroscopic work on pyrrole has been extensive.

The infra-red spectrum of liquid pyrrole has been obtained twice previously.[1,2] In the Raman effect, numerous studies of pyrrole have been made,[3–9] including a careful determination of the depolarization factors of the Raman lines by Reitz.[8] One deuterium derivative, pyrrole-*N*-*d*, has also been studied in the Raman effect.[10,11] It seemed to the authors that the analysis of the spectra of pyrrole might best be accomplished with the help of the spectra of the deuterium derivatives. The preparation of several of the symmetrically substituted derivatives is not difficult. We have accordingly undertaken an investigation of pyrrole, pyrrole-*N*-*d*, symmetrical pyrrole-d_4, and pyrrole-d_5 in both the Raman effect and in infra-red absorption.

EXPERIMENTAL METHODS

Preparation of the Compounds

It has been shown by Koizumi and Titani[12] that all the hydrogens in the pyrrole molecule will exchange in solutions of $p\mathrm{H} \lesssim 1$. We have confirmed and extended this work, and have found that such exchange furnishes a convenient method for preparing the symmetrically deuterated derivatives. Details of the method are to be described elsewhere.† It should be mentioned here, however, that in all our spectra only two bands are found which can reasonably be assigned to isotopic impurity (Table XII). Both of these are in the infra-red, and both are weak. From this we conclude that our exchange was very nearly as complete as the purity of our heavy water (99.6+ percent) would allow.

* Chemical Foundation Fellow, 1938–1942.
[1] W. W. Coblentz, *Investigations of Infra-Red Spectra* (Carnegie Institution of Washington, Washington, D. C., 1905) pp. 99, 143, 278.
[2] R. Manzoni-Ansidei and M. Rolla, Atti accad. Lincei **27**, 410 (1938).
[3] S. Venkateswaran, Ind. J. Phys. **5**, 145 (1930).
[4] G. B. Bonino, R. Manzoni-Ansidei, and P. Pratesi, Zeits. f. physik. Chemie **B22**, 21 (1933).
[5] A. Stern and K. Thalmayer, Zeits. f. physik. Chemie **B31**, 403 (1936).
[6] A. W. Reitz, Zeits. f. physik. Chemie **B33**, 179 (1936).
[7] G. B. Bonino and R. Manzoni-Ansidei, Ricerca Scient. **7** (1), No. 11–12, 2 pp. (1936). *Or*: Atti accad. Lincei **25**, 489 (1937).
[8] A. W. Reitz, Zeits. f. physik. Chemie **B38**, 275 (1938).
[9] R. Manzoni-Ansidei, Ricerca Scient. **10**, 328 (1939).
[10] G. B. Bonino and R. Manzoni-Ansidei, Ricerca Scient. **7** (2), No. 3–4 (1936). *Or*: Atti accad. Lincei **25**, 494 (1937).
[11] O. Redlich and W. Stricks, Monats. **68**, 47 (1936).
[12] M. Harada and T. Titani, Bull. Chem. Soc. Jap. **11**, 465–74 (1936); M. Koizumi and T. Titani, *ibid.*, **12**, 107–8 (1937); *ibid.*, **13**, 85–94 (1938).
† To appear shortly in J. Am. Chem. Soc.

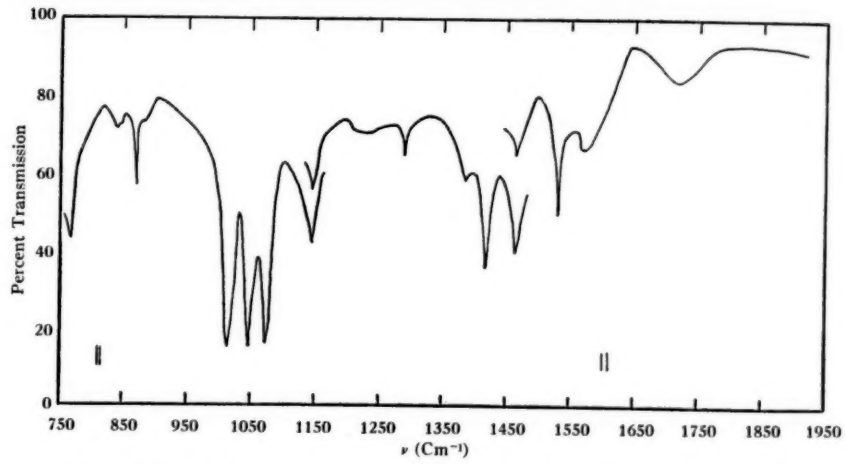

FIG. 1. Infra-red transmission curve for pyrrole. Cell thickness = 0.020 mm.

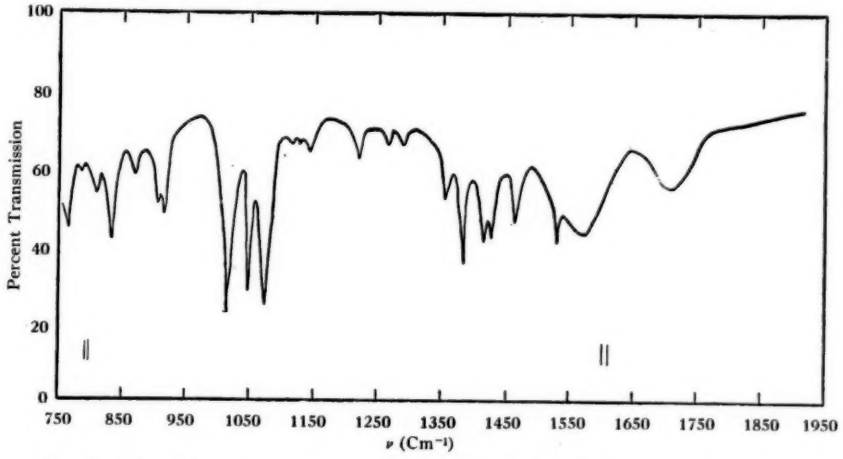

FIG. 2. Infra-red transmission curve for pyrrole-*N*-*d*. Cell thickness = 0.020 mm.

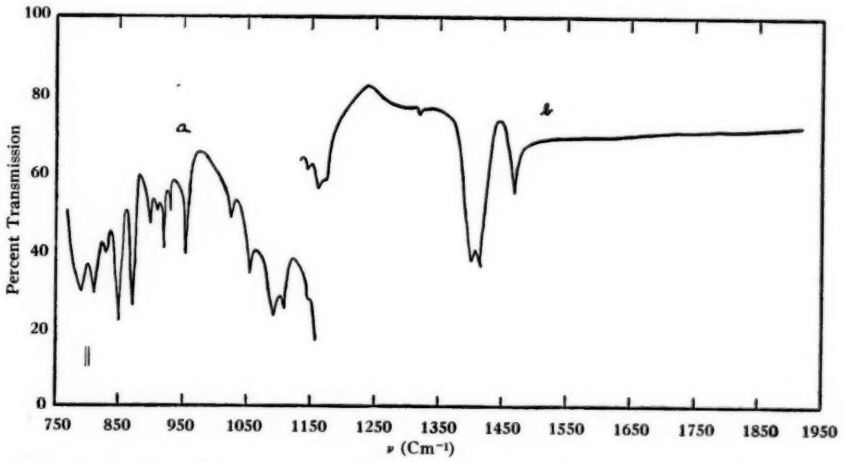

FIG. 3. Infra-red transmission curve for *sym*-pyrrole-d_4. Cell thickness: *a* − 0.045 mm. *b* − 0.020 mm.

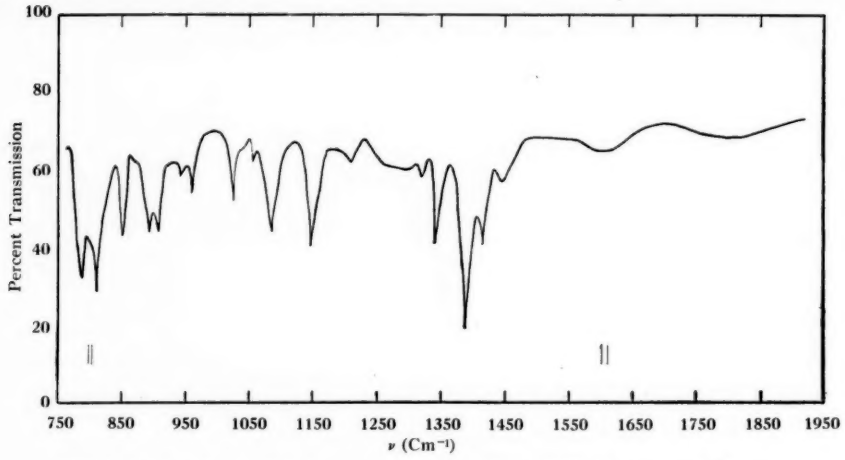

FIG. 4. Infra-red transmission curve for pyrrole-d_5. Cell thickness = 0.028 mm.

The chief difficulty encountered in obtaining the Raman spectrum of pyrrole is the removal of the last traces of fluorescent impurities. To accomplish this removal the pyrrole was distilled four times and then sealed in the Raman tube, the entire series of operations being carried out in vacuum. After exposures totalling as much as 70 hours, samples were still free from fluorescence.

Spectroscopic Procedures

The Raman spectra were photographed with Hg 4358A excitation. To isolate this frequency we used a filter of saturated aqueous $NaNO_2$ of sufficient thickness to remove Hg 4047A almost completely. For a few exposures Rhodamine 5 GDN Extra was also used.[13] The removal of background by this filter was offset by the somewhat longer exposure times which its use necessitated. The light source consisted of six General Electric H-2 type mercury arcs. These lamps are not particularly intense, but they have excellent background characteristics and are easily operated. The spectrograph is a plane grating instrument with an extremely fast camera, which was usually operated at a stop of f: 3.8. The grating, ruled by Professor R. W. Wood of the physics department, is of the echelette type. Its ruled surface is 4×6 inches, it has a total of 90,000 lines, and in the blue-green region it throws some 80 percent of the reflected light into one of the first orders. The dispersion in the blue-green is 55A/mm. Details of the construction of this instrument, as well as of the illuminator and filter cell, will be published elsewhere. The plates were Eastman Super Panchro Press, which are very fast but coarse-grained. For this reason a fine-grain developer was used (Eastman DK-20). Exposures varied from 1 to 24 hours, depending on the filters. The plates were enlarged 20 times, and the frequencies were measured from these enlargements by linear interpolation between standard lines of the iron arc with the help of a correcting curve. Sharp lines are probably accurate to ±1 cm^{-1}, diffuse ones to ±3 cm^{-1}.

The infra-red spectra were obtained in the liquid state in the range 750–1900 cm^{-1}. This work was done at the Stamford laboratories of the American Cyanamid Company through the kindness of Dr. R. Bowling Barnes, Director of the Physics Division, and Dr. Van Zandt Williams. The spectrometer is an automatic recording instrument which uses two rocksalt prisms in a Littrow mount.** The cells containing the liquid were made of rocksalt plates spaced at the proper distance by metal washers. The cell thicknesses were 0.020, 0.028, and 0.045 mm. The spectral slit widths varied from about 8 cm^{-1} at 1600 cm^{-1} down to 5 cm^{-1} at 800 cm^{-1}. Cell thicknesses and slit widths employed in obtaining the various curves are indicated on Figs. 1–4. The accuracy of the transmission

[13] J. T. Edsall and E. B. Wilson, Jr., J. Chem. Phys. **6**, 125 (1938).

** A diagrammatic sketch of the instrument will be found in Rev. Sci. Inst. **13**, 50 (1942).

TABLE I. Raman spectra of the four pyrroles.

Pyrrole $\Delta\nu$(cm^{-1})	I	Pyrrole-*N*-*d* $\Delta\nu$(cm^{-1})	I	Symmetrical pyrrole-d_4 $\Delta\nu$(cm^{-1})	I	Pyrrole-d_5 $\Delta\nu$(cm^{-1})	I
545–585	0*b*	420–475	0*b*	514	1	425–475	1*b*
(618)	0	606	3*p*	560	6*b*	516	1
647	3	708	3	692	4*p*	565	4
711	3	(780)	0	730	2	693	3*p*
837	2	831	3*p*	769	1	728	2*p*
866	1	869	2	848	4*p*	766	1
880	½	911	2	917	4*p*	808	1
1015	½	1010	1	953	1	892	5*p*
1045	1	1074	5*p*	1094	10*p*	909	5*p*
1076	3	1135	10*p*	1319	7*p*	1084	10*p*
1144	10	1210	0	1401	9*p*	1115–1170	3*b*
1237	½	1237	½	1463	1	(1211)	0
1379	9*b*	1320–80	3*b*	2309	7*p*	1317	5*p*
1468	5	1384	9*p*	2358	7*p*	1389	8*p*
(1484)	0	1465	6*p*	3365–3455	3*b*	(1413)	½
1528	½	2490–2560	5*b*	—	—	1455	½
3100	4	(2709)	0	—	—	2309	8
3111	4	3104	8*p*	—	—	2350	6*p*
3133	9	3131	10*p*	—	—	2368	6*p*
3345–3460	4*b*	—	—	—	—	2505–2560	6*b*
		—	—			2679	½

( ) Observed on only one plate, but believed real.
b Broad.
p Estimated to be polarized.

TABLE II. Raman spectrum of pyrrole: comparison with earlier work.

V. (1930)[a] $\Delta\nu$	I	S. T. (1936)[b] $\Delta\nu$	I	B. M.-A. (1936)[c] $\Delta\nu$	I	R. (1938)[d] $\Delta\nu$	I	Depol	L. M. (1942) $\Delta\nu$	I
530	0	550	0	—		556	0	*dp.*	545–585	0*b*
—		—		574	0	—			—	
628	0	—		—		—			(618)	0
—		646	2*d*	649	1	646	2	0.92	647	3
704	1	711	2*d*	708	2	708	4	.94	711	3
843	0	840	1	835	½	835	3	.89	837	2
—		873	1	866	2	865	3	.92	866	1
—		—		—		—			880	½
1003	1	1000	0	1001	0	—			1015	½
—		1051	2	1046	½	1048	4	*dp.*	1045	1
—		—		1084	½*f*?	1072	1	*p.*	1076	3
—		1091	2	—		—			—	
1144	8	1145	10	1142	10	1144	12	.18	1144	10
1202	0	—		1204	?	—			—	
—		1233	0	1235	0	1235	1	.33	1237	½
—		1313	0	—		—			—	
1384	4*b*	1382	6	1380	6	1379	8*b*	.36	1379	9*b*
—		1416	0	1414	½*f*?	—			—	
1470	3	1465	5	1465	5	1469	6	.22	1468	5
—		—		—		—			(1484)	0
—		1524	1	—		—			1528	½
—		1558	1	—		1562	1?		—	
—		1593	0	—		—			—	
—		1631	0	—		—			—	
—		2676	0	—		—			—	
—		2777	1	2786	0Hg?	—			—	
—		2880	0	—		—			—	
—		2926	1	—		2917	0	*p.*	—	
3057	0	3056	1	3062	½Hg?	3045	1?	−(Hg)	—	
—		—		—		—			3100	4
—		3108	3	3107	3	3108	8	*p*(Hg)	3111	4
3139	6	3134	5	3138	5	3138	7*b*	.44(Hg)	3133	9
3308	0*b*	—		—		—			—	
—		3388	2*d*	3390	3 dif.	3383	3*b*	.49(Hg)	3345–3460	4*b*

( ) Found on only one plate, but believed real. [a] Reference 3. [b] Reference 5. [c] Reference 7. [d] Reference 8.

TABLE III. Raman spectrum of pyrrole-*N*-*d*: comparison with earlier work.

R. S. (1936)[a] $\Delta\nu$	*I*	B. M.-A. (1936)[b] $\Delta\nu$	*I*	L. M. (1942) $\Delta\nu$	*I*
291	0	—		—	
—		456	0	420–475	0*b*
537?	0	—		—	
—		572	0	—	
608	2	608	½	606	3
—		652	0	—	
708	2	710	2	708	3
—		—		(780)	0
832	2	835	1	831	3
—		867	1	869	2
—		912	2	911	2
—		1012	½	1010	1
—		1046	½	—	
1072	3*b*	1080	4	1074	5
—		1104	00	—	
1136	10	1136	10	1135	10
1147	1	—		—	
—		—		1210	0
—		1236	½	1237	½
—		—		1320–80	3*b*
1386	9	1383	7	1384	9
—		1414	0-*f*?	—	
1465.5	4	1465	5	1465	6
2357	0	—		—	
—		2536	3*d*	2490–2560	5*b*
—		—		(2709)	0
—		2788	½	—	
—		3023	0?	—	
—		3051	0-Hg	—	
3104.5	3	3109	3	3104	8
3135	5	3138	5	3131	10

( ) Found on only one plate.
[a] Reference 11.
[b] Reference 10.

TABLE IV. Infra-red spectra of the four pyrroles.

Pyrrole cm^{-1}	*I*	Pyrrole-*N*-*d* cm^{-1}	*I*	*sym*-pyrrole-d_4 cm^{-1}	*I*	Pyrrole-d_5 cm^{-1}	*I*
768	*s*	766	*s*	793	*s*	789	*vs*
839	*w*	783	*vw*	812	*s*	813	*vs*
844	*vw*	786	*vw*	830	*w*	852	*s*
869	*m*	808	*m*	849	*vs*	893	*s*
884	*w*	835	*s*	872	*vs*	910	*s*
1015	*vs*	870	*m*	899	*m*	943	*w*
1047	*vs*	905	*m*	910	*w*	961	*m*
1076	*vs*	915	*s*	920	*s*	1025	*s*
1146	*s*	1015	*vs*	931	*m*	1039	*vw*
1289	*m*	1026	*w*	956	*s*	1058	*w*
1384	*m*	1048	*vs*	1027	*m*	1085	*s*
1418	*s*	1074	*vs*	1058	*m*	1131	*vw*
1466	*s*	1116	*vw*	1093	*s*	1147	*s*
1531	*s*	1126	*vw*	1111	*m*	1210	*m*
		1143	*w*	1147	*vw*	1318	*w*
		1220	*m*	1163	*s*	1341	*s*
		1265	*w*	1178	*vw*	1389	*vs*
		1290	*w*	1318	*vw*	1415	*s*
		1354	*m*	1401	*vs*	1442	*w*
		1384	*s*	1415	*vs*		
		1418	*s*	1468	*s*		
		1428	*s*				
		1464	*s*				
		1532	*m*				

vs Very strong. *s* Strong. *m* Medium. *w* Weak. *vw* Very weak.

TABLE V. Infra-red spectrum of pyrrole: comparison with earlier work.

C. (1905)[a] cm^{-1}	*I*	M.-A. and R. (1938)[b] cm^{-1}	*I*	L. M. (1942) cm^{-1}	*I*
		647	*m*		
—		728	*vs*		
—		—		768	*s*
781	*vw*	—		—	
—		826	*w*	—	
—		—		839	*w*
—		—		844	*vw*
873	*s*	864	*w*	869	*m*
—		—		884	*w*
972	*vw*	—		—	
1005	*vs*	—		1015	*vs*
—		1026	*s*	—	
1052	*w*	—		1047	*vs*
1075	*vs*	1069	*s*	1076	*vs*
1130	*s*	1149	*w*	1146	*s*
1202	*w*	—		—	
1273	*w*	—		—	
—		—		1289	*m*
—		—		1384	*m*
1418	*vs*	1418	*vs*	1418	*s*
—				1466	*s*
1540	*vs*			1531	*s*
1600	*vw*			—	
1710	*m*			—	
2100	*w*				
2260	*w*				
2530	*s*				
2800	*vw*				
3100	*vw*				
3390	*vs*				

vs Very strong. *s* Strong. *m* Medium. *w* Weak. *vw* Very weak.
[a] Reference 1. [b] Reference 2.

minima varies from about 5 cm^{-1} in the 1600-cm^{-1} region to 2 cm^{-1} in the 800-cm^{-1} region. The upper limit of 1900 cm^{-1} to the spectral range studied was dictated by considerations of time. The only fundamental frequencies beyond this region are the "hydrogen" stretching frequencies, which are Raman active, and concerning whose interpretation there is no serious question.

EXPERIMENTAL RESULTS

Raman Spectra

The results of the Raman studies on the four pyrroles are given in Table I. The intensities listed there have been visually estimated on an arbitrary scale of 10. Those lines which seemed to be polarized, judging from their sharp appearance on the plates, are labelled *p*.[14] In

[14] This method of estimating polarization is not entirely trustworthy, as has been pointed out by J. R. Nielsen and N. E. Ward (J. Chem. Phys. **10**, 87 (1942)). Our assignments contravene our estimates of depolarization in 5 instances.

TABLE VI. Selection rules for pyrrole: C_{2v} symmetry.

Class	Essential symmetry elements $C_2^{(z)}$	$\sigma_v^{(y)}$	T and R	Ring	Normal vibrations Hydrogen Stretching	Hydrogen Bending	Total	Selection rules Ram.	I. R.
A_1	+	+	T_z	4	3	2	9	$+p$	+
B_1	−	+	T_x, R_y	3	2	3	8	$+dp$	+
A_2	+	−	R_z	1	0	2	3	$+dp$	−
B_2	−	−	$T_y R_x$	1	0	3	4	$+dp$	+

TABLE VII. Selection rules for D_{5h} symmetry.*

Class	Essential symmetry elements $C_5^{(y)}$	$C_2^{(z)}$	$\sigma_h^{(y)}$	T and R	Normal vibrations C	H	Total	Selection rules Ram.	I. R.	Vibrations become in C_{2v} Class	No.
A'_1	+	+	+		1	1	2	+	−	A_1	2
A'_2	+	−	+	R_y	0	1	1	−	−	B_1	1
A''_1	+	+	−		0	0	0	−	−	A_2	0
A''_2	+	−	−	T_y	0	1	1	−	+	B_2	1
E'_1	$\epsilon^{\pm}$	±	+	T_{xz}	1	2	3	−	+	A_1	7
E'_2	$\epsilon^{\pm 2}$	±	+		2	2	4	+	−	B_1	7
E''_1	$\epsilon^{\pm}$	±	−	R_{xz}	0	1	1	+	−	A_2	3
E''_2	$\epsilon^{\pm 2}$	±	−		1	1	2	−	−	B_2	3

* For the derivation of this table see, e.g., Tisza, Zeits. f. Physik **82**, 48 (1933), or Rosenthal and Murphy, Rev. Mod. Phys. **8**, 317 (1936).

TABLE VIII. Moments of inertia for the pyrroles: C_{2v} symmetry. ($\times 10^{-40}$ g cm^2).

	Pyrrole	Pyrrole-*N*-*d*	*sym*-Pyrrole-d_4	Pyrrole-d_5
I_x	89	97	102	109
I_y	186	194	221	228
I_z	97	97	119	119

Table II our results for pyrrole are compared with those of previous investigators. It will be seen that there is general agreement except for a number of weak frequencies reported by Stern and Thalmayer. There seems to be some question as to the purity of the sample used by these investigators, however,[7,9] and we feel that this is a fair way of explaining these weak lines. Owing to the high resolving power of our instrument, two lines (866 and 3108 cm^{-1}) have each been resolved into two components in our spectra. Inasmuch as our work agrees generally with earlier results, we feel that our frequencies for pyrrole represent fairly its Raman spectrum. In Table II we have also included the results of Reitz' depolarization measurement.[8]

Two previous studies have been made of pyrrole-*N*-*d*.[10,11] These results are compared with ours in Table III. The agreement is reasonably satisfactory. Bonino and Manzoni-Ansidei report finding more lines than were found by either Redlich and Stricks or by ourselves. Frequencies which they alone report are 572, 652, 1046, 1104, 1414, 2788, 3023, and 3051 cm^{-1}. We shall see later that two of these, 1046 and 1414, are unquestionably fundamental frequencies in pyrrole-*N*-*d*; we have found them in the infra-red. Bonino and Manzoni-Ansidei themselves suggest that 2788 and 3051 cm^{-1} may be caused by weak lines of their Hg arcs. This is supported by the facts that these same frequencies appear in their spectrum of pyrrole, and that we do not find them on our plates. 3023 is presumably an overtone or combination tone. 1104 is reported as exceedingly weak; we find no trace of it. This leaves 572 and 652 to be explained. It is to be noted that both of these frequencies appear in the Raman spectrum of pyrrole reported by Bonino and Manzoni-Ansidei. 572, however, is of low intensity in pyrrole, and it is surprising that Bonino and Manzoni-Ansidei should have observed it in pyrrole-*N*-*d* if it really is caused by isotopic impurity. On the other hand, this is the N−H out-of-plane bending frequency in pyrrole (Table XI); hence it is a frequency which should be very sensitive to any N−H impurity in a sample of pyrrole-*N*-*d*. The 652 frequency is somewhat stronger in pyrrole, and can probably show up weakly in the Raman spectrum of pyrrole-*N*-*d* contaminated with ordinary pyrrole.

TABLE IX. Frequency product ratios (τ's): C_{2v} symmetry.

Class		$\frac{\text{Pyrrole}}{\text{Pyrrole-}d_5}$	$\frac{\text{Pyrrole}}{\text{Pyrrole-}d_4}$	$\frac{\text{Pyrrole}}{\text{Pyrrole-}N\text{-}d}$	$\frac{\text{Pyrrole-}N\text{-}d}{\text{Pyrrole-}d_5}$	$\frac{\text{Pyrrole-}N\text{-}d}{\text{Pyrrole-}d_4}$	$\frac{\text{Pyrrole-}d_4}{\text{Pyrrole-}d_5}$
A_1	Calc.	5.46	3.89	1.40	3.89	2.77	1.40
	Obs.	5.21	3.75	1.37	3.81	2.74	1.39
B_1	Calc.	4.93	3.56	1.38	3.58	2.59	1.38
	Obs.	4.60	3.36	1.35	3.41	2.49	1.37
A_2	Calc.	1.80	1.80	1.00	1.80	1.80	1.00
	Obs.	1.80	1.80	1.00	1.80	1.80	1.00
B_2	Calc.	2.43	1.82	1.35	1.83	1.35	1.36
	Obs.	—	—	1.29	—	—	—

TABLE X. Infra-red and Raman spectra of the four pyrroles.

Pyrrole				Pyrrole-*N*-*d*				*sym*-pyrrole-d_4				Pyrrole-d_5			
Raman		Infra-red		Raman		Infra-red		Raman		Infra-red		Raman		Infra-red	
cm^{-1}	*I*	cm^{-1}	*I*	cm^{-1}	*I*	cm^{-1}	*I*	cm^{-1}	*I*	cm^{-1}	*I*	cm^{-1}	*I*	cm^{-1}	*I*
565	0*b*			450	0*b*			514	1			450	1*b*		
(618)	0			606	3			560	6*b*			516	1		
647	3			708	3			692	4			565	4		
711	3			—		766	*s*	730	2			693	3		
—		768	*s*	(780)	0	783	*vw*	769	1	—		728	2		
837	2	839	*w*	—		786	*vw*	—		793	*s*	766	1	—	
—		844	*vw*	—		808	*m*	—		812	*s*	—		789	*vs*
866	1	869	*m*	831	3	835	*s*	—		830	*w*	808	1	—	
880	½	884	*w*	869	2	870	*m*	848	4	849	*vs*	—		813	*vs*
1015	½	1015	*vs*	911	2	905	*m*	—		872	*vs*	—		852	*s*
1045	1	1047	*vs*			915	*s*	—		899	*m*	892	5	893	*s*
1076	3	1076	*vs*	1010	1	1015	*vs*	—		910	*w*	909	5	910	*s*
1144	10	1146	*s*	—		1026	*w*	917	4	920	*s*	—		943	*w*
1237	½	—		—		1048	*vs*	—		931	*m*	—		961	*m*
—		1289	*m*	1074	5	1074	*vs*	953	1	956	*s*	—		1025	*s*
1379	9*b*	1384	*m*	—		1116	*vw*	—		1027	*m*	—		1039	*vw*
—		1418	*s*	—		1126	*vw*	—		1058	*m*	—		1058	*w*
1468	5	1466	*s*	1135	10	—		1094	10	1093	*s*	1084	10	1085	*s*
(1484)	0	—		—		1143	*w*	—		1111	*m*	—		1131	*vw*
1528	½	1531	*s*	1210	0	—		—		1147	*vw*	1145	3*b*	1147	*s*
				—		1220	*m*	—		1163	*s*	(1211)	0	1210	*m*
				1237	½	—		—		1178	*vw*	1317	5	1318	*w*
				—		1265	*w*	1319	7	1318	*vw*	—		1341	*s*
				—		1290	*w*	1401	9	1401	*vs*	1389	8	1389	*vs*
				1350	3*b*	1354	*m*	—		1415	*vs*	(1413)	½	1415	*s*
				1384	9	1384	*s*	1463	1	1468	*s*	—		1442	*w*
				—		1418	*s*					1455	½	—	
				—		1428	*s*								
				1465	6	1464	*s*								
				—		1532	*m*								
3100	4			2525	5*b*			2309	7			2309	8		
3111	4			(2709)	0			2358	7			2350	6		
												2368	6		
3133	9			3104	8			3410	3*b*			2535	6*b*		
3400	4*b*			3131	10							2679	½		

( ) Observed on only one plate, but believed real.

Redlich and Stricks report a line at 1147 cm^{-1}; this is probably the corresponding strong line of pyrrole. We also found no trace of the frequencies reported by them at 291 and 537 cm^{-1}. These same authors seem to have made an error, perhaps typographical, in the N − D stretching frequency. They report it at 2357 cm^{-1}, whereas it actually occurs in the neighborhood of 2530 cm^{-1}. Apart from these exceptions, there is general agreement between the three spectra.

The assignment of lines to the proper exciting frequencies in *sym*-pyrrole-d_4 was straightforward and offered no problem. In pyrrole-d_5, the 808-cm^{-1} Raman frequency excited by Hg 4358A coincides with the 909 frequency excited by Hg 4339A. The intensity of this line, however, which is greater than that of the 909 Raman line caused by Hg 4348A, leaves no doubt that 808 cm^{-1} is real. The 1413 frequency, although measured on only one plate, can be seen on several others.

It occurs as a wing on the edge of the strong 1389-cm^{-1} band, and any overexposure tends to merge the two.

Infra-Red Spectra

The infra-red transmission curves for the four pyrroles are shown in Figs. 1–4. The frequencies of the transmission minima have been tabulated in Table IV with a qualitative estimate of their intensities.

The infra-red absorption spectrum of pyrrole has been obtained previously by Coblentz[1] and by Manzoni-Ansidei and Rolla.[2] Both of these studies were made on the liquid, although Manzoni-Ansidei and Rolla do not explicitly say so. The latter authors give no cell sizes, but since they compare their work with that of Coblentz without comment on the state of aggregation, we must presume that their studies, like his and like ours, were made on the liquid. These results are compared in Table V. The general agreement of the spectra in regions where they overlap is not bad. Most noteworthy are the facts that the 1015–1047 cm^{-1} doublet is reported as unresolved by Manzoni-Ansidei and Rolla at 1026 cm^{-1}, and that the strong frequency found by us at 768 cm^{-1} must be considered as unreported by Manzoni-Ansidei and Rolla or else identified with the very strong absorption reported by them at 728 cm^{-1}. The infra-red spectra of the other three pyrroles have not been obtained previously.

DISCUSSION OF RESULTS

As a working hypothesis we will assume that the pyrrole molecule has C_{2v} symmetry. This is in accordance with chemical evidence for the structure of pyrrole, and with the results of the electron diffraction studies.[15] The allocation of the 24 vibrational degrees of freedom to the various C_{2v} symmetry classes, and the selection rules for these classes, are shown in Table VI. The 2-fold axis through the nitrogen atom is picked as the z axis. The y axis is chosen perpendicular to the plane of the molecule and intersecting the z axis at the center of gravity. The x axis is then picked perpendicular to the y and z axes and passing through their intersection. It will later prove convenient to have also the allocation of frequencies for a planar 10-atom molecule of D_{5h} symmetry. This is given in Table VII.

The usefulness of the spectra of deuterium derivatives for purposes of vibrational analysis is greatly enhanced by application of the Teller product rule. This rule has been discussed in detail elsewhere.[16] By its use one can calculate, independently of spectroscopic observation, the ratio (denoted by τ) between the product of a certain set of frequencies in one isotopic form of a molecule, and the product of the same set in another isotopic form. By a "set" one means a collection of frequencies whose modes of vibration have a common symmetry. If the two isotopic forms under consideration belong to the same symmetry group (as will be true in our case), the sets to which the product rule is applicable are simply the symmetry classes of that group. In order to calculate these theoretical τ's, a knowledge of the moments of inertia of the several pyrroles is essential. These moments have been calculated from the geometrical data given by Schomaker and Pauling,[15] with the additional assumptions that the C–H distance is 1.09A, the N–H distance 1.02A, and that the C–H bond line bisects the ring angle when extended into the ring. The moments are given in Table VIII. The theoretical τ's for the various symmetry classes and for the various pairs of deuterium derivatives are given in Table IX.

We now proceed to the assignment of the various frequencies to their symmetry classes. For convenience in discussing the spectroscopic data, the infra-red and Raman results are brought together in Table X. Table V will summarize our assignments, and will be of aid in tracing a given frequency through the four pyrroles.

1. Class A_1

The C_{2v} model requires nine totally symmetrical vibrations. Of these, two are C–H stretching frequencies and one the N–H stretching frequency, which we can assign without

[15] V. Schomaker and L. Pauling, J. Am. Chem. Soc. **61**, 1776 (1939). This work, of course, leaves open the question of the positions of the hydrogen atoms.

[16] Angus, Bailey, Hale, Ingold, Leckie, Raisin, Thompson, and Wilson state the product rule without proof (J. Chem. Soc., p. 978 (1936)). It was first published with proof by O. Redlich, who found it independently (Zeits. f. physik. Chemie **B28**, 371 (1935)).

TABLE XI. Frequency assignments: C_{2v} symmetry.

Class	No.	Pyrrole	Pyrrole-*N*-*d*	*sym*-pyrrole-d_4	Pyrrole-d_5
A_1	1	711	708	692	693
	2	1076	1074	812	813
	3	1144	1135	1094	1084
	4	1237	1237	919	909
	5	1384*	1384	1319	1317
	6	1467	1465	1401	1389
	7	3100	3104	2309	2309
	8	3133	3131	2358	2350
	9	3400	2525	3410	2535
B_1	10	647	606	560	565
	11	1015	1012	793	789
	12	1046	1048	848	808
	13	(1146)	915	1163	892
	14	1418	1418	1415	1415
	15	1530	1532	1465	1455
	16	3111	(3104)	(2309)	(2309)
	17	(3133)	(3131)	(2358)	2368
A_2	18	[510]	[510]	[440]	[440]
	19	(711)	(708)	514	516
	20	868	869	769	766
B_2	21	565	450	(560)	450
	22	768	766	[610]	[590]
	23	838	833	730	728
	24	(1046)	1026	872	852

( ) Used twice.
[ ] Calculated with the help of the product rule.
* The infra-red frequency value. The Raman band is diffuse.

hesitation to the 3100 and the 3400 cm^{-1} regions, respectively. The shifts in the deuterium derivatives are completely in accordance with this assignment.[17] We are then left with six vibrations to be located in the region below 2000 cm^{-1}. Reitz has found five polarized lines in this region (Table II), and these five lines can be assigned bodily to the A_1 class. The sixth frequency then remains to be located. One would expect to find this well below 1000 cm^{-1}, since there must be one totally symmetric ring bending vibration, and since none of the five polarized lines lies below 1000 cm^{-1}. As a matter of fact, analogy with other ring compounds whose spectra have been analyzed leads one to expect this frequency at about 600–700 cm^{-1}. We select for it the frequency 711 cm^{-1}. 711 is found to be completely depolarized, as are all the other lines in this region, but this may be caused by the fact that the 711 line is a composite of a strong non-totally symmetrical frequency and a considerably less intense symmetrical frequency. This interpretation is borne out by the broad nature of the 711 line and by the frequency changes in *sym*-pyrrole-d_4 and pyrrole-d_5. A sharp line appears in both of these compounds at 692 cm^{-1} which can scarcely have any other analogue in pyrrole than 711 cm^{-1}. The interpretation is further substantiated by the Raman spectrum of furan,[8] in which there appears only one polarized line of frequency less than 1000 cm^{-1}. This line, whose depolarization factor has the rather large value 0.63, occurs at 724, a value sufficiently close to 711 to enable us to call the two lines analogous. The other constituent of the 711 line of pyrrole will be discussed under the A_2 symmetry class.

All six of the low A_1 frequencies can be traced unambiguously through the four deuterium derivatives. The agreement of the observed product rule τ's with the calculated τ's (Table IX) is quite satisfactory in view of the usual small deviations that are expected because of anharmonicity.

The intensity changes produced by deuterium substitution are very marked, and the spectra would be exceedingly difficult to analyze without having both the Raman and infra-red data. The A_1 class is no exception to this. A case in point is the 1076 frequency. This appears with great intensity in both the Raman and infra-red spectra of pyrrole and pyrrole-*N*-*d*. The analogous frequency in *sym*-pyrrole-d_4 and pyrrole-d_5, 812 cm^{-1}, is, however, completely missing in the Raman effect. It is true that there is a frequency in the Raman spectrum of pyrrole-d_5 at 808 cm^{-1}, but this is better ascribed to a B_1 vibration. Another case is the totally symmetric "breathing" frequency (1145 cm^{-1} in pyrrole), which undergoes very marked intensity changes in the infra-red. Inasmuch as there is no trouble whatever in tracing this very intense and highly polarized line in the Raman effect, we know exactly where to look for it in the infra-red. A rather broad band of marked intensity is indeed observed in the infra-red spectrum of pyrrole. We prefer, however, not to identify this band with the totally symmetric "breathing" frequency. In the first place, the analogous band is *completely* missing from the infra-red spectrum of pyrrole-*N*-*d*. Secondly, it should be noticed

[17] It may be worth mentioning that the N–H frequencies appear as very broad bands in the Raman spectra. This can doubtless be attributed to hydrogen bonding.

that for a molecule of D_{5h} symmetry, this vibration is forbidden to appear in the infra-red (Table VII). Therefore one would expect that in a C_{2v} molecule which does not deviate too much from one of D_{5h} symmetry, the frequency will appear only weakly in the infra-red. We have, moreover, a satisfactory alternative assignment for this band in pyrrole which will be discussed later. The weak A_1 frequency at 1237 cm^{-1} is missing from the infra-red spectra of pyrrole and pyrrole-*N*-*d*, but the analogous frequencies in the other two compounds (919 and 909 cm^{-1}) are strong in both the Raman effect and the infra-red. The quantitative frequency changes, however, leave little doubt that these frequencies are to be assigned to the same modes of vibration. The remaining totally symmetrical frequencies occur with more or less regular intensity changes.

2. Class B_1

The location of the B_1 frequencies can be facilitated if one notes that all but one of the B_1 frequencies of the C_{2v} molecule are derived from the E_1' and E_2' frequencies of the D_{5h} molecule by the release of the double degeneracy of the latter (Table VII). Those $E'_{1,2}$ frequencies which do not become B_1 frequencies go into class A_1 upon the release of the degeneracy. In consequence we might expect that the A_1 frequencies should to a certain extent be paired up with the B_1 frequencies, except for those two A_1 vibrations which correspond to the totally symmetrical vibrations of the D_{5h} molecule and for the single B_1 vibration which corresponds to the A'_2 vibration of D_{5h}. The latter is essentially one of hydrogen bending. All the B_1 ring frequencies should thus occur in the neighborhood of their A_1 counterparts. These A_1 frequencies are 711, 1384, and 1467 cm^{-1} in pyrrole (cf. Table XI). The frequencies nearby are 647, 1418, and 1530 cm^{-1}. These we assign to class B_1. Of the five hydrogen vibrations in class B_1, two are essentially C−H stretching, two C−H bending, and one N−H bending. The C−H stretching frequencies are to be assigned to the 3100-cm^{-1} region. By analogy with the A_1 bending frequencies, we assign the lines at 1015 and 1046 to C−H bending.

The N−H bending frequency is more difficult to locate. There are several general statements which we may make, however, before starting a methodical search for it. First, if it is as high as 1500–1600 cm^{-1}, it should shift to 1100–1200 cm^{-1} in the N−D substituted compounds. We then expect that this frequency will never interact with the C−H or C−D bending frequencies except in pyrrole-*N*-*d*, for in both *sym*-pyrrole-d_4 and pyrrole-d_5 the C−D bending frequencies are much too low. If on the other hand the N−H frequency is considerably lower, we might expect to find marked evidence of interaction with C−H bending vibrations in pyrrole, and with C−D bending vibrations in pyrrole-d_5. We observe the following facts: (a) There are no Raman nor infra-red frequencies in the 1500–1600-cm^{-1} region whose frequency changes upon deuterium substitution are compatible with the mass change of two. (b) The difference in the 800–1000-cm^{-1} region between the spectra of pyrrole and pyrrole-*N*-*d*, and between *sym*-pyrrole-d_4 and pyrrole-d_5 is marked. These differences indicate strongly that some interaction is occurring. At first one might ascribe this interaction to members of the B_2 class, but we will show later that the N−H frequency in B_2 lies entirely outside of this region at 565 cm^{-1}. Since the B_1 class is the only other class containing an N−H bending frequency, we are virtually compelled to locate the N−D frequency in the 800–1000-cm^{-1} region. This puts the N−H frequency at about 1000–1200 cm^{-1}. A search of the infra-red and Raman spectra in this region reveals only one significant change on passing from pyrrole to pyrrole-*N*-*d*. This is the absence, referred to earlier, of the 1146-cm^{-1} band in the infra-red spectrum of pyrrole-*N*-*d*. We therefore ascribe the 1146-cm^{-1} band in pyrrole to the N−H bending. The shift in the N−H frequency upon deuterium substitution should put it in the neighborhood of 850–900 cm^{-1}. Actually there is observed a new Raman frequency and a new infra-red band in pyrrole-*N*-*d* at 915 cm^{-1}. The unexpected appearance of a frequency in this neighborhood can scarcely be understood on any other basis. This assignment is substantiated by the spectra of pyrrole-d_4 and pyrrole-d_5. In the latter compounds the N−H and N−D frequencies occur, respectively, at 1163 and 892 cm^{-1}.

As can be seen from Table IX, the product rule is reasonably well satisfied by these assignments. Corroboration of the assignments is also indicated by the remarkable frequency and intensity changes which occur in the 800–900 cm^{-1} region in going from *sym*-pyrrole-d_4 to pyrrole-d_5. The 848 Raman line in the former compound changes markedly in frequency and intensity, dropping to 808 cm^{-1} in pyrrole-d_5 and becoming much less intense. The change can be readily understood if we attribute it to interaction between this C−D and the N−D bending frequencies. Such an interaction will cause the two frequencies to separate and their Raman intensities to mix. We thus can understand the remarkable drop from 848 to 808, the accompanying loss of intensity, and the great increase in the intensity of the N−D frequency at 892 cm^{-1} in the Raman effect. The only remaining comment on the B_1 frequencies is to remark the surprising constancy of the 1418 cm^{-1} ring vibration. The fact that this frequency shifts by only a few wave numbers in going from pyrrole to pyrrole-d_5 is presumably to be ascribed to the lack of appreciable participation of the hydrogen atoms in the mode of vibration.

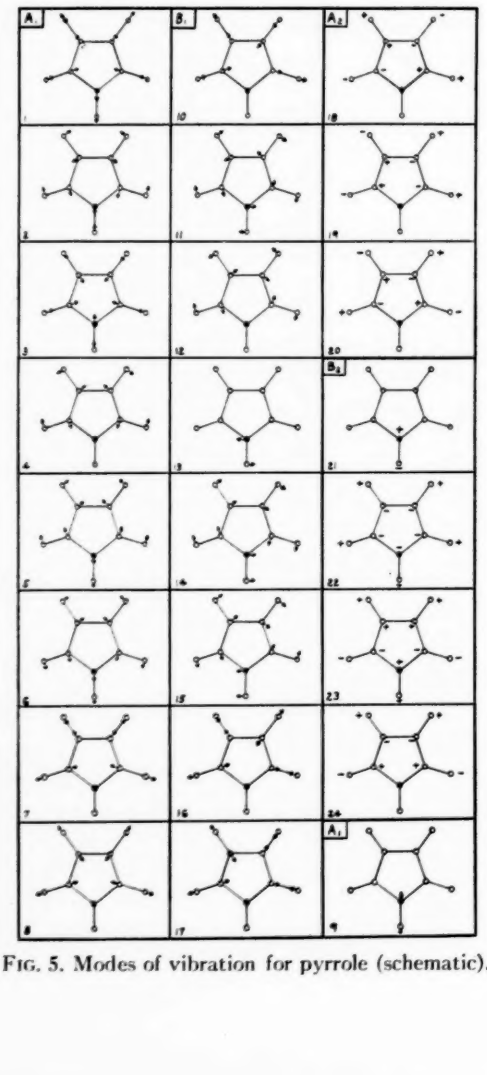

FIG. 5. Modes of vibration for pyrrole (schematic).

3. Class A_2

It should in principle be easy to locate the A_2 frequencies, for these should show no change in going from pyrrole to pyrrole-*N*-*d*, and from *sym*-pyrrole-d_4 to pyrrole-d_5. Moreover, they should be missing from the infra-red spectra. Unfortunately the infra-red measurements do not extend to sufficiently low frequencies to cover the region of all the A_2 vibrations. In addition we may note that in the case of benzene analogous frequencies appear with some intensity in the infra-red spectrum of the liquid, although they are missing in the spectrum of the vapor.[18] Analogy with benzene leads us to assign the 711 Raman line to the A_2 class. This frequency shifts by the proper amount to 515 cm^{-1} in pyrrole-d_4 and pyrrole-d_5. Another Raman line satisfying the A_2 criterion is 868 in pyrrole. This leaves one additional A_2 frequency, which we suppose is not Raman active. This is not surprising, inasmuch as ring distortion vibrations of this type are generally weak in the Raman effect. It is possible that the numerical value of this frequency will not be far from the analogous frequency in furan. An extremely weak Raman line is observed in the latter molecule at 500 cm^{-1}.[6,8] If we assume that an A_2 frequency lies at 510 cm^{-1} in pyrrole, we can explain several overtones and combination tones which are otherwise hard to understand. This should shift to the neighborhood of 450 cm^{-1} in *sym*-pyrrole-d_4 and pyrrole-d_5. One combination tone in the spectrum of the former can be explained by the assumption of a fundamental at 440 cm^{-1}. These values fit the product rule for class A_2.

4. Class B_2

Of the B_2 frequencies, the easiest one to assign is the N−H out-of-plane bending vibra-

[18] Bailey, Hale, Ingold, and Thompson, J. Chem. Soc., p. 931 (1936).

TABLE XII. Left-over frequencies and suggested assignments.

Pyrrole			Pyrrole-*N*-*d*			*sym*-pyrrole-d_4			Pyrrole-d_5		
Cm^{-1} Obs.	Cm^{-1} Calc.	Assignment	Cm^{-1} Obs.	Cm^{-1} Calc.	Assignment	Cm^{-1} Obs.	Cm^{-1} Calc.	Assignment	Cm^{-1} Obs.	Cm^{-1} Calc.	Assignment
618	616	$\nu_5-\nu_{22}$	783	778	$\nu_5-\nu_{10}$	830	—	—	943	939	$\nu_6-\nu_{21}$
844	*		786	787	$\nu_4-\nu_{21}$	899	901	$\nu_{14}-\nu_{19}$	961	966	$\nu_{19}+\nu_{21}$
882	883	$\nu_{15}-\nu_{10}$	808	812	$\nu_{14}-\nu_{10}$		905	$\nu_{15}-\nu_{10}$	1025	1032	$2\nu_{19}$
1289	1294	$2\nu_{10}$	905	900	$2\nu_{21}$	910	—	N-D impurity	1039	—	—
1484	1485	$\nu_{10}+\nu_{23}$	1116	1116	$\nu_{10}+\nu_{18}$	931	—	—	1058	—	—
			1126	*		955	954	$\nu_{18}+\nu_{19}$	1131	1130	$2\nu_{10}$
			1143	—	N-H impurity	1027	1028	$2\nu_{19}$		1130	$2\nu_{10}$
			1210	1212	$2\nu_{10}$	1058	—	—	1147(*b*)	1143	$\nu_1+\nu_{21}$
			1220	1218	$\nu_{18}+\nu_{19}$	1111	1120	$2\nu_{10}$		1180	$2\nu_{22}$
			1265	1276	$\nu_{18}+\nu_{22}$	1147	—	—			
			1290	1283	$\nu_{21}+\nu_{23}$	1178	—	—	1210	1216	$\nu_{20}+\nu_{21}$
			1354	1350	$3\nu_{21}$					1209	$\nu_1+\nu_{19}$
				1365	$\nu_{13}+\nu_{21}$				1341	1350	$3\nu_{21}$
			1428	1425	$\nu_{13}+\nu_{18}$				1442	—	—
			2709	2702	$\nu_4+\nu_6$				2679	—	—

* Cannot be explained as binary combination tone.

tion. This frequency occurs as a fuzzy line at 565 cm^{-1} in the N−H compounds and at 450 cm^{-1} in the N−D compounds. The large shift marks it immediately.[19] It is perhaps rather surprising that a hydrogen frequency should be so low. This low value is doubtless associated with the flatness of the potential curve for the bending. In the ammonia molecule the potential curve for the symmetrical bending vibration has two minima separated by a low maximum. In pyrrole, resonance between electronic structures involving a neutral and a positively charged nitrogen atom may wash out this maximum, leaving a flattened potential curve with a single minimum at the point where the N−H bond lies in the ring plane.

Of the remaining B_2 frequencies, one should be strongly active in the infra-red, namely, the one associated with the anti-translational mode of vibration (ν_{22}, Fig. 5). Our curves show a strong absorption at 768 cm^{-1}, which is a reasonable place for this vibration to appear. We find no evidence of a 768 frequency in the Raman effect, which is compatible with the fact that the corresponding D_{5h} frequency (A''_2) is forbidden. Unfortunately we cannot observe this frequency in the infra-red spectra of *sym*-pyrrole-d_4 and pyrrole-d_5 as it lies below 750 cm^{-1}. One of the two remaining B_2 frequencies may be assigned to the line at 838 cm^{-1}. A reasonable shift to 730 cm^{-1} is observed for this in the heavier compounds. The other B_2 frequency has been tentatively located by the difficulty of otherwise assigning a band shoulder at 1026 cm^{-1} in pyrrole-*N*-*d*. We have not been able to get a satisfactory explanation of this frequency as a combination tone, and we tentatively assign it to B_2. A reasonable shift for this frequency in the deuterium derivatives would place it at about 850 cm^{-1} and indeed two very similar bands, one at 872 cm^{-1} in pyrrole-d_4 and the other at 852 in pyrrole-d_5, have been found. By means of the product rule we can place this frequency at about 1045 cm^{-1} in pyrrole, where it coincides with a B_1 frequency. By the same procedure we can calculate a value of 610 and of 590 cm^{-1} for the unobserved ν_{22} frequency in pyrrole-d_4 and pyrrole-d_5.

A summary of the foregoing assignments is given in Table XI. In Fig. 5 we have represented schematically the modes of vibration for the C_{2v} model of pyrrole. These are determined to some extent by symmetry and by the orthogonality relationships.[20] In addition, the assumption of a valence-force potential system for pyrrole enables one to make a rough guess at the form of the vibrations. It is to be emphasized that the modes pictured in Fig. 5 are simply approximations which can be helpful when one is estimating frequency shifts, spectroscopic intensities, and the like.

[19] In pyrrole-d_4 the 560-cm^{-1} N−H frequency overlies the 565-cm^{-1} B_1 frequency. This is clearly indicated by the fuzziness of the line; in pyrrole-d_5, the B_1 frequency at 565 cm^{-1} is sharp.

[20] E. Teller, *Hand- und Jahrbuch der chemischen Physik* **9** (2), pp. 95 ff.

5. Left-Over Frequencies

Now that we have completed our analysis of the fundamental frequencies, we are in a position to consider the assignment of overtones and combination tones. Owing to the fact that the infra-red spectra have been run on the liquid, and that the selection rules for overtones restrict one very little, it is not surprising that a number of weak overtones and combination tones are obtained in the infra-red spectra. The assignment of these, with few exceptions, can be made without difficulty, but under the circumstances the assignment is of no great significance. The frequencies and our suggested assignments are tabulated in Table XII.

The two left-over frequencies which most urgently require explanation are the strong infra-red bands at 1354 cm^{-1} in pyrrole-*N*-*d* and 1341 cm^{-1} in pyrrole-d_5. Any attempt to explain these as N−D fundamentals is ruled out by the complete lack of any frequencies in the 1800-cm^{-1} region in pyrrole and pyrrole-d_4. We suggest that they be assigned to $3\nu_{21}$. The corresponding overtone at $2\nu_{21}$ is observed in pyrrole-*N*-*d*, although it is obscured in pyrrole-d_5 by the broad, intense doublet 893–910. 1354 also appears in the Raman effect for pyrrole-*N*-*d*. This can hardly be explained as $3\nu_{21}$, but it will be noticed that it might well be the combination tone $\nu_{13}+\nu_{21}$.[21] The broad nature of the Raman band is doubtless due to the fact that two N−H vibrations are involved. A corresponding band might then be expected in the Raman spectrum of pyrrole-d_5, but actually none is found. ν_{13} in pyrrole-d_5 is interacting strongly with the C−D bending vibrations, and this interaction may lead to a large change in the combination tone's influence on the molecular polarizability.

The only other unassigned frequency of marked intensity is one which occurs in both the infra-red and Raman spectra of pyrrole-d_5 at 1147 cm^{-1}. The Raman band is very broad, whereas the infra-red band is quite sharp. This difference leads us to believe that the two should be given different interpretations. A credible interpretation of the Raman frequency would be its assignment to the first overtone of either ν_{22} or ν_{10}. These overtones have total symmetry and could pick up intensity from the nearby totally symmetrical line at 1084 cm^{-1}. The exactly analogous overtone is observed in the Raman spectrum of benzene-d_6. The chief objection to this interpretation is the already mentioned breadth of the Raman band. This breadth might at first be thought to be associated with some N−D vibration, but it is difficult to understand the intensity of this band if it is an overtone or a combination tone without ascribing it to resonance interaction with a nearby fundamental. The only nearby fundamental is the 1084 vibration of class A_1. No combination tone of total symmetry involving an N−D vibration lies in this neighborhood, and therefore this line probably cannot be ascribed to a combination tone involving an N−D degree of freedom. It seems to us more plausible to suppose that the breadth is due to the presence of several overtones in this neighborhood. At least two of these are totally symmetrical, namely $2\nu_{22}$ and $2\nu_{10}$. Moreover, the combination tone $\nu_1+\nu_{21}$, which involves the broad out-of-plane N−D vibration, should also fall hereabouts. Perhaps the net result of these coincidences is their apparent fusion into one broad band. This interpretation is substantiated to some extent by the appearance of a shoulder on the low frequency side of the 1147-cm^{-1} infra-red band in pyrrole-d_5. Confirmation from the infra-red spectrum of pyrrole-d_4 is difficult because of the presence of the N−H planar bending frequency at 1163 cm^{-1}. There is some sign, however, of a diffuse companion on the high frequency side of the 1094 Raman line in pyrrole-d_4. The sharp character of the 1147 band in the infra-red spectrum enables us to make a more definite assertion about its origin. It may very well arise solely from the overtone $2\nu_{22}$. In this case our estimate of ν_{22} in *sym*-pyrrole-d_4 and pyrrole-d_5 from the product rule calculation will have to be revised downward by 15 cm^{-1}. Clearly experimental determination of this fundamental in the infra-red is most desirable.

The interpretation of the remaining frequencies requires no especial discussion except to remark that assignment of all the left-over frequencies in pyrrole-d_4 and pyrrole-d_5 is hardly feasible until experimental values are obtained for ν_{18} and ν_{22}.

[21] This combination has A_2 symmetry, so that it cannot be used to explain the infra-red band.

CONCLUSIONS

From the foregoing discussion it is clear that a postulated symmetry of C_{2v} is quite adequate to explain the spectroscopic results. In particular, the agreement of the frequencies assigned to the A_1 and B_1 classes with the product rule τ's for these classes is quite satisfactory. Many of the intensity changes attendant upon deuterium substitution are likewise understandable. The question now remains: Will any other symmetry serve equally well to interpret the spectra? Symmetries higher than C_{2v} can be eliminated immediately on the grounds that they are not compatible with chemical evidence and with electron diffraction results. Furthermore, as Reitz[8] has already pointed out, too many polarized Raman lines are found to allow postulation of a higher symmetry.

There are two possible lower symmetries, C_1 and C_s. C_1 can be excluded, for it demands that all the Raman lines be polarized and this is obviously not the case. To obtain the product rule ratios (τ's) for C_s symmetry, one merely multiplies together the τ's for C_{2v} symmetry in the following manner:

$\tau : C_s$	$\tau : C_{2v}$
A'	$A_1 \times B_2$
A''	$B_1 \times A_2$

It is obvious that if the product rule is obeyed for all classes of a C_{2v} symmetry, it will also be obeyed for a C_s symmetry. The converse, however, is not necessarily true. In fact, it seems to us that it would be an improbable accident for the frequencies of a C_s molecule to fit the product rule for each of the four classes of a C_{2v} structure. The A' frequencies, for example, of a C_s structure are all mechanically interconnected. When one imputes to a C_s molecule a C_{2v} symmetry, one asserts in effect that the A' frequencies can be split into two groups (classes A_1 and B_2 of C_{2v}) which are mechanically independent. Unless the special nature of the C_s molecular potential system is such that this assertion is valid, it is impossible for the frequency changes caused by deuterium substitution to satisfy a product rule for C_{2v} symmetry. Hence, although a C_s symmetry cannot be rigorously excluded on these grounds, it is made most unlikely. This conclusion is given strong support by the number of polarized Raman lines;[8] thirteen are demanded for C_s symmetry while only eight are found which can be established as fundamentals (Table II). We are, therefore, convinced that pyrrole is a C_{2v} molecule.

As we have remarked earlier, the complete survey of the infra-red spectra down to 400 cm^{-1}, preferably in the vapor, will be necessary before the spectroscopic investigation can be regarded as complete. We hope to carry out such an investigation in the near future if circumstances permit.

ACKNOWLEDGMENTS

We are indebted to the Rockefeller Foundation for a grant which made this research possible. Acknowledgment is also made for a grant-in-aid from the Hynson, Westcott, and Dunning Fund. We wish to thank Dr. R. B. Barnes and the American Cyanamid Company for the use of their infra-red spectrometer. One of us (F. A. M.) also wishes to thank the Chemical Foundation for the award of a fellowship for graduate study.

Energy Relations of the Surfaces of Solids

II. Spreading Pressure as Related to the Work of Adhesion Between a Solid and a Liquid*

WILLIAM D. HARKINS AND H. K. LIVINGSTON
George Herbert Jones Laboratory, University of Chicago, and the Universal Oil Products Company, Chicago, Illinois

(Received December 19, 1941)

This is the second paper in a series which gives theoretical values for the free and total surface energy of the diamond, and experimental values for the total and free energy, the latent heat, and the entropy of adhesion between various crystalline solids and liquids. This second paper deals with the oldest part of the subject, but a part which has always been treated incorrectly. The total energy ($\epsilon_{A(SL)}$) required to separate water from solids of the general type of $BaSO_4$, TiO_2, and $ZrSiO_4$, has been found by Harkins and Boyd to vary from 600 to 1000 erg cm^{-1}, while to separate octane from these solids requires only from 150 to 250 erg cm^{-2}. The free energy of separation, designated by $W_{A(SL)}$, is smaller. It is generally believed that

$$W_{A(SL)}=\gamma_L(1+\cos\theta_{SL}), \qquad (A)$$

which gives values, for solids thus far investigated, from 47.5 to 144 erg cm^{-2} at 25°C if the liquid is water, and much smaller values if organic liquids are used. Indeed *the maximum value of the work of adhesion between water and any solid at this temperature is given by this equation as only 144 erg cm^{-2}*. That the work of adhesion should be so small a fraction of the free surface energy of the solid itself as these numbers suggest, is, in the case of solids of high melting point, entirely incredible, since even polar solids of this type must have free surface energies in excess of 1000 erg cm^{-2}. For such a solid the work of adhesion toward water would be only ten or less percent of the free surface energy of the solid. The correct equation is

$$W_{A(SL)}=f_{E(SV^\circ)}+\phi^S{}_{LV^\circ}+\gamma_L=f_{E(SL)}+\gamma_L. \qquad (24)$$

Thus the work of adhesion is the sum of three terms which may be determined experimentally: (1) The solid, initially in a vacuum, is immersed in the vapor of the liquid with a decrease of free energy equal to $f_{I(SV^\circ)}$. The reversal of this process separates the solid from the vapor, with an increase of free energy of $f_{E(SV^\circ)}$, the free energy of emersion of the solid from the vapor. Equations of this type are in general written to correspond to a separation of phases, while the experimental processes take place in the opposite direction. (2) The free energy of transfer ($\phi^S{}_{LV^\circ}$) of the solid from the interior of the liquid to the interior of the saturated vapor, without a change in any other interfacial areas than that of the solid represented by the symbol S, and that of the solid-liquid interface SL. It is shown that $\phi^S{}_{LV^\circ}=\phi_{L/S'}$, where the term on the right is the spreading pressure of the liquid L over the surface of the solid S', which is in equilibrium with the saturated vapor V° of the liquid. (3) The free surface energy of the liquid. The quantity listed in (2) above is defined by Eq. (17) as follows:

$$\phi^S{}_{LV^\circ}=\phi_{L/S'}=\gamma_{SV^\circ}-\gamma_{SL}. \qquad (17)$$

It will be designated by either of the terms given in (2) but more commonly as the *spreading pressure*. This would be identical with what was defined by Freundlich as a *Haftspannung*, usually translated as the *adhesion tension* (A), but unfortunately the adhesion tension has never been defined nor used correctly (see Section 6), since it is designated by two equations which give magnitudes which are extremely different, and one of the two equations is incorrect. The term "adhesion tension" has also carried with it the unfortunate implication that it gives, through Eq. (A), which may be written $W_{A(SL)}=A+\gamma_L$, a measure of the free energy of emersion of a solid ($f_{E(SL)}$), from which the work of adhesion may be obtained by merely adding the surface tension of the liquid. This is extremely erroneous, since the adhesion tension, if correctly defined, is equal to only the minor term $\phi_{L/S'}$ in the expression

$$f_{E(SL)}=f_{E(SV^\circ)}+\phi_{L/S'}.$$

On account of the unfortunate implication of the term itself, and because it has always been defined and used incorrectly, it is recommended that *the term "adhesion tension" should be discarded*, and the correctly defined and more suitable term (*spreading pressure*) be substituted for it. If the angle between a liquid-liquid (L_1-L_2) interface meets the surface of a solid with the angle α, the displacement pressure (D) is defined by the equation

$$D=\gamma_{L_1L_2}\cos\alpha. \qquad (35)$$

It is shown that the equations in the literature which relate the displacement pressure to the adhesion tension, are incorrect and entirely too simple. The true relation (that between D and $\phi_{L/S'}$) is much more complicated.

SYMBOLS

A	adhesion tension, or as a subscript, *adhesion*.
α	angle of contact between a solid and a liquid-liquid interface.
B	$\cos\theta$.
γ	free surface energy (erg cm^{-2}) or surface tension (dyne cm^{-1}).
D	displacement pressure, D_{WO} displacement pressure of water toward oil.
E	emersion or emergence, reversal of the process of immersion.
ϵ	increase in internal energy due to an increase in

* This paper combines and extends the relations of Harkins and Dahlstrom, "Wetting of pigments and other powders," Ind. Eng. Chem. **22**, 897 (1930); and of Harkins, "A general thermodynamic theory of the spreading of liquids . . .," J. Chem. Phys. **9**, 552 (1941).

area of 1 cm², commonly designated as the total surface or interfacial energy.

f free energy per unit area, as a subscript designates a film.

$f_{I(SL)}$ free energy of immersion in erg cm^{-2} of a solid, initially in a vacuum, in a liquid.

$f_{E(SL)}$ free energy of emersion of a solid from a liquid into a vacuum, the process is the reverse of that of immersion.

H Gibbs heat function for any area, and h for unit area.

θ angle of contact between the surface of a solid and that of a liquid.

I immersion.

L liquids, L' liquid with its surface saturated with the material of another phase.

l latent heat.

O oil.

S solid, S' surface of a solid in equilibrium with the saturated vapor of a liquid.

s entropy per unit area.

Σ total area, σ area per molecule.

τ transfer from one phase to another.

V vapor, V° saturated vapor.

ϕ spreading pressure, $\phi_{L/S}$ initial spreading pressure of a clean liquid over the clean surface of a solid, $\phi_{L/S'}$ semi-final spreading pressure of a clean liquid over the surface of a solid already covered with a film in equilibrium with the saturated vapor of the liquid, $\phi_{L'/S'}$ final spreading pressure of a liquid over a solid with all interfaces mutually saturated, $(-\phi_f)$ hypothetical surface tension (opposite of pressure) of film on the surface of a solid $=\gamma_{SV}-\gamma_{SL}$.

$\phi^S{}_{(P_2P_3)}$ free energy of transfer of a finely divided solid, sheets or powder, from the interior of phase 2 to the interior of phase 3.

W water, W_A work of adhesion, W_C work of cohesion.

I. INTRODUCTION

ONE of the most important of all of the branches of surface chemistry is that which deals with the energy relations of the surfaces of solids, and of their interfaces with liquids and vapors. Nevertheless there are no experimental data in the literature which give the magnitude of any of the surface energy quantities involved.[1]

This paper is the second of a series in which such data, already obtained, are presented. In this paper attention is focused upon the free energy changes which accompany (1) the spreading of a liquid over the surface of a solid, and (2) the displacement of one liquid by another on such a surface. A knowledge of (1) is essential to the determination of the amount of work (W_A) or increase of free energy (f_A), required to separate a liquid from a solid for 1 cm² of interface between the two (Fig. 1). It is also one of the two experimentally determinable terms whose sum gives the free energy of emersion (f_E) of a finely divided solid from a liquid.

Since the difference between the total energy of adhesion (ϵ_A), which has been determined by a direct calorimetric measurement, and f_A, gives the latent heat of adhesion (l_A), and since l_A/T is the entropy of adhesion (s_A), the determination of (1) is also an important step in the process of obtaining the latent heat and entropy of adhesion.

If a liquid and a solid are completely separated from an interface of 1 cm² (Fig. 1) the increase of free energy is

$$f_{A(SL)}=W_{A(SL)}=\gamma_S+\gamma_L-\gamma_{SL}, \qquad (1)$$

since unit area of the surface of the solid and of the liquid appear, and unit area of the interface disappears. The subscript S by itself signifies that the solid is in a vacuum. A lower case letter, if it indicates an energy quantity, refers to unit area. Thus, if $f_{A(SL)}$ is considered as an example,

$$f_{A(SL)}=(\partial F_{A(SL)}/\partial\Sigma)_{T,p}.$$

If, in the separation of the solid and the liquid no other process occurs, the increase in the internal energy of the system is equal to the increase of total surface energy ($\epsilon_{A(SL)}$), but the quantity which is measured more directly is the

FIG. 1. Cylinder of solid (S) and liquid (L), with an interface (SL) of area 1 cm².

[1] See paper I, W. D. Harkins, J. Chem. Phys. **10**, 268 (1942).

heat function ($h_{A(SL)}$), so it is important to obtain the difference between ϵ and h.

In general

$$h=(\partial H/\partial\Sigma)_{T,p}=(\partial E/\partial\Sigma)_{T,p}+p(\partial v/\partial\Sigma)_{T,p} \\ =\epsilon+p(\partial v/\partial\Sigma)_{T,p}. \quad (2)$$

However, $(\partial v/\partial\Sigma)_{T,p}$ is extremely small, and p is not large at atmospheric pressure, so the last term is negligible, and

$$\epsilon\approx h. \quad (3)$$

By considering the process of the separation, equations involving h or ϵ may be written, and these are analogous to (1) in form.

$$h_{A(SL)}=h_S+h_L-h_{SL}, \quad (4)$$

$$\epsilon_{A(SL)}=\epsilon_S+\epsilon_L-\epsilon_{SL}, \quad (5)$$

in which the relation between any total and the corresponding free energy is:

$$\epsilon=\gamma+l=\gamma-T(\partial\gamma/\partial T)_{p,\Sigma}. \quad (6)$$

It is pointed out earlier in this introduction that the primary purpose of this paper is to consider certain free energy changes which must be evaluated correctly if the work of adhesion between a solid and a liquid, and the decrease of free energy which accompanies the immersion of a finely divided solid in a liquid, are to be calculated. A secondary and, to the writer, a less agreeable purpose, is to correct the incorrect equations which seem universally to accompany the treatment of this subject in the literature, as, for example, in the books of Rideal and of Adam.[2]

Therefore, if later in this paper the equations of certain workers in this field seem to have been selected for criticism, this is only because the number of equations developed by them is larger, but not that they are more incorrect, than those of others.

In practically all treatments of the subject Eq. (1) for the work of adhesion is given correctly, but one of the two expressions for what has been designated by Freundlich as the "adhesion tension" (A) is always incorrect. The result of this is to introduce an equation for the work of adhesion, which is as follows:

$$W_A=\gamma_L(1+\cos\theta). \quad (A)$$

The general opinion of the importance of this equation is reflected accurately in the following quotation of a statement by Adam.

> This equation has been known for over a century; it was given in 1805 by Young (without proof!) and by Dupré; it can be deduced also from Laplace's theory of capillarity, or indeed from any theory of the cohesive forces, since it can be obtained from consideration of energies only. Until recently it has been little noticed, which is unfortunate, as the meaning of the contact angles is much clarified when the work of adhesion is introduced, and the surface tensions of the solid surfaces, which are not measurable, are eliminated. Most authors are now, however, expressing their results in terms of the work of adhesion or of closely related expressions.

The equation is said to have been developed by Young,[3] but no such equation is to be found in his paper, where he expresses the relations in words, whose significance is not clear. According to Adam it was given by Dupré.[4]

In contrast with this opinion, the viewpoint of the present paper is that it is extremely unfortunate that this equation came into notice at all, since it gives not only a very false idea of the magnitude of the adhesional free energy, but also excludes the particular term, considered later, which is characteristic of the nature of the surface of the solid.

In addition to this, the adhesion tension, when defined correctly, is not a measure of the tension of adhesion at all. On the basis of these facts it is suggested that the use of the term "adhesion tension" should be discontinued, both on account of its association with incorrect equations, and because the term itself is misleading. It is shown later that the use of the spreading pressure (ϕ) is much more satisfactory.

The importance of Eq. (A) lies in the fact that if correct it would give an extremely simple means for the determination of the fundamental quantity $W_{A(SL)}$. This would be specially important, since only one of the three terms in the fundamental Eq. (1) for the work of adhesion can be determined experimentally, and

[2] E. K. Rideal, *Surface Chemistry* (Cambridge University Press, 1930), p. 6. N. K. Adam, *The Physics and Chemistry of Surfaces* (Clarendon Press, Oxford, 1938), p. 179.

[3] T. Young, Phil. Trans. 54 (1805): *Works* (ed. Peacock) Vol. 1, p. 432.

[4] Dupré, *Théorie Mécanique de la Chaleur*, p. 393 (1869) as cited by Adam.

this term, γ_L, is the least important of the three. The effect of Eq. (A) has been to give rise to the almost universal belief that the extremely low values which are obtained by its use represent the actual adhesion between the solid and the liquid. It is difficult to imagine any other concept which could possibly have brought greater confusion into the subject of the surface energy relations of solids. The logical deduction from these low values would be that the work of adhesion between a liquid and a solid is very much lower than is usually the case.

A considerable number of the incorrect equations in the literature have their origin in the fact that the equation for the adhesion tension (A) is written as either

$$A=\gamma_S-\gamma_{SL}=\gamma_L\cos\theta, \qquad (B)$$

or

$$A=\gamma_{SA}-\gamma_{SL}=\gamma_{LA}\cos\theta. \qquad (B')$$

When, for example, Eq. (B) is combined with another equation in which γ_S represents the free surface energy in a vacuum, the γ_S of Eq. (B) is assumed to have the same value, and is substituted for it. This amounts to the assumption that the γ_S of Eq. (B) is also the free surface energy of the solid in a vacuum, as the symbol states. But if this is true, then

$$\gamma_S-\gamma_{SL}\gg\gamma_L\cos\theta,$$

so these two values cannot be equated.

II. CHANGE OF INTERFACIAL ENERGY WHICH ACCOMPANIES THE TRANSFER (τ) OF A FINELY DIVIDED SUBSTANCE FROM THE INTERIOR OF ONE PHASE TO THE INTERIOR OF ANOTHER (ENERGY OF PHASE TRANSFER)

Since the amount of material in 1 cm² of any interface is excessively small, the amount of surface energy is also excessively small. Thus the value of h_L for the surface of water at room temperatures is only 1/280,000 of a calorie, so 2.8×10^5 cm² of surface must disappear in a calorimeter if the amount of heat to be measured is one calorie. It is obvious, therefore, that if the energy of any interface is to be determined calorimetrically, the area must be made very large, as by the use of very many extremely thin sheets, or of very minute particles of the material. This may be illustrated by the fact that if one gram of water at 20° is in the form of spherical droplets 1μ in diameter, the number of droplets is 1.9×10^{12}, but the total energy (ϵ_τ) of transfer of these droplets from inside the vapor phase to inside the liquid phase of water is only -0.165 calorie, while the corresponding free energy (f_τ) is an even smaller negative quantity (-0.103 cal.).

The equations for phase transfer, which are written below, are very simple. Symbols of the type of $\overset{P_1}{\epsilon_\tau(P_2P_3)}$ indicate the increase of energy per cm² due to a transfer of the finely divided phase (1) from the interior of phase (2) to the interior of phase (3).

Internal energy or heat content:

$$\overset{P_1}{\epsilon_\tau(P_2P_3)}=\epsilon_{P_1P_3}-\epsilon_{P_1P_2}\approx h_{P_1P_3}-h_{P_1P_2}=\overset{P_1}{h_{\tau(P_2P_3)}}. \qquad (7)$$

Free energy:

$$\overset{P_1}{f_{\tau(P_2P_3)}}=f_{P_1P_3}-f_{P_1P_2}. \qquad (8)$$

Latent heat:

$$\overset{P_1}{l_{\tau(P_2P_3)}}=l_{P_1P_3}-l_{P_1P_2}=-T\left[\frac{\partial(\gamma_{P_1P_3}-\gamma_{P_1P_2})}{\partial T}\right]_\Sigma. \qquad (9)$$

Entropy:

$$\overset{P_1}{s_{\tau(P_2P_3)}}=\overset{P_1}{l_{\tau(P_2P_3)}}/T. \qquad (10)$$

Relation between free and total energy:

$$\overset{P_1}{h_{\tau(P_2P_3)}}=\overset{P_1}{f_{\tau(P_2P_3)}}+\overset{P_1}{l_{\tau(P_2P_3)}}. \qquad (11)$$

The term *free energy of immersion* has been applied to the decrease of free energy which accompanies the transfer of a finely divided phase from a *vacuum* (immersed in only its own vapor) into the interior of another phase. In order that the free energy may increase, it is only necessary exactly to reverse this process, and the increment of free energy per unit area will be designated by the symbol f_E. This is the free energy increase per unit area which accompanies the *emersion* (or emergence) of the thin sheets or the powder from the liquid into a vacuum. Equations (7) to (10) may be rewritten for this case by the substitution of the symbol S for P_1. Since most of the solids used in this type of work have a negligible vapor pressure, the symbol $f^S{}_{E(LVS)}$, which is read as the free energy

of the emersion of the solid from the liquid into the vapor of the solid, is simplified to $f_{E(SL)}$, which is read as the free energy of emersion of the solid from the liquid into a vacuum. The experimental process used for the determination of the total energy is that of immersion, which is brought about by breaking a bulb, or pushing out the ends of a cylinder, which contains the clean powder in a vacuum, after the bulb has been immersed in the liquid, and it and its contents have come into thermal equilibrium with the liquid.

For emersion from a liquid Eq. (8) becomes:

$$f_{E(SL)} = f_{\tau(SL)} = \gamma_S - \gamma_{SL}, \tag{12}$$

or from a vapor:

$$f_{E(SV)} = f_{\tau(SV)} = \gamma_S - \gamma_{SV}. \tag{13}$$

If the vapor is saturated the symbol V is replaced by V°.

An equation analogous to (12) can be written for the increase of internal energy:

$$\epsilon_{E(SL)} = \epsilon_{\tau(SL)} = \epsilon_S - \epsilon_{SL}. \tag{14}$$

III. THE TOTAL ENERGY OF ADHESION ($\epsilon_{A(SL)}$) AND OF EMERSION ($\epsilon_{E(SL)}$)

The primary purpose of this paper is to consider the quantities which must be determined in order to obtain the work of adhesion ($W_{A(SL)}$) between a solid and a liquid. Since, however, the free surface energy γ_S of Eq. (1) has not been determined for any solid, and since γ_{SL} is also unknown, it is impossible at present to use Eq. (1) to calculate $W_{A(SL)}$. Thus it is necessary to resort to less direct methods in order to obtain the work of adhesion. Before these methods are considered it seems advisable to learn the general order of magnitude to be expected for $W_{A(SL)}$ in representative cases.

While the work of adhesion, $W_{A(SL)}$, cannot be obtained in a single experiment, the total energy of immersion $-\epsilon_{I(SL)}$ can be determined directly by its measurement in a calorimeter, and $-\epsilon_{I(SL)} = \epsilon_{E(SL)}$.

From Eqs. (1) and (14)

$$\epsilon_{A(SL)} = \epsilon_{E(SL)} + \epsilon_L$$
$$= f_{E(SL)} - T(\partial\gamma_{E(SL)}/\partial T)_{p,\Sigma}$$
$$+ \gamma_L - T(\partial\gamma_L/\partial T)_{p,\Sigma}. \tag{15}$$

Since $(\partial\gamma_L/\partial T)_{p,\Sigma}$ is known to be negative, and since it may be predicted that $(\partial\gamma_{E(SL)}/\partial T)_{p,\Sigma}$ is also negative, it is to be expected that $f_{A(SL)}/\epsilon_{A(SL)} < 1$, but from what is known about the relations of interfaces it may be concluded that this fraction is not very small at ordinary temperatures.

A relation between the free and the total energies of adhesion is given by

$$\partial\left(\frac{f_A}{T}\right) \Big/ \partial T = -\epsilon_A/T^2. \tag{16}$$

It is therefore of interest to consider carefully the values of $\epsilon_{E(SL)}$, as obtained in unpublished work by Harkins and Boyd, for representative solids and liquids. These are in erg cm^{-2} of interface: $BaSO_4$, 490(610), TiO_2 520(640), SiO_2 600(720), ZrO_2 600(720), SnO_2 680(800), $ZrSiO_4$ 850(970). The numbers in parentheses give $\epsilon_{A(SL)}$ the energy of adhesion. The ratio of the energy of *emersion* of a given liquid to that of water ($\epsilon_{E(L)}/\epsilon_{E(H_2O)}$) is, for eight liquids and all of the solids listed above: H_2O 1.00; butyric acid, 0.77; ethyl acetate 0.75; butyl alcohol, 0.71; nitrobenzene, 0.58; carbon tetrachloride, 0.47; benzene, 0.30; and iso-octane 0.18.

With graphite the total energies of *emersion* are in an altogether different ratio, and in erg cm^{-2} are: H_2O, 265; ethyl alcohol, 250; carbon tetrachloride, 195; and benzene, 225.

Until recently no values of the work of adhesion between a liquid and a solid have been known, but a few determinations of this quantity have just been made in this laboratory, as described later. In these few instances $f_{A(SL)}$ has exhibited values of the order of 60 percent of those of $\epsilon_{A(SL)}$ given above for TiO_2 and SiO_2.

IV. THE SPREADING PRESSURE, OR THE FREE ENERGY OF TRANSFER ($\phi^S{}_{LV^\circ}$) FROM A LIQUID TO ITS SATURATED VAPOR

An important quantity in the determination of the work of adhesion between a solid and a liquid, is the *spreading pressure* of the liquid on the solid. This is the increase of free energy of phase transfer of the finely divided solid from a liquid into its vapor, and is designated as $\phi^S{}_{LV^\circ}$. The value of this quantity is given by the relation

$$\phi^S{}_{LV^\circ} = -f^S{}_{\tau(V^\circ L)} = \gamma_{SV^\circ} - \gamma_{SL}. \tag{17}$$

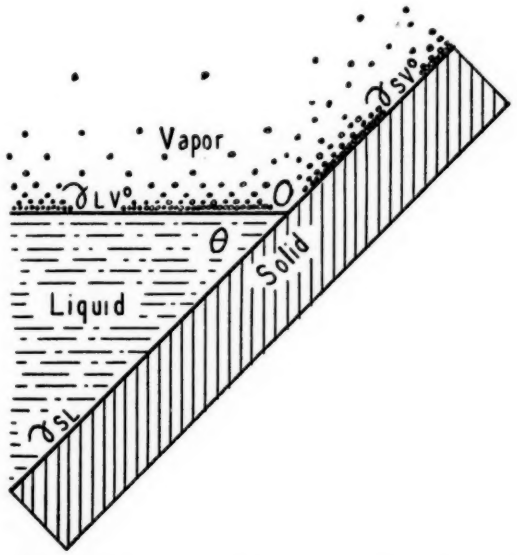

FIG. 2. Angle of contact (θ) between a solid and a liquid.

Now if any certain material, can be obtained as a fine powder, with all of the faces of the same type (e.g., all 110 faces) and if the same face of a larger crystal is available, then an additional relation which expresses (17) can be obtained (Fig. 2). The forces which act along the lines of contact, between the edge of a lens of the liquid and the surface of the solid, perpendicular at 0 to the plane of the diagram may be resolved as follows:

$$\gamma_{SV^\circ} - \gamma_{SL} = \gamma_L \cos \theta_{LS}. \tag{18}$$

This, from Eq. (17) is equal to the spreading pressure ϕ for the same process, or

$$\phi^S{}_{LV^\circ} = \gamma_{SV^\circ} - \gamma_{SL} = \gamma_L \cos \theta_{SL}. \tag{19}$$

The symbol for the spreading pressure may be expressed in another form as $\phi_{L/S}$ in order to bring out its points of resemblance to the initial spreading coefficient, $S_{b/a}$, used by Harkins[5] to express the initial spreading pressure of a duplex film of one liquid on the surface of another. By the convention already used $\phi_{L/S}$ represents the spreading of the liquid on the clean surface of the solid, so

$$\phi_{L/S} = \gamma_S - \gamma_{SL}, \tag{20}$$

while

$$\phi_{L/S'} = \gamma_{SV^\circ} - \gamma_{SL} = \phi^S{}_{LV^\circ} \tag{21}$$

is the spreading pressure which has been used in the earlier equations of this section, since S' represents the solid covered by a film which is in equilibrium with the liquid L.

If the material of the solid spreads on the surface of the liquid the spreading pressure becomes $\phi_{L'/S'}$, and

$$\phi_{L'/S'} = \gamma_{L'} \cos \theta_{S'L'}, \tag{22}$$

in which the prime on L indicates that the surface of the liquid is covered by a film of the material S in equilibrium with S. If the solid is an organic substance of the polar-non-polar type $\gamma_{L'}$ may be much lower than γ_L, and $\theta_{S'L'}$, may have a value which differs greatly from that of θ_{SL}.

V. THE WORK OF ADHESION BETWEEN A SOLID AND A LIQUID

It has been pointed out that of the three terms (γ_S, $-\gamma_{SL}$, and γ_L) of Eq. (1), whose sum gives the value of the work of adhesion, only one (γ_L) can be determined at the present time. However, it is possible to consider a series of processes which bring together the surface of a solid (initially in a vacuum) and that of a liquid, to form the interface SL.

Let us suppose that the crystalline solid exists in the form of many extremely thin sheets, so that the total area available is very large in comparison with the volume, and that all of the crystal faces are of the same type (as 110).

Process 1

The vapor of the liquid is admitted very slowly into the vacuum which surrounds the sheets of solid, until the vapor finally becomes saturated. The decrease of free energy on immersion, $-f_{I(SV^\circ)}$, of the solid in the saturated vapor is given by the relation

$$-f_{I(SV^\circ)} = \gamma_S - \gamma_{SV^\circ} = f_{E(SV^\circ)}. \tag{13b}$$

The positive value of $-f_{I(SV^\circ)}$ corresponds to the increase of free energy on the reversal of the process of immersion, that is on emersion.

Process 2

The finely divided solid is transferred from the saturated vapor of the liquid to the liquid. The free energy decrease is $\phi^S{}_{V^\circ L}$.

[5] W. D. Harkins, J. Chem. Phys. **9**, 552 (1941); W. D. Harkins and A. Feldman, J. Am. Chem. Soc. **44**, 2665 (1922).

From Eq. (17), this is equal to $\gamma_{SV^\circ}-\gamma_{SL}$, and neither of these is known. However, it is also equal to

$$\gamma_L \cos\theta_{SL}.$$

By these two processes the solid is transferred from a vacuum into the liquid, and

$$-f_{I(SL)}=-f_{I(SV^\circ)}-\phi^{S}{}_{V^\circ L}$$
$$=-f_{I(SV^\circ)}+\gamma_L\cos\theta_{SL}. \quad (23)$$

Since

$$W_A=-f_{I(SL)}+\gamma_L \quad \text{and} \quad -f_{I(SL)}=f_{E(SL)}$$

it is also given by

$$W_{A(SL)}=f_{E(SV^\circ)}+\phi^{S}{}_{LV^\circ}+\gamma_L, \quad (24)$$
$$=f_{E(SV^\circ)}+\gamma_L(1+\cos\theta), \quad (25)$$
$$=f_{E(SL)}+\gamma_L. \quad (26)$$

These equations, in a somewhat different form, were developed by Harkins and Dahlstrom.[6]

It is of interest to note a few examples of the preliminary values obtained for the three terms of Eq. (24), which in erg cm^{-2} are given below.

$W_A(TiO_2, H_2O)=227.6+72.2+72.2=372$
$W_A(TiO_2\text{-}n\ \text{Heptane})=38+20+20=78$
$W_A(\text{Graphite-}H_2O)=58+72.2+5.8=136.$
$(t=24°C)$

VI. THE "ADHESION TENSION"

Freundlich[7] has defined a "Haftspannung," usually translated as the "adhesion tension" (A_{SL}), by two equations, as follows:

$$A_{L/S}=\gamma_{SG}-\gamma_{SL}, \quad (C)$$
$$A_{L/S'}=\gamma_{LG}\cos\theta. \quad (27)$$

Of these (27) is correct, since it is a definition, while (C) is correct if γ_{SG} designates surface of the solid in equilibrium with the saturated vapor (V°) of the liquid, and incorrect if it indicates surface of the solid in nothing but a permanent gas or a vacuum. Unfortunately it is this latter incorrect significance with which it has been universally associated, since the value of γ_{SG} is substituted for the γ_S in Eq. (1) for W_A, in which the surface of the solid is in a vacuum. Thus in the application of Eq. (C) it is the universal custom to use it as if it were written

$$A_{L/S'}=\gamma_S-\gamma_{SL}. \quad (C')$$

This gives actually the value of $\phi_{L/S}$ which is very much larger than the $\phi_{L/S'}$ of the correct equation.

The work of adhesion between a solid and a liquid is given correctly by

$$W_{A(SL)}=\gamma_S+\gamma_L-\gamma_{SL}. \quad (1)$$

If this is to be combined with Eq. (C) the proper method would be to substitute the value of γ_{SL} as given by Eq. (C), in Eq. (1), since the two values of γ_{SL} are the same. Instead of this, however, it has become the custom to substitute the value of γ_{SG} of Eq. (C) for the γ_S of Eq. (1), although the two are extremely different. As a result the following equation

$$W_{A(SL)}=\gamma_{LV^\circ}(1+\cos\theta), \quad (A)$$

which is obviously very different from the correct equation ((24), (25), (26)) is obtained.[8]

If Eq. (A) were to be changed to

$$W_{A(SV^\circ,\,L)}=\gamma_{LV^\circ}(1+\cos\theta) \quad (1')$$

it would become correct, provided this is intended to represent the decrease of free interfacial energy involved in bringing into contact the liquid and the surface of the solid, already covered with a film in equilibrium with the saturated vapor of the liquid. The signs in this equation are correct if this process is exactly reversed. While in this equation W_A is a work of adhesion, it is not the work of adhesion between the solid and the liquid, since the interface at which the separation occurs does not lie exactly at the surface of the solid, but very slightly inside the liquid. Other incorrect equations which have been developed from Eq. (C) are considered later.

A real adhesion tension between high melting inorganic polar solids and water should have a value of twenty thousand atmospheres or more, while what is known as the adhesion tension represents a very much smaller value.

[6] W. D. Harkins, and R. Dahlstrom, Ind. Eng. Chem. **22**, 897 (1930).
[7] H. Freundlich, *Kapillar Chemie* (Leipzig, 1900), Vol. 1, p. 223.
[8] D. H. Bangham and R. I. Razouk, Trans. Faraday Soc. **33**, 1459 (1937), point out that this equation does not give the work of adhesion as specifically defined by Harkins.

On the basis of the unsuitability of the term, and the fact that it is universally associated both with incorrect equations and erroneous and deceptive magnitudes, it is recommended that the expression "adhesion tension" should be discarded, and the term "spreading pressure" substituted, in treatments of the adhesional energy between a solid and a liquid.

VII. SPREADING PRESSURE ($\phi_{L/S'}$) WITH THE CONTACT ANGLE (θ) GREATER THAN ZERO

If the contact angle between a solid and a liquid is greater than zero, the only difficulty in obtaining a correct value of the spreading pressure lies in the determination of a correct equilibrium contact angle. Almost the only contact angle which has an established value within not too wide limits is that between paraffin and water. Since solid paraffins differ in composition it is not to be expected that exact agreement should be obtained between the contact angles obtained by the use of different samples.

It was found[9,10] that by the use of the tilting plate method it was possible with water and a given paraffin surface to determine the angle of contact to within $\pm 0.2°$ of the mean value in entirely independent determinations. The surfaces were prepared by a quick dipping of cold, dry microscope slides into a pure molten paraffin of b.p. 210–220° at 3-mm pressure. The paraffin solidified rapidly to give a smooth even surface. With this paraffin the contact angle exhibited a mean value of 109.7° as determined by F. M. Fowkes, while G. Jura obtained an angle of $109.3 \pm 0.2°$ with a different, but similar sample of paraffin. These values may be compared with that of Nietz, 109.5°, found by the use of a sample of b.p. 218–225° at 4-mm pressure.

Of all of the known methods for the measurement of the contact angle, that of the tilting plate, if used in its most recent form, is the most accurate. The initial simple type of apparatus of Adam and Jessup[11,12] was too simple, and gave considerable hysteresis in the angle. Improvements have been introduced successively by Nietz,[13] Sumner,[14] and Harkins and Fowkes,[9,10] and as a result of all of these improvements a high degree of accuracy can be attained provided the surface can be produced in a sufficiently smooth state. Thus Harkins and Fowkes were able, *for the first time*, to obtain values of the contact angle which exhibited no hysteresis, and their work has been confirmed in this respect by the experiments of G. Jura, in this laboratory.

An inspection of Table I reveals the fact that with minerals the method of the tilting plate has given results very different from those of Rehbinder[15] by the measurement of the profiles of drops of liquid on the surface of the mineral and of bubbles of air under the surface of the mineral.

The measurement of the profiles of drops and bubbles has been used very widely for the determination of the contact angle, but has suffered from a great disadvantage as compared with the use of the tilting plate, since in the application of the plate method the surface is cleaned frequently by sweeping. As an additional precaution Harkins and Fowkes used a film balance in the water to determine the cleanliness of the surface. The writer has introduced, with drops and bubbles, a "sweeping" of the surface, which may be less effective, however, than that employed with a plane surface. The drop or bubble is produced on a very clean solid surface, and with clean water drawn from *inside* a comparatively large body of water. Just before the photograph is taken, or the direct measurements are made, the surface of the drop or bubble is cleaned by suction, by the use of a very fine tube, the plane of whose opening lies almost perpendicular to the surface of the water. This is moved over the surface, and its proper use gives a considerable cleaning action.

The values of θ obtained by Rehbinder are relatively very low, and this is the effect to be expected if impurities are present in the water.

Since the attainment of equilibrium is exces-

[9] W. D. Harkins and F. M. Fowkes, J. Am. Chem. Soc. **60**, 1511 (1938).
[10] F. M. Fowkes and W. D. Harkins, J. Am. Chem. Soc. **62**, 3377 (1940).
[11] N. K. Adam and Jessup, J. Chem. Soc. **1925**, 1865.
[12] N. K. Adam and Morrell, J. Soc. Chem. Industry, **53**, 255T (1934).
[13] A. H. Nietz, J. Phys. Chem. **32**, 255 (1928).
[14] C. G. Sumner, *Wetting and Detergency* (Chemical Publishing Company, New York, 1937), p. 41.
[15] P. Rehbinder, Marie Lipetz, Marie Rimskaja, and A. Taubman, Kolloid Zeits. **65**, 268 (1933).

TABLE I. Solid liquid contact angles with water.

Substance	Tilting Plate H and F[a]	Tilting Plate A and J[b]	Water drops R[c]	Bubble in water R[c]
Ceylon graphite	85.7		55–60	59
Talc	87.8		69–77	52
Stibnite	84.2			
Paraffin	108–111	105		
Long chain acids and alcohols		100		

F. E. Bartell and H. H. Zuidema, J. Am. Chem. Soc. **58**, 1449 (1936) obtained 86° for water on talc by making measurements of drop dimensions. Our value of 87.8° is in excellent agreement with this, especially since different samples of talc were used.

[a] H & F = Harkins and Fowkes.
[b] A & J = Adam and Jessup.
[c] R = Rehbinder and associates.

sively sensitive to differences of temperature the method of the sessile bubble is the only one which has thus far been used with sufficient attention to the attainment of saturation. However, as applied, this method has suffered from the great disadvantage that no attempt has been made to eliminate impurities from the surface.

To make certain what the values of the contact angles actually are when minerals and water or an oil are involved, the writer is constructing a gas tight tilting plate apparatus, together with a thermostat in the liquid of which it is to be buried.

In order that some idea of the magnitude of the spreading pressure may be obtained a few values are given in Table II.

VIII. SPREADING PRESSURE AND ADHESION TENSION WITH THE CONTACT ANGLE (θ_{SL}) EQUAL TO ZERO

Inorganic solids, such as quartz and glass, exhibit a zero contact angle with water, and are classed as hydrophilic, while others (talc, graphite, galena, etc.) give a finite contact angle and are designated as hydrophobic. Solids are also classed as oleophilic and oleophobic. Clean glass, clean metals, etc. are both hydro- and oleo-philic, and barium stearate multilayers are both hydro- and oleo-phobic.[16]

While it might seem that when θ_{SL} is zero, the semi-final* spreading pressure $\phi_{L/S'}$ may be obtained very simply, since

$$\phi_{L/S'}=\gamma_L\cos\theta=\gamma_L\cos 0=\gamma_L,$$

in papers on adhesion tension it is considered that the equation loses its validity in this case.

It is difficult to ascertain the origin of this concept, but its consequences are discussed very fully in the papers of Bartell and his associates.[17] The fundamental idea seems to be obtained from the equation

$$A=\gamma_S-\gamma_{SL}=\gamma_L\cos\theta \qquad (D)$$

by the type of reasoning outlined below.

(1) The equation should be valid for partial spreading, i.e., if

$$\theta>0 \quad \text{so} \quad \cos\theta<1 \quad \text{and} \quad A<\gamma_L.$$

(2) The equation should be valid if the free energy difference

$$\gamma_S-\gamma_{SL}=\gamma_L\cos 0=\gamma_L,$$

so, it is said, $A=\gamma_L$.

(3) The equation is not valid if

$$\gamma_S-\gamma_{SL}>\gamma_L,$$

since this would give an excess of free energy over that needed for complete spreading, so now

$$A=\gamma_S-\gamma_{SL}=K\gamma_L,$$

where K is greater than unity.

Thus the equation $A=\gamma_L\cos\theta$ is not general, and $\cos\theta$ should be replaced by K. The value of K is equal to that of $\cos\theta$ if θ is greater than zero, but if θ is zero, then the value of K must be obtained in some indirect way. Bartell's method for doing this is discussed in Section 11.

This point of view arises from a confusion in which the concepts of an initial ($\phi_{L/S}$) and a final ($\phi_{L/S'}$) spreading pressure are inextricably mixed. It is true that with high melting polar

TABLE II. Final ($\phi_{W/S'}$) and initial ($\phi_{W/S}$) spreading pressures of water on solids at 24°C (dyne cm^{-1} or erg cm^{-2}).

	θ	$\phi_{L/S'}=\gamma_W\cos\theta$	$\phi_{L/S}$
Graphite	85.7	5.8	80
Talc	87.8	2.8	
Stibnite	84.2	7.3	
Paraffin	109.7	−24.4	
Liquid petrolatum (Squibbs, 20°)		−24.2	
Anatase (TiO_2)	0	72.1	300

[16] I. Langmuir, Science **87**, 493 (1938).

* While this has the form of the semi-final spreading pressure, for insoluble solids which do not contaminate the surface of the liquid, it is the final coefficient, and will be designated as such in later discussions.

[17] F. E. Bartell and H. J. Osterhof, Ind. Eng. Chem. **19**, 1277 (1927); F. E. Bartell and C. E. Whitney, J. Phys. Chem. **36**, 3122 (1932), Table IV; references 18 and 14b also.

solids γ_S is much greater than γ_{SL}, and that their difference $\gamma_S - \gamma_{SL}$ is very much larger than $\gamma_L \cos 0 = \gamma_L$. Thus if it were desired to express the value of the difference as a function of γ_L, the equation $\gamma_S - \gamma_{SL} = C\gamma_L$ might be used. Thus we might write

$$\phi_{W/TiO_2} = \gamma_S - \gamma_{SW} = C\gamma_W$$

as the initial spreading coefficient of water in TiO_2. This is a correct equation, but the term on the extreme right is useless, and $K = C$ only if θ is greater than zero.

The value obtained in this laboratory by Livingston, Boyd, and Harkins for the quantity is 300 erg cm^{-2} at 24.0°C, and in the form of $C\gamma_W$ this could be written 4.16×72.13, or $C = 4.16$ and this would be a correct, but a useless expression for the initial spreading pressure, since the value 300 dyne cm^{-1} tells what we want to know more simply. The value of such a C is different for every combination of solid, liquid, and temperature, and it has already been shown (Eqs. (19), (20), (21)) that the useful expression is

$$\begin{aligned} \phi_{L/S} &= \gamma_S - \gamma_{SL} = \gamma_S - \gamma_{SV^\circ} + \phi_{L/S'} \\ &= \gamma_S - \gamma_{SV^\circ} + \gamma_L \cos \theta_{SL}. \end{aligned} \tag{27}$$

While it is correct, but useless, to write $\phi_{L/S} = C\gamma_L$, the relation

$$\gamma_S - \gamma_{SL} = \gamma_L \cos \theta,$$

given so universally in treatments of the subject, *is always incorrect.*

Thus it is not possible to express the *initial* spreading coefficient for the spreading of a liquid over the clean surface of a solid by $\gamma_L \cos \theta$ whether θ is equal to or larger than zero.

Whatever value the contact angle may have, its equilibrium value is obtained when the surface of the solid is covered by a film of the material of the liquid, and this film has the same vapor pressure as the pure liquid (except for any minute effect of gravitation).

If the equilibrium contact angle is not zero, then this film differs in its free surface energy from the surface of the pure liquid. Therefore, at equilibrium the surface of the solid cannot be covered completely by a duplex film of the liquid.

In this connection it is of interest to consider that Bartell and Bartell[18] obtain for the *adhesion tension* of several solids with water the values 76.6 for silica, 76.7 for Al_2O_3, and 76.4 for barite, and these are as nearly the same as if a single solid has been used. This suggests that when the contact angle is zero their displacement pressure method measures a property of the water surface and gives no measure of any surface energy relation of the solids involved. That the quantity measured is the surface tension of water is indicated by the fact that the values obtained are only 5 percent too high if this is the case, which is a small error for so complicated a method.

IX. THEORY OF THE SPREADING PRESSURE WHEN THE CONTACT ANGLE IS ZERO

The writer's equation for the initial spreading coefficient of a duplex film is the same for a solid as for a liquid subphase, and may be written

$$\begin{aligned} S_{L/S} &= W_{A(SL)} - W_{C(L)} \\ &= \gamma_S - \gamma_{SL} - \gamma_L = \phi_{L/S} - \gamma_L. \end{aligned} \tag{28}$$

If this is positive a duplex film of the liquid *can* spread over the *clean* surface of the solid. This does not show that of necessity a duplex film will spread, since there may be some other film of a lesser free energy which may spread before the duplex film can do so. The relations are similar to those involved in the spreading of oils on water. Thus an oxidized lubricating oil spreads first (in general) as a duplex film, which changes later to a monolayer and a lens with a reduction of free surface energy.[19] With a material like oleic acid the monolayer may spread in advance of the duplex film, and a duplex film cannot spread over the monolayer since that would involve an increase in free energy.

The free energy of a liquid surface covered by a monolayer or a duplex film is designated by the symbol γ_f. If we designate the free surface energy of a solid covered by a film by the same symbol, then

$$\gamma_{f(SV^\circ)} = \gamma_{f(SL)} + \phi_{LS'}. \tag{29}$$

Thus it may be considered that the free energy

[18] F. E. Bartell and L. S. Bartell, J. Am. Chem. Soc. **56**, 2205 (1934).

[19] W. D. Harkins, J. Chem. Phys. **9**, 552 (1941).

of the film covered surface is the same as that of the interface solid-liquid, plus a term (usually positive, but possibly negative as with water on paraffin) which makes allowance for the fact that the film has an upper surface in addition to the interface (SL).

Let it be supposed that the plane surface of a solid, which gives a zero contact angle with a given liquid, is already in equilibrium with the vapor of the liquid. If a drop of the liquid is now placed upon the film thus formed, it spreads over it. In order that it may do this the effective surface tension of the film ($-\phi_f$) must be equal to or greater than that of the liquid, or $-\phi_f \geqq \gamma_L$. This becomes $\gamma_{f(SV^\circ)} = \gamma_{SL} + (-\phi_f) \geqq \gamma_{SL} + \gamma_L = \gamma_d$ if the entire free surface energy $\gamma_{f(SV^\circ)}$ is considered. Now if

$$\gamma_{f(SV^\circ)} = \gamma_{SL} + (-\phi_f) > \gamma_{SL} + \gamma_L,$$

then the surface covered with the film, obtained by equilibrium with the saturated vapor, and therefore with the liquid, has a greater tension, or free surface energy, than the duplex film. This indicates that the duplex film d will become thinner, while the film f will thicken, until at equilibrium

$$\gamma_{f(SV^\circ)} = \gamma_{SL} + (-\phi_f) = \gamma_{SL} + \gamma_L, \quad (31)$$

or

$$-\phi_f = \gamma_L. \quad (32)$$

Since ϕ_f is a pressure, the *positive* value of the *tension* is $-\phi_f$. This indicates that the equation

$$\gamma_{SV^\circ} - \gamma_{SL} = \gamma_L \cos\theta \quad (18)$$

is to be taken literally, even if the contact angle is zero. Thus if the relation is written

$$\phi_{L/S'} = \gamma_{SV^\circ} - \gamma_{SL} = K\gamma_L,$$

then K is merely a shorthand expression for $\cos\theta$, and cannot therefore be greater than unity, as it is commonly supposed to be.

TABLE III. Initial spreading coefficients of liquids on solids or on mercury (erg cm^{-2}).*

TiO_2 (Anatase)		Mercury	
Liquid	$S_{L/S}$	Liquid	$S_{L/Hg}$
Water	228	Water	32
n-Propyl alcohol	90	Ethyl alcohol	89
n-Heptane	38	*n*-Octane	79
SiO_2 (Quartz)		Hexane	79
Water	244	Nitro-ethane	63
n-Propyl alcohol	110	Nitro-benzene	82
Heptane	39	Acetone	60
Acetone	85	Benzene	90
Benzene	52	*m*-Xylene	90
$BaSO_4$		*o*-Xylene	91
Water	246	*p*-Xylene	97
n-Propyl alcohol	77	Chloroform	97
n-Heptane	38	iso-Butyl alcohol	110
Graphite		*n*-Octyl alcohol	102
Water	−8.0	Carbon disulfide	108
n-Heptane	(60)	Oleic acid	122
n-Propyl alcohol	(73)	Acetylene tetra-bromide	114
( ) = correct if $\theta = 0$		Ethyl iodide	135
		Methyl iodide	137

* The values of the initial spreading coefficients have been calculated from those for $\gamma_S - \gamma_{SV^\circ}$, which is the same as $f_{E(SV^\circ)}$, taken from the Ph.D. thesis of H. K. Livingston. The values of the latter were obtained by integration of the Gibbs adsorption Eq. (678), which is $d\pi = \Gamma_2 d\mu_2$, by a method suggested by Bangham and Razouk, reference 8, which will be given in a paper by H. K. Livingston, G. E. Boyd, and W. D. Harkins (unpublished). The value of $f_{E(SV^\circ)}$ for water on graphite was found in this work to be 58 erg cm^{-2}. The spreading pressure of water on graphite is 6 erg cm^{-2}. These values indicate a *negative initial* spreading coefficient (−8.0 erg cm^{-2}). While even the *initial* coefficient is probably negative on paraffin (final coefficient = −24 to −25), this is a somewhot surprising result with graphite, where the final coefficient is −6. However, since the values of $f_{E(SV^\circ)}$ are, seemingly, less accurate for graphite than for the other solids, the error in its initial spreading coefficient may be more than 8 erg cm^{-2}, so this coefficient may actually have a positive value. For the other solids the initial spreading coefficient and $f_{E(SV^\circ)}$ have the same value in every case.

X. THEORY OF THE SPREADING PRESSURE WHEN THE CONTACT ANGLE IS GREATER THAN ZERO

If the contact angle is greater than zero, then

$$\phi_f = \phi_{L/S'} < \gamma_L, \quad (33)$$

and the free surface energy of the film covered surface is less than that of the duplex film (γ_d).

$$\gamma_{f(SV^\circ)} < \gamma_{SL} + \gamma_L = \gamma_d. \quad (34)$$

This indicates that the upper surface of the film and the interface have now come so close together that they have merged into a single interface, with a resultant decrease of free energy, which may be designated as the free energy of interaction between the interface SL and the surface L. For water on graphite at 24°C

$$\gamma_{f(SV^\circ)} - \gamma_{SL} = (72.1 - 66.3) \text{ erg cm}^{-2},$$

so the interaction energy is 66.3 erg cm^2, which indicates that the film of water must be much thinner than a duplex film. For films on water this type of interaction energy may be large for liquids which do not give stable duplex films. For example the free energy of a water surface covered by a monolayer of methylene iodide in equilibrium with the liquid phase, is 24.2 erg cm^{-2} below that of the duplex film. The fact

Table IV. Initial ($S_{b/a}$) and final ($S_{b'/a'}$) spreading coefficients and spreading pressures (ϕ) for water on oil, and oil on water.

A. Water on oil

Oil	$S_{W/O}$	$\phi_{W/O}$	$\gamma_{O(dry)}$	$\gamma_{O(wet)}$	γ_{WO}	γ oily water	$\phi_{W'/O'}$	$S_{W'/O'}$
Higher hydrocarbon[a]	−97.6	−24.8	30.7		55.5			
CS_2	−90.0	−17.2	31.4	31.8	48.6	70.5	−16.8	−87.3
CH_2I_2	−67.9	+4.8	50.7	50.5	45.9	72.0	+4.6	−67.4

B. Oil on water

	$S_{O/W}$	$\phi_{O/W}$	$\phi_{O'/W'}$	$S_{O'/W'}$
Higher[a] hydrocarbon	−14.1	17.3		
CS_2	−8.2	24.2	21.9	−10.0
CH_2I_2	−23.8	26.9	26.3	−24.2
Benzene	8.84	37.8	27.3	−1.5
n-Heptyl alcohol	37.8	64.8	20.5	−5.9

[a] Stanolax.

that the interaction energy is 175 percent greater than this with water on graphite is not surprising, since the free surface energy of graphite, while its magnitude is unknown, is very much higher than that of water.

It is found that the film of water on a fine anatase (TiO_2) powder has, at 24°C, a mean thickness of 2.7 water molecules when the water vapor is only 87 percent saturated. The form of the adsorption curve is such as to indicate that at complete saturation the film is much thicker than this. The thickness of the film was calculated from the amount of water adsorbed per cm^2. The area was calculated by the use of the theory of Brunauer, Emmett, and Teller.[20] On graphite the water film was thinner—1.4 molecules thick at 85 percent saturated.

Although the mean thickness of the water film on graphite appears to be greater than that of a monolayer, the surface of this solid is presumably not so smooth as that of a liquid, and it is probable that the thickness of the water film on high spots is less than in the depressions, i.e., there is an effect due to the roughness of the surface. It is not improbable, however it may be brought about, that parts of even the equilibrium film may be monomolecular, though its mean thickness is greater than this.

In order to give some idea of the relative magnitudes of the initial spreading coefficients of various liquids on crystalline solids and on mercury, Table III is given below, while Table IV exhibits values of both initial and final spreading coefficients for water on organic liquids and for organic liquids on water.

The initial spreading coefficient of water on the polar solids is very high, on graphite it may be negative, while on mercury it has a moderately low value.

Table III exhibits several relations of importance:

1. Any one of the three liquids listed can spread on any one of the polar solids to give a duplex film.
2. The initial spreading coefficients are much higher than those on water.
3. The initial spreading coefficient of water on any of the polar solids is very much higher than on mercury.
4. The initial spreading coefficients of non-polar oils are much smaller on the polar solids than on mercury.
5. Polar-non-polar oils seem to exhibit initial spreading coefficients of the same general order of magnitude on the polar solids as on mercury.

It is unfortunate that those who have dealt with the free energy relations of the interfaces between solids and liquids have given so little attention to the relations at the liquid-liquid interface, since these are similar, especially if the liquids are only slightly soluble in each other. In order to exhibit the relations for the liquid-liquid interface Fig. 3 has been prepared. This gives both the *free* and the *total energy values* of the following: surfaces of (1) water and of (2) various oils; (3) interfaces between water and oil; (4) immersion of water in the oil; (5) adhesion between water and oil.

[20] S. Brunauer, P. H. Emmett, and E. Teller, J. Am. Chem. Soc. **60**, 309 (1938).

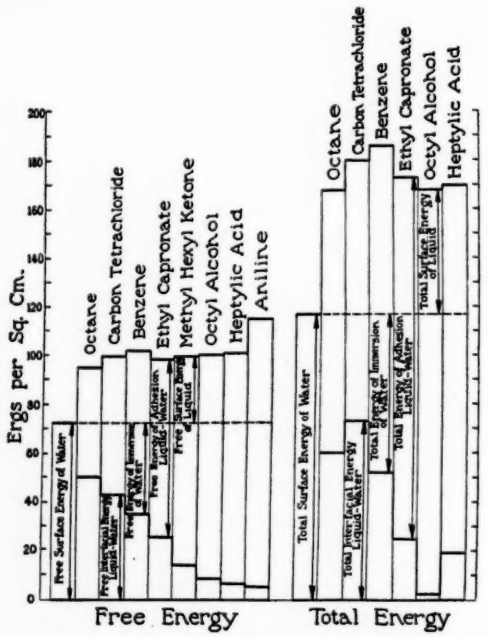

FIG. 3. Free and total surface and interfacial energy relations between water and other liquids. On the left of each section the surface energy of water is plotted by itself, and the magnitudes are represented by arrows. Each of the other arrows refers to all of the subdivisions of a certain level, and not merely to the vertical section in which it is given. The energies of immersion (or emersion) are for the immersion of water in, or emersion from, the organic liquid, so $f_{E(WO)}=\gamma_W-\gamma_{WO}$, which is positive, while that for the emersion of oil from water is given by $f_{E(OW)}=\gamma_O-\gamma_{WO}$, which may be either positive or negative.

The energy relations for the immersion of polar inorganic solids are very much the same as for the immersion of water, except for the much higher magnitudes of the energies of immersion in the case of the solids. Obviously $\epsilon_A-\epsilon_I$ and also f_A-f_I have the same magnitudes for both.

XI. THE ANGLE BETWEEN A WATER-OIL INTERFACE AND THE SURFACE OF A SOLID: THE DISPLACEMENT PRESSURE $(D)_{WO}$

If a water-oil interface meets the surface of a solid with the contact angle α, measured in the water phase, the displacement pressure (D_{WO}) from water toward oil is given by

$$D_{WO}=\gamma_{WO}\cos\alpha_{S(WO)}. \qquad (35)$$

With water and hexane at 20° the value of γ_{WO} is 51 dyne cm^{-1}, so the maximum values of D_{WO} are +51 and −51.

In addition we may write (Fig. 4) the equation

$$D_{WO}=\gamma_{12}-\gamma_{13}=\gamma_{WO}\cos\alpha_{S,WO}.$$

The question now arises, is γ_{12} the same as γ_{SO}, and γ_{13} the same as γ_{SW}?

This may be answered by a consideration of the numerical values of Livingston, Boyd, and Harkins for anatase (TiO_2), which give

$$\gamma_{SO}-\gamma_{SW}=(\gamma_S-\gamma_{SW})-(\gamma_S-\gamma_{SO})$$
$$=300-58=242=\gamma_{WO}\cos\theta$$
$$=\gamma_{WO}=51\text{ erg cm}^{-2},$$

which is a discrepancy of 191 erg cm^{-2}. Obviously the correct relation is:

$$D_{WO}=\gamma_{S'O'}-\gamma_{S'W'}=\gamma_{W'O'}\cos\alpha_{S,W'O'}, \qquad (36)$$

since at equilibrium each phase is saturated with the others.

It is considered by Rehbinder that the value of $B=\cos\alpha$ gives the best known measure of the hydrophilic and of the hydrophobic characteristics of the surfaces of solids. If B lies between 0 and 1 the surface is hydrophilic, and if between 0 and −1, hydrophobic. Gypsum ($B=1$), is considered as entirely hydrophilic, and paraffin ($B=-1$) as perfectly hydrophobic. As a representative oil he uses benzene. His values for minerals, given in Table V exhibit hysteresis. Thus if α is measured by the use of a drop of water on the surface of molybdenite (MoS_2) in benzene, $\alpha=145°$ ($B_{WO}=-0.819$) and with a

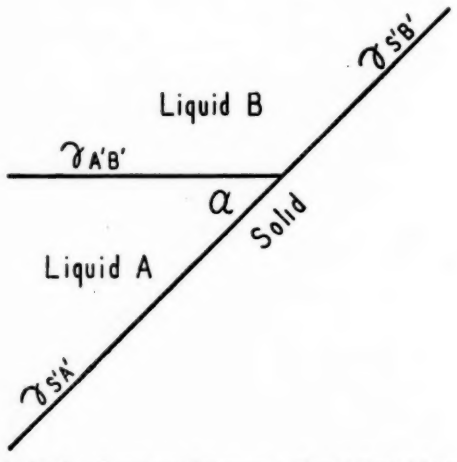

FIG. 4. Angle of contact between a liquid-liquid interface and the surface of a solid.

TABLE V. Displacement pressure (D) of water toward benzene on the surface of minerals (calculated from the contact angles (α) determined by Rehbinder and collaborators' values of D in dyne cm^{-1} or erg cm^{-2}).

Mineral	Cleaved C or ground G	Water drop in benzene $B=\cos\alpha$	D from water toward benzene	Benzene drop in water $B=\cos\alpha$	D from water toward benzene
Gypsum	C	1	35.0	1	35.0
Calcite $CaCO_3$	C	0.940	32.9	0.719	25.2
Barite $BaSO_4$	C	0.866	30.3	0.777	27.2
Fluorite CaF_2	C	0.755	26.4	0.707	24.8
Malachite $CuCO_3 \cdot Cu(OH)_2$	G	0.866	30.3		
Smithsonite $ZnCO_3$	G	0.755	26.4	0.819	28.7
Antimonite, Sb_2S_3	G	0.105	3.7	0.839	29.4
Sphalerite ZnS	G	0.017	0.6	0.809	28.3
Galena PbS					
Ground in water		0	0.0	0.766	26.8
Ground in benzene		−0.643	−22.5	0.656	23.0
Pyrites (single crystal) FeS_2					
Ground in water		−0.707	−24.8	0.819	28.7
Ground in benzene		−0.602	−21.1	0.602	21.1
Molybdenite MoS_2	$C.G.$	−0.819	−28.7	−0.656	−23.0
Graphite (Ceylon single crystal)	C	−0.602	−21.1	−0.602	−21.1
Chalcopyrites (single crystal) $CuFeS_2$	G	−0.656	−23.0	0.500	+17.5
Chalcopyrites (aggregate)	G	+0.469	+16.4	0.619	+21.7
Talc	C	−0.743	−26.0	−0.559	−19.6
Paraffin		−1.0	−35.0	−1.0	−35.0

drop of benzene in water $\alpha=135°$ ($B_{OW}=-0.656$). He designates $h=B_{OW}-B_{WO}=0.163$ as the "static wetting hysteresis." If the average value of α is taken as 140° then $D_{WB}=35.0 \cos 140°=-26.8$ dyne cm^{-1}. Thus on the surface of MoS_2, benzene exhibits a displacement pressure of 26.8 dyne cm^{-1} toward water. Table V gives the displacement pressures for other minerals as calculated from Rehbinder's values of $\cos\alpha$.

It is probable that this hysteresis may be eliminated by the proper use of the tilting plate but it is difficult to obtain crystal faces large enough for the use of this method, except for relatively few minerals. If the drop method is used the water-oil interface should be cleaned, as described earlier.

At this point it seems essential to consider the method devised by Bartell and Osterhof[21] for the determination of the value of K in the equation

$$A=K\gamma_L, \qquad \text{(D)}$$

when the contact angle θ_{SL} is zero. Whitney[22] has used the procedure for the evaluation of K for water and 13 organic liquids. The values vary from 1.07 for water and 1.08 for brombenzene to 2.68 for butyl acetate.

The equations of Bartell and Osterhof are given below.

$$A_{SW}=\gamma_S-\gamma_{SW}=K_{SW}\gamma_S$$
$$=\cos\theta_{SW}\gamma_W \quad \text{if } \theta_{SW}>0, \qquad \text{(E)}$$

$$A_{SO}=\gamma_S-\gamma_{SO}=K_{SO}\gamma_O$$
$$=\cos\theta_{SO}\gamma_O \quad \text{if } \theta_{SO}>0. \qquad \text{(F)}$$

The difference is

$$A_{SW}-A_{SO}=\gamma_{SO}-\gamma_{SW}=K_{WO}\gamma_{WO}$$
$$=\cos\alpha_{WO}\gamma_{WO}, \qquad \text{(G)}$$

or

$$A_{SW}-A_{SO}=\gamma_{WO}\cos\alpha_{S(WO)}. \qquad \text{(H)}$$

It is important to realize the fact that the true difference between the values of A_{SO} and A_{SW} can be obtained only if it is recognized that in the Eq. (E) and (F), the meaning of γ_S is very different from that associated with this symbol by Bartell and Osterhof. In (E) it designates $\gamma_{SV^{\circ}W}$ and in F, $\gamma_{SV^{\circ}O}$, which differ in magnitude by 242 erg cm^{-2} if the oil is heptane, and the solid anatase (TiO_2).

[21] F. E. Bartell and H. J. Osterhof, Ind. Eng. Chem. 19, 1277 (1927).

[22] C. E. Whitney, Dissertation, University of Michigan (1931).

A subtraction of the correct equations

$$\phi^{S}{}_{V^{\circ}O}O = A_{SO} = \gamma_{SV^{\circ}O} - \gamma_{SO} \cos\theta_{SO}, \quad (37)$$

$$\phi^{S}{}_{V^{\circ}W}W = A_{SW} = \gamma_{SV^{\circ}W} - \gamma_{SW} = \gamma_{W} \cos\theta_{SW}, \quad (38)$$

gives

$$\phi^{S}{}_{V^{\circ}W}W - \phi^{S}{}_{V^{\circ}O}O = A_{SW} - A_{SO}$$
$$= (\gamma_{SV^{\circ}W} - \gamma_{SV^{\circ}O}) + (\gamma_{SO} - \gamma_{SW})$$
$$= \gamma_{W} \cos\theta_{SW} - \gamma_{O} \cos\theta_{SO}, \quad (39)$$

which is very different from (H).

Thus Bartell's equation omits the term $\gamma_{SV^{\circ}W} - \gamma_{SV^{\circ}O}$, which is the only term distinctly characteristic of the nature of the surface of the solid, and obtains the difference of the two adhesion tensions as a function of the contact angle α, for which there is no justification.

The true value of the term $\gamma_{SO} - \gamma_{SW}$ in their Eq. (G) is, for TiO_2, heptane and TiO_2, water

$$\gamma_{SO} - \gamma_{SW} = (\gamma_{S} - \gamma_{SW}) - (\gamma_{S} - \gamma_{SO})$$
$$= f_{I(S\cdot W)} - f_{I(S\cdot O)} = 300 - 58$$
$$= 242 \text{ erg cm}^{-2}.$$

The term omitted is:

$$\gamma_{SV^{\circ}W} - \gamma_{SV^{\circ}O} = (\gamma_{S} - \gamma_{SV^{\circ}O}) - (\gamma_{S} - \gamma_{SV^{\circ}W})$$
$$= 38 - 227 = -191.$$

Thus actually $A_{SW} - A_{SO} = 242 - 191 = 51$ erg cm^{-2}.

Thus Eq. (G) gives the difference of the adhesion tensions as 242 erg cm^{-2}, while the correct result is 51 erg cm^{-2}.

Furthermore for this case it gives

$$\gamma_{WO} \cos\alpha_{WO} = 51 \cos\alpha_{WO} = 242,$$

an impossible result, since the maximum value of 51 cos α_{WO} is 51.

While the equations which give the spreading pressure and related quantities are very simple, the fact that the "adhesion tension" has always been expressed by equations which have been used incorrectly, indicates that great care must be taken to understand the relations between such equations and the phenomena which they represent.

A Superliquid in Two Dimensions and a First-Order Change in a Condensed Monolayer

II. Abnormal Viscosity Relations of Alcohol Monolayers in Condensed Liquid Phases

L. E. COPELAND, WILLIAM D. HARKINS, AND G. E. BOYD
George Herbert Jones Chemistry Laboratory, University of Chicago, Chicago, Illinois

(Received March 19, 1942)

The new LS phase found in alcohol monolayers has the compressibility of a solid and, at temperatures near that of the first-order $L_2 \rightleftharpoons LS$ transition, the low viscosity of a very highly fluid liquid. The viscosity is almost independent of pressure, but varies in an abnormal way with temperature. For example, octadecanol exhibits a minimum viscosity at about 8.8°C. As is normal, the viscosity increases with decrease of temperature over the small range from 8.8° to 7.5°C where a transition to the S phase occurs. However, above 8.8°C an increase of temperature of 16° increases the viscosity of the LS phase by a factor of 25, and changes it from Newtonian to non-Newtonian. At a pressure of 18 dynes cm^{-1} the logarithm of the viscosity above 12°C varies nearly either as T, or as $1/T$. At other pressures (Fig. 5) the relations are different. At 1 dyne cm^{-1} the viscosity of the condensed liquid (L_2) phase decreases in a normal way with temperature, but at 12 dynes cm^{-1} the relation is reversed and is abnormal, since the viscosity increases very rapidly as the temperature rises, to correspond with that of the LS phase. This makes the pressure relations extremely abnormal, since the LS phase at 25°C and the S phase at 5°C do not differ greatly in their behavior from normal liquids, which follow the relation $\log \eta = \log \eta_0 + k\pi$. However, at the intermediate temperatures in the range of 8.85 to 10° the viscosity of this phase decreases only slowly with pressure at low pressure, but more and more rapidly as the pressure increases, until the extremely rapid decrease is stopped by a transition to the LS phase. The viscosity relations indicate that the transition $S \rightleftharpoons LS$ occurs very close to a molecular area of 19.98A^2. While the area for the transition is almost constant, its temperature increases slowly with pressure. At 16 dynes cm^{-1} an *increase* of 0.07A in mean molecular distance *increased* the viscosity by a factor of 55. It should be noted that this effect is in the abnormal direction. The S phase is the only one of the three condensed phases which exhibits normal viscosity relations. In both the S and the LS phases the molecules may be assumed to be oriented perpendicular to the surface. In three-dimensional crystals the hydrocarbon chains occupy an area of 18.5A^2, in the S alcohol films from 19.5 to 20.0A^2, in the LS films from 20 to 20.75, and in the L_2 films from 19.8 to 22.7. The highest temperature employed was 35°C. An increase above this temperature would increase the upper limits of area for the LS and L_2 monolayers. It is obvious that the possibility exists for hydrogen bonding between the −OH groups of the alcohols themselves, or between these groups and the water molecules. What is needed for the explanation of the abnormal relations of the L_2 and LS phases of the alcohols is to determine what type of binding will increase in energy as the molecular distance is increased, either by increase of temperature or decrease of pressure. The *normal* behavior of the solid surface phase of the alcohols is similar to that of the acids, which has been discussed in earlier papers.

1. INTRODUCTION: GENERAL VISCOSITY RELATIONS OF CONDENSED MONOLAYERS

THE viscosity relations of monolayers of the n long paraffin chain alcohols are anomalous and remarkable. For example, the viscosity of a monolayer of octadecanol at a pressure of slightly more than 12 dynes cm^{-1} is about 5×10^{-3} surface poise if the temperature is 8.85°C, but if the temperature is either raised or lowered the viscosity increases with great rapidity. However, earlier work[1] at 25°C revealed no abnormality in the effect of pressure on the viscosity of any of the alcohols investigated, which included the five n alcohols with from 14 to 18 carbon atoms in the chain. At sufficiently low temperatures also (as 5°C with octadecanol) the pressure effect is again normal, but highly abnormal at intermediate temperatures.

According to Eyring's theory, as applied to monolayers by Moore and Eyring[2] the effect of pressure upon the viscosity of a liquid monolayer should be expressed by the relation (1) that the logarithm of the viscosity is a linear function of the pressure, or

$$\log \eta = \log \eta_0 + k\pi, \qquad (1)$$

which is the equation found empirically in the

[1] L. Fourt and W. D Harkins, J. Phys. Chem. **42**, 897 (1938).

[2] W. J. Moore and H. Eyring, J. Chem. Phys. **6**, 391 (1938).

laboratory, as represented graphically in Fig. 1, which represents the behavior of the normal long chain paraffin acids at 25°C.[3]

The relation is linear at 25°C up to about 16.5 dyne cm^{-1} with the 18 and 19 C atom acids, and up to 24 dyne cm^{-1} if there are 20 C atoms in the molecule.

The curves obtained by Fourt and Harkins at 25°C with the long chain alcohols are exhibited in Fig. 2. The alcohol films undergo a transition from the liquid condensed (L_2) phase to the high pressure phase at a much lower pressure than those of the corresponding acids, so the linear portion of the curve as expressed by (1) is much shorter than with the acids.

The following additional relations emerge from these diagrams:

2. At low film pressure the liquid condensed (L_2) film of octadecanol has a viscosity about 14 times higher than that of the corresponding acid.

3. The viscosity is increased by a factor of about 2 for the alcohols and of about 3 for the acids for each additional carbon atom in the chain. Thus the viscosities become more nearly equal as the chains lengthen.

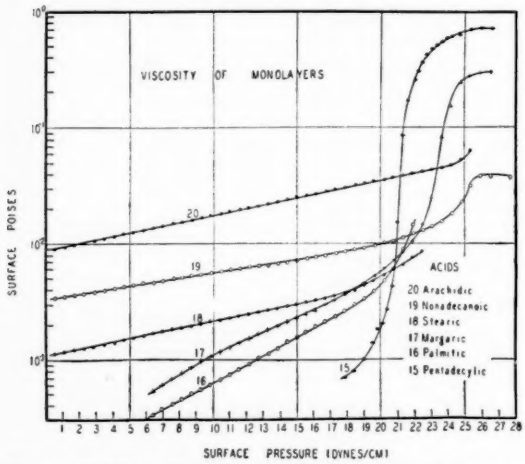

FIG. 1. Exhibits the linear relation between film pressure and the logarithm of the viscosity in the liquid condensed phase or low pressure phase. The viscosity of this phase increases rapidly, while that of the high pressure phase decreases rapidly, with increase in the number of carbon atoms in the hydrocarbon chain. The second-order transition between these phases is marked by an extremely rapid increase in viscosity. The second-order transition affects the viscosity both several dynes below and several above the transition, while the compressibility exhibits no effect except exactly at the pressure of the transition itself.

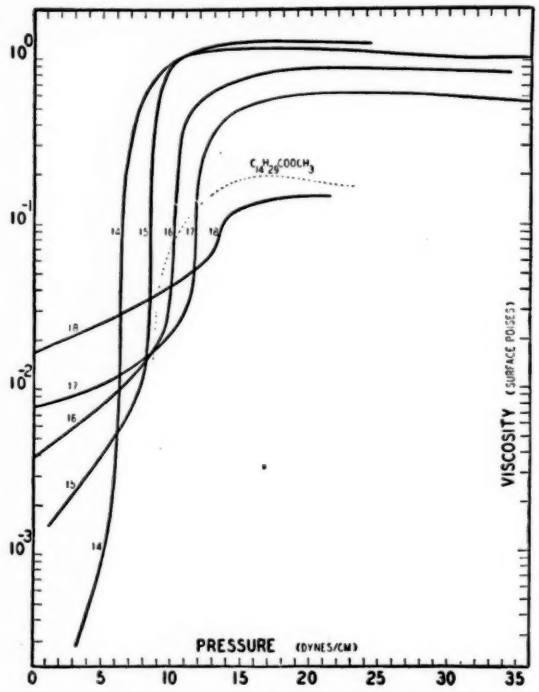

FIG. 2. Similar to Fig. 1, except that it represents the normal long paraffin chain alcohols, with methyl myristate added for comparison. The alcohol monolayers have much higher viscosities than the corresponding acids. The transition from liquid condensed to high pressure phase occurs at a much lower pressure than in the case of the acids, so the linear relation between pressure and logarithm of viscosity in the liquid condensed phase is more obscured than with the acids.

4. The liquid (L_2) films exhibit a Newtonian viscosity.

5. The high pressure condensed film exhibits a non-Newtonian viscosity which decreases slightly as the pressure increases. A non-Newtonian viscosity is defined as one which varies with the rate of shear.

6. The second-order transition between the low and high pressure phases (L_2 and S) of a long chain acid is represented on a pressure-area ($\pi - \sigma$) diagram by a kink produced by the meeting of two straight lines of different slope. This is true also for alcohols in the case of the transition $L_2 \rightleftharpoons S$, and nearly true for that of $L_2 \rightleftharpoons LS$ if the temperature is sufficiently far above that of the first-order transition. The relation seems always to be linear on the high pressure side. Thus the pressure-area diagram

[3] W. D. Harkins and G. E. Boyd, J. Chem. Phys. **7**, 203 (1939); E. Boyd and W. D. Harkins, J. Am. Chem. Soc. **61**, 1188 (1939).

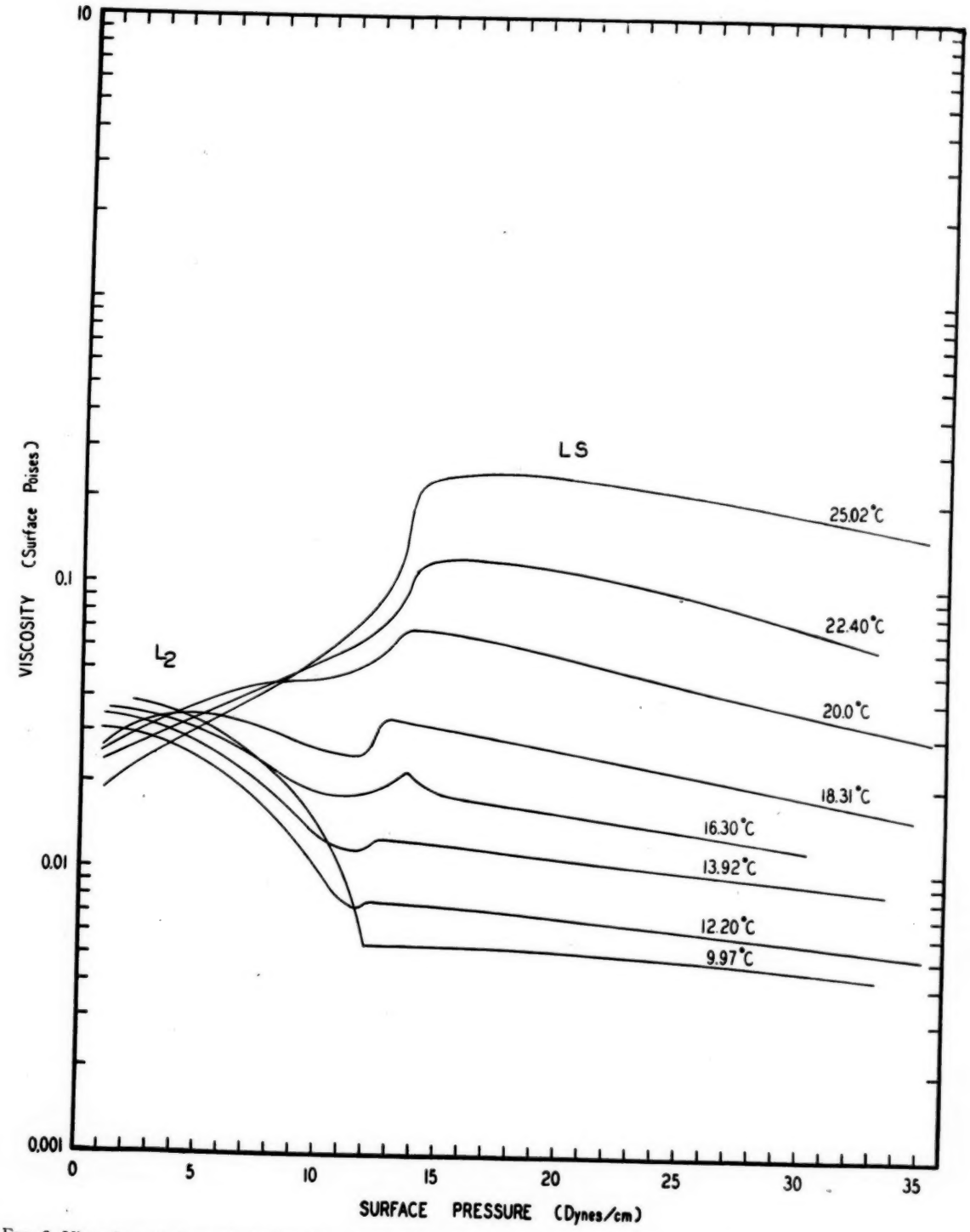

FIG. 3. Viscosity relations of the liquid condensed and *LS* phases of monolayers of octadecanol. Exhibits the normal effect of temperature on viscosity at a pressure of one dyne, and the abnormal effect at the larger pressures. The effects of pressure itself are extremely abnormal.

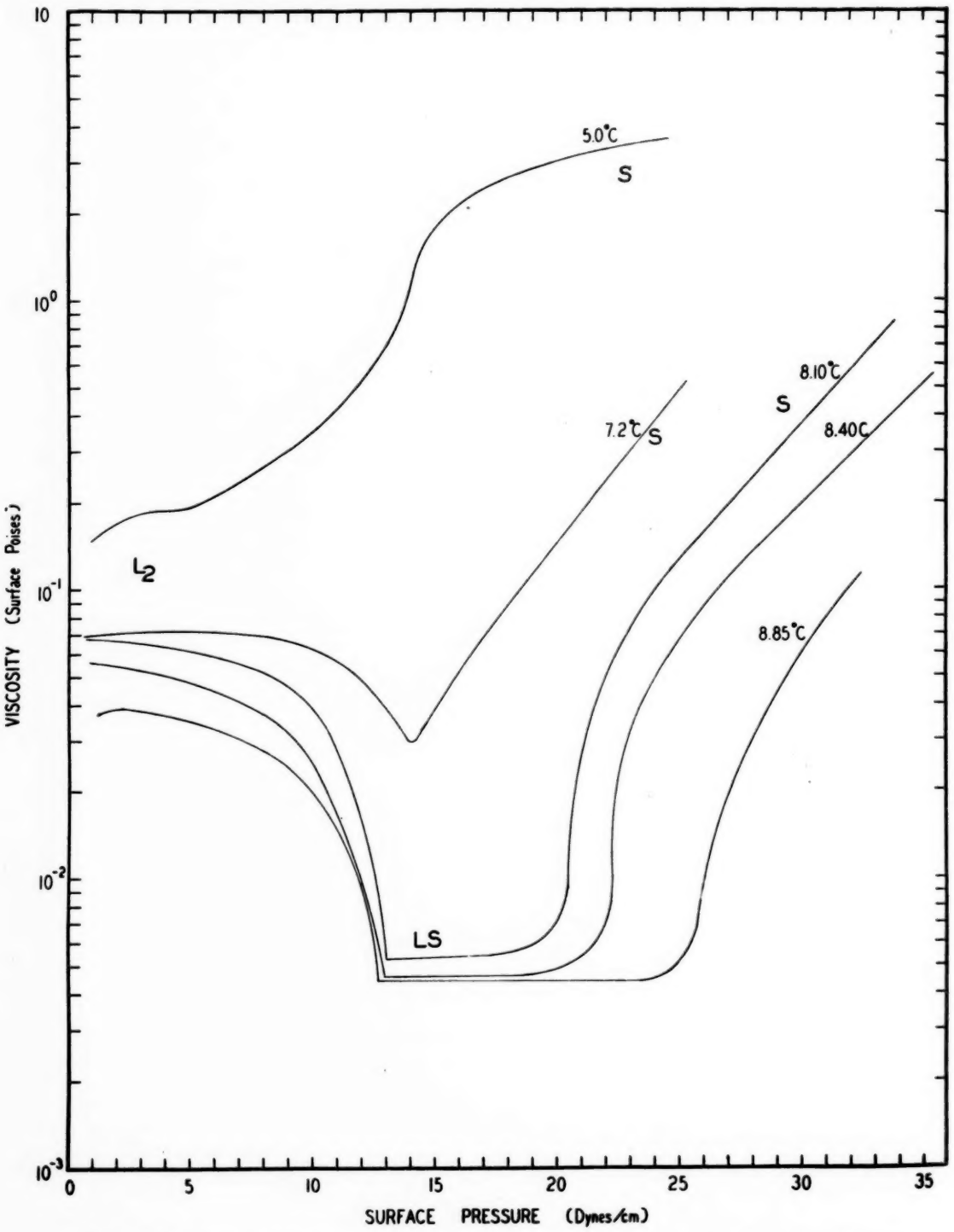

FIG. 4. Viscosity relations of the liquid condensed, and the *LS* and *S* phases of monolayers of octadecanol.

usually gives no hint that a change of phase is to occur until the pressure and area of the second-order transition are attained. In contrast with this, Fig. 1 shows very plainly that the linear relation between pressure and logarithm of viscosity begins to disappear at pressures several dynes below that of the transition, and that the approximately constant viscosity of the high pressure phase does not appear until the pressure is several dynes above that of the transition.

7. While the Newtonian viscosity of the liquid condensed (L_2) monolayer increases rapidly, the non-Newtonian viscosity of the high pressure phase decreases almost as rapidly, as the chain length is increased.

2. ABNORMAL VARIATION OF THE VISCOSITY OF LIQUID CONDENSED PHASE OF AN ALCOHOL WITH TEMPERATURE AND WITH PRESSURE (FIGS. 3 AND 4, AND TABLE I)

Effect of Temperature

At very low film pressures the viscosity of the liquid condensed (L_2) monolayer of a normal long chain paraffin alcohol decreases with increasing temperature, as is normal. Thus the value is about seven times lower at 25°C than at 5°C. However, in Fig. 3 the curves for this phase are seen to cross each other at higher pressures, with the result that at the highest pressures at which this phase exists the viscosity in surface poises decreases from a little over 0.1 at 25°C to about 0.0045 at 8.85°C, or to about a twenty-fifth of its value in a *decrease* of temperature of 16°C. This is extremely remarkable, since in general the viscosity of a phase *rises* rapidly as the temperature is decreased.

As the temperature is decreased still further (Fig. 4), the viscosity of the liquid condensed (L_2) phase, at the highest pressures at which it exists, increases from about 0.045 at 8.85°C to about one surface poise, or the increase is by a factor of about 200 for a temperature increment of 4°C.

Effect of Pressure

At both 5°C and 25°C the effect of pressure upon the viscosity of the L_2 film of octadecanol may be described as normal. As the temperature rises from the lower or falls from the higher value, the effect becomes increasingly abnormal as 9°C is approached. At 9.97°C the viscosity decreases with increasing rapidity, from about 0.04 at low pressure to 0.005 surface poise at a pressure of 12 dynes cm^{-1}. At 8.10°C the decrease is from 0.07 to slightly below 0.006 surface poise by an increase of pressure to 13 dynes cm^{-1}. This behavior is extremely abnormal since the viscosity is reduced to an eighth or tenth of its value by an increase of pressure which should give threefold or fourfold increase.

TABLE I. Surface viscosity of octadecanol[a] (in surface poises).

t° C	Pressure (dynes/cm) 1	10	18	25
5.1°	0.150	0.352	2.65	—
7.2	.0700	.0620	0.0890	0.490
8.1	.0673	.0392	.00555	.126
8.4	.0560	.0250	.00450	.0655
8.8	.0370	.0196	.00440	.00515
10.0	.0390	.0136	.00530	.00493
12.2	.0302	.00955	.00710	.00620
13.9	.0340	.0127	.0115	.0102
16.3	.0357	.0187	.0170	.0140
18.3	.0270	.0260	.0292	.0207
20.0	.0260	.0457	.0612	.0452
22.4	.0238	.0532	.1020	.0935
25.0°	0.0192	0.0570	0.249	0.206

[a] Note that at a film pressure of one dyne per cm the viscosity decreases with increasing temperature, as is normal, from 0.150 poise at 5.1° to 0.0192 at 25°C. At 10 dynes per cm the viscosity decreases (normal) from 0.352 at 5.1° to 0.0096 poise at 12.2°C, but increases (abnormal) from this temperature up to 0.0570 at 25°C. In all of the above changes the monolayer is in the liquid condensed (L_2) state. At 18 dyne cm^{-1} the viscosity in the S state decreases with extreme rapidity with increase of temperature, from 2.65 poises at 5.1° to 0.0890 poise at 7.2° and still lower. Then a transition to the LS state occurs, after which the viscosity falls much more slowly to a minimum of not far from 0.0044 poise at about 8.8°C. Then the direction of the change changes and the viscosity of the LS phase increases rapidly with increase of temperature (abnormal) until it becomes 0.249 at 25°C.

3. A SUPERLIQUID PHASE WITH EXTREMELY ABNORMAL VISCOSITY RELATIONS

Figures 3 and 4 indicate the existence of a new phase which exhibits extremely remarkable viscosity relations as follows:

1. Although the viscosity is Newtonian, it is essentially independent of pressure. In this constancy of viscosity with increase of pressure, it resembles solid monolayers, which, however, have a non-Newtonian viscosity.

2. Although the phase exists in the same range of high pressures as the S (usually designated as solid) phase, its viscosity at temperatures of 8

to 12°C is much lower than that which is exhibited at low pressures by the liquid (L_2) phase from which it is formed by increase of pressure.

3. The viscosity of this phase is lowest at those temperatures at which it is formed by a *first-order* transition from the liquid condensed (L_2) phase, by increase of pressure.

4. As the temperature is increased in the range of the second-order transition $L_2 \rightarrow LS$, the viscosity rises very rapidly and takes on more and more the characteristics commonly exhibited by the S phase, although there seems to be no indication of any change of phase. At 25° the viscosity of the LS phase has become non-Newtonian, high (*ca.* 0.25 surface poise), and decreases slightly with increase of pressure. Since the viscosity is non-Newtonian, the value cited refers to the rate of shear employed in this work. A Couette type of apparatus has been designed and will be used later to determine the relation between viscosity and rate of shear.

4. THE TRANSITION $L_2 \rightleftharpoons LS$ AND $LS \rightleftharpoons S$ AS REVEALED BY ABRUPT CHANGES IN VISCOSITY

At temperature between 8 and 10° (Figs. 3 and 4 and Table II) the slope ($\partial \log \eta / \partial \pi$) takes on an extremely large negative value as the pressure approaches about 13 dynes cm^{-1}, but at this pressure changes abruptly to zero. The pressures and temperatures of these abrupt changes correspond to phase transitions from the condensed liquid to a high pressure phase as revealed by the pressure-area ($\pi - \sigma$) diagram of Fig. 2, Paper I. At 8.10, 8.40, 8.85, and 9.97°C the viscosity remains constant for increases of pressure of 4, 5.5, 11, and more than 22 dynes cm^{-1}, respectively.

TABLE II. Effect of pressure on $d \log_{10} \eta / d\pi$.

π	Temperature (°C) 5.1°	7.2°	8.85°	10.0°	25.0°
1	0.0732	0.00647	0.0529	−0.00448	−0.0684
3	.0245	.00487	−.0162	− .0187	.0470
5	.0292	−.00268	−.0228	− .04282	.0470
7	.0494	−.00652	−.0355	− .07560	.0551
9	.0634	−.0216	−.0741	− .08145	.0570
11	.0840	−.0534	−.1412	− .0945	.0701
13	.125	−.0998	.00037	− .000315	.0180
15	.109	.129	.00037	− .000408	.0126
17	.046	.114	.00037	− .00235	.00418
19	.0232	.106	.00037	− .00386	− .00779
21	0.0187	.106	.00037	− .00477	− .0107
23	—	.106	.00037	− .00586	− .0123
25	—	0.106	.1355	− .00724	− .0130
27	—	—	.2304	− .00805	− .0140
29	—	—	.1426	− .00797	− .0140
31	—	—	0.1132	−0.00870	−0.0156

η = surface viscosity in surface poises.

At all of these temperatures except the highest the viscosity begins to increase rapidly at the end of these intervals, and at 8.10° and 8.40°C the slope of the curve takes on an almost infinite *positive* value, after which it decreases, but remains high.

The most obvious explanation of this extremely high slope is that it corresponds to a phase transition, which would seem to be from the LS to the S phase. This assumption is the basis for the inclusion, in Fig. 3 of Paper I, of a boundary between these two phases, which, as obtained from the viscosity relations, is found to be linear, with a slope which indicates a rise in the transition pressure of 6.4 dynes cm^{-1} per degree C.

The evidence for the existence of the transition from the LS to the S phase is not that of the viscosity alone, since the effect of the transition is apparent in the entropy and energy relations. These exhibit discontinuities at this transition, and also at that between the L_2 and S phases. At a molecular area of 19.98A^2 the $L_2 \rightleftharpoons S$ transition occurs at a pressure of 17.61 dynes cm^{-1}, and the $LS \rightleftharpoons S$ transition at 23.73 dynes cm^{-1}. These pressures agree with those obtained from the viscosity relations.

5. ABNORMAL VISCOSITY RELATIONS OF MONOLAYERS OF EICOSANOL (FIG. 5)

The pressure-area relations indicate that the temperature of the first-order transition rises about 5°C per carbon atom added to the hydrocarbon chain of an alcohol. Thus with 20 C atoms (eicosanol) the general viscosity diagram ($\eta - \pi - T$) at 20° should resemble that of the 18 C alcohol (octadecanol) at 10°C, and this is found to be true, as shown plainly by Fig. 5. The lowest viscosity with 18 C atoms was found at 8.85°C, and had a value of 0.0045 surface poise for the LS phase. At 20.0°C with 20 C atoms the viscosity is 0.01 surface poise, but the temperature of the minimum viscosity is

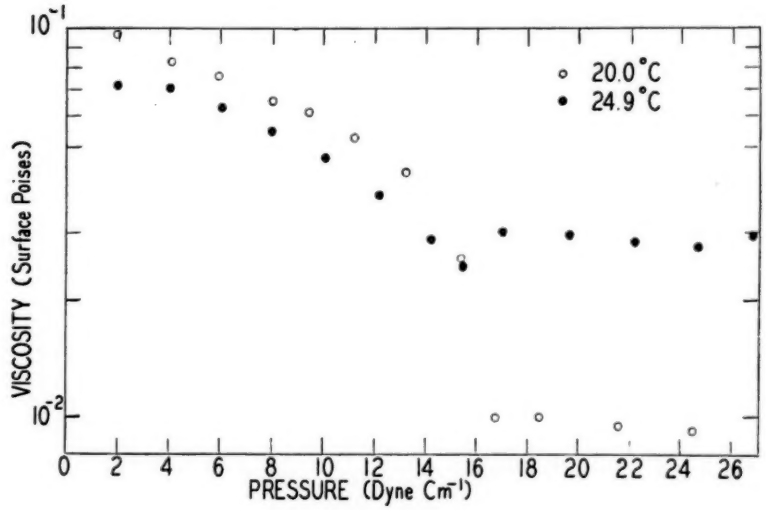

FIG. 5. Viscosity of the low (L_2) and high (LS) pressure phases of the normal long paraffin chain 20 carbon atom alcohol. Note that the curves cross each other. The relations are similar to those of the 18 carbon alcohol at a lower temperature.

probably slightly lower than this. At a temperature 5° higher (24.9°C) the viscosity of this phase is 0.03 surface poise. The L_2 phase exhibits the same relation of exhibiting a high viscosity at low pressure, which decreases rapidly with increase of pressure, as was found with the shorter chain alcohol. Also, there is to be seen in the curve at 24.9°C the same lowering of the viscosity below that of the LS phase just before the L_2 phase is transformed into it by increase of pressure. Whether or not this represents a failure to obtain equilibrium quickly enough has not been determined.

Since the $\pi-\sigma$ diagram indicates that the pressure of the transition $L_2 \rightleftarrows LS$ is increased by increase in the number of carbon atoms, it is to be expected that this will be revealed in the viscosity relations also. This is shown in Fig. 5 to be true, since the viscosity changes its slope from highly negative to zero at 16.7 dynes cm^{-1}, while with octadecanol this occurs at 12.6 dynes cm^{-1}.

Thus the phase transitions, the energy relations, the compressibility, and the viscosity are very much the same for monolayers of the 18, 19, and 20 C atom alcohols in their relation to the pressure, area, temperature region in which the first-order phase transition occurs.

6. DISCUSSION

The molecular area at which the transition $LS \rightleftarrows S$ occurs in octadecanol seems to be almost independent of pressure and temperature, and what little work has already been done with the 20 C alcohol seems to indicate that the area for its similar transition is almost the same. Also, the range in area of the first-order transition seems to be affected only slightly by an increase in the number of carbon atoms, while both the pressure and the temperature are increased materially. These facts seem to suggest that the mechanism involved is extremely sensitive to the distance between the molecules in the monolayer. Furthermore, since similar abnormalities in pure three-dimensional liquids involve only minor changes of viscosity, the enormous effects found here would seem to be associated with the presence of the aqueous subphase. This can effect the relations in two ways:

1. By orientation of the molecules, the hydroxyl groups (also the hydrocarbon chains) of the alcohols are brought into proximity.

2. The hydroxyl groups are brought into contact with molecules of water.

By (1) there could be some type of bonding between the hydroxyl groups of the alcohols, or by (2) between these groups and the water.

To explain the results, it is necessary to assume a type of bonding which is extremely sensitive to changes of intermolecular distance. In either (1) or (2) hydrogen bonding is likely to be involved, but it seems advisable to await the accumulation of further data before attempting to discover if the formation and dissolution of these bonds can be made to accord with all of the bizarre relations presented here. The transition $S \rightleftharpoons LS$ takes place at a molecular area not far from 19.98A² at any pressure at which both phases are stable. This corresponds to a temperature close to 8.6°C. The curve in Fig. 4 which is the nearest to this temperature is that at 7.2°C. At this temperature the viscosity of the L_2 phase is almost constant with increase of pressure up to 9 dynes cm^{-1} and then decreases more and more rapidly until at 14 dynes cm^{-1} the monolayer changes directly into the S phase. At the transition point the viscosity is slightly less than 0.03 surface poise, but that of the S phase rises rapidly with pressure, until at 25.5 dynes cm^{-1} it is 0.5 surface poise.

At 8.85°C and 16 dynes cm^{-1} the molecular area is 20.0A² and the viscosity, which is that of the LS phase, is 0.0044 surface poise. If at this pressure the molecular area of this phase is increased to 20.75A² by increase of temperature, the viscosity increases by a factor of 55 to 0.2400. *Thus the binding is increased greatly by an increase of molecular area and temperature, both of which should normally decrease it very greatly.*

The extremely high fluidity of the LS film is exhibited only when the molecules are tightly packed and when the temperature is relatively low. Increase of molecular distance is accompanied by an extremely rapid rise of viscosity. Thus at a pressure of 16 dynes cm^{-1} the viscosity is increased 55 times by *increase* of 0.07A in mean molecular distance.

While the viscosity of the condensed liquid (L_2) phase of the alcohols decreases at low pressures with the temperature, which is normal, this is reversed at high pressures. At higher and lower temperatures, increase of pressure gives the normal increase of viscosity with pressure, but at intermediate temperatures the viscosity decreases more and more rapidly as the pressure increases, until finally a phase transformation occurs.

The behavior of liquid sulfur, in a three-dimensional system, presents some features which are analogous. The viscosity decreases from 0.1094 to 0.0709 poise[4] with increase of temperature from 123° to 149.5°C. At 160°C the value of $(\partial\eta/\partial T)_p$ becomes extremely high, and at 200° the viscosity itself attains the extremely high value of 21,500 poises, after which it decreases with rise of temperature. Farr and McLeod attribute this rapid increase of viscosity with temperature to a rapid increase in the percentage of S_8 in liquid S in this temperature range as found by Smith and Holmes, and by Carson.[5] Rhombic or monoclinic sulfur is considered by Warren and Buswell[6] to consist of puckered 8-atom rings, with an S−S distance of 2.12A, but closest distance of approach of atoms in adjoining rings of 3.3A. They explain the increase of viscosity with increase of temperature to breaking of the rings. Ewell and Eyring[7] find the slope $(\partial \log \eta)/\partial(1/T)$ to be much larger above 250° than at 160°C and calculate the unit of flow at the higher temperature to be about S_{36}. The viscosity increase above 160°C for sulfur is much larger than that of the LS film above 8.85°C. Unfortunately, the effect of pressure upon the viscosity of liquid sulfur has not been investigated.

If the logarithm of the surface viscosity of the liquid condensed film of octadecanol at a pressure of 1 dyne cm^{-1} is plotted against the reciprocal of the absolute temperature, a curve is obtained with two linear portions: one below 10°C and the other above 18°C. These indicate heats of activation for viscous flow of 38,400 and 12,100 cal. mole, respectively. For stearic acid monolayers, Moore and Eyring obtained values from 12,100 to 16,150 cal. $mole^{-1}$ and concluded, since these values are two to three times larger than for stearic acid in bulk, that the unit of flow is not a single molecule of stearic acid.

If the logarithm of the viscosity of the LS phase is plotted against various functions of the

[4] C. C. Farr and D. B. McLeod, Proc. Roy. Soc. **97**, 80 (1920).
[5] A. Smith and Holmes, Zeits. f. physik. Chemie **54**, 257 (1905); C. M. Carson, J. Am. Chem. Soc. **29**, 499 (1909).
[6] B. E. Warren and J. T. Buswell, J. Chem. Phys. **3**, 6 (1935).
[7] R. H. Ewell and H. Eyring, J. Chem. Phys. **5**, 726 (1937).

temperature is is found that linearity is obtained at temperatures above 12°C at pressures of 18 dynes cm^{-1} if the function chosen is the temperature (Fig. 6), and is almost as linear *versus* the reciprocal of the temperature.

The *S* phase of the alcohols is the only one of their three condensed phases which exhibits normal viscosity relations. In both the *S* and the *LS* phases the molecules may be assumed to be oriented perpendicular to the surface. In three-dimensional crystals the hydrocarbon chains occupy an area of 18.5A^2, in the *S* alcohol films from 19.5 to 20.0A^2, in the *LS* films from 20 to 20.75, and in the L_2 films from 19.8 to 22.7. The highest temperature employed was 35°C. An increase above this temperature would increase the upper limits of area for the *LS* and L_2 monolayers. It is obvious, as has been mentioned earlier, that the possibility exists for hydrogen binding between the −OH groups of the alcohols themselves, or between these groups and the water molecules. What is needed for the explanation of the abnormal relations of the L_2 and *LS* phases of the alcohols is to determine what type of binding will increase in energy as the molecular distance is increased, either by increase of temperature or decrease of pressure. The distance between the two heavier nuclei at the ends of a hydrogen bond is in the range from 2.5 to 2.8A.

The non-Newtonian viscosity of a monolayer of methyl pentadecylate in what is usually designated as the *S* phase, is about 0.2 surface poise, and is somewhat lower than that of the acid or alcohol with 15 or 16 C atoms in the normal chain. Since the ester should not exhibit

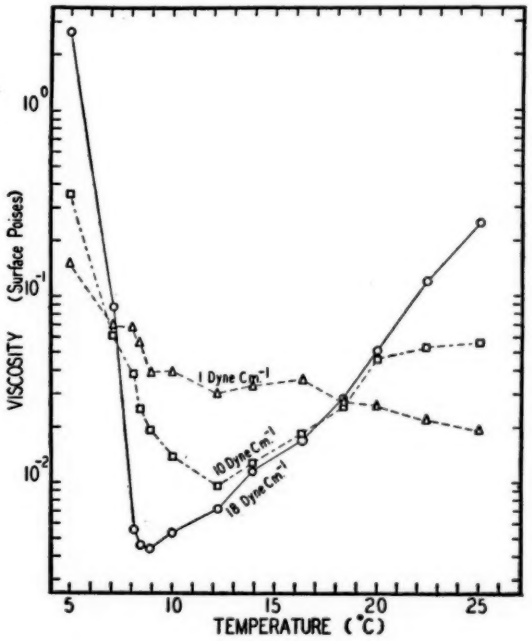

FIG. 6. Relation between the logarithm of the viscosity and the temperature of a monolayer of octadecanol at pressures of 1, 10, and 18 dynes cm^{-1}.

hydrogen bonding between molecules in the monolayer itself, it is unfortunate that the viscosities in the liquid condensed state have not been determined.

This publication was made possible by funds granted by the Carnegie Corporation of New York. That Corporation is not, however, the author, owner-publisher, or proprietor of this publication, and is not to be understood as approving by its grant any of the statements made or views expressed therein.

Mechanism of the Thermal Reaction Between Hydrogen and Oxygen[1]

GUENTHER VON ELBE[2] AND BERNARD LEWIS[3]
Bureau of Mines and Carnegie Institute of Technology, Pittsburgh, Pennsylvania

(Received January 24, 1942)

Explosion limits and reaction rates of hydrogen and oxygen have been measured in spherical quartz and Pyrex vessels of varying diameter, clean and coated with various substances and for various temperatures, pressures, and mixture compositions, including addition of inert gases. Clean and B_2O_3-coated surfaces give rise to rapid and erratic reaction, indicating a surface chain-breaking efficiency $\epsilon \ll \lambda/d$ (ratio of mean free path to vessel diameter); the reaction is self-accelerating, probably due to poisoning of the surface by H_2O, which decreases ϵ. By coating with various salts such as KCl, $BaCl_2$, $K_2B_2O_4$, $K_2B_4O_7$, and Na_2WO_4, the condition $\epsilon \gg \lambda/d$ is established in the region between second and third explosion limits. The limits are farther apart, the rates much lower and not accelerating, and both rates and limits are reproducible and identical for the various salts. For $K_2B_4O_7$, $\epsilon \backsimeq \lambda/d$ for small reaction rates. The chain-breaking mechanism on clean and salt-coated surfaces is discussed. With the elimination of the surface as a variable by coating with salts, data of explosion limits and rates can be used to derive the mechanism of the reaction. From a critical analysis of all imaginable reactions of the system and the present and earlier experimental results, the following mechanism is deduced.

i. $H_2O_2+M=2OH$
1. $OH+H_2=H_2O+H$
2. $H+O_2=OH+O$
3. $O+H_2=OH+H$
6. $H+O_2+M=HO_2+M$
11. $HO_2+H_2=H_2O_2+H$
12. $2HO_2 \xrightarrow{\text{surface}} H_2O_2+O_2$
5. $H+O_2+H_2O_2=H_2O+O_2+OH$
7. $HO_2+H_2O_2=H_2O+O_2+OH$
13. $H_2O_2 \xrightarrow{\text{surface}} H_2O+\frac{1}{2}O_2$
14. $H_2+O_2 \xrightarrow{\text{surface}} H_2O_2$

$H, O, OH \xrightarrow{\text{surface}}$ destruction

The surface destruction of H, O, and OH is important only at the first explosion limit and depends on the nature of the salt. Reaction 2 leads to chain branching by the formation of two new free valences. It is counteracted by reaction 6. H_2O is a much more efficient third body than any other molecule investigated and, therefore, powerfully suppresses chain branching. Hence, explosions and reaction rates near the explosion limits are strongly inhibited by H_2O, either added or formed during the reaction. If H_2O is formed during the preparation of the mixture in the reaction vessel, the rates and limits measured may be very different from the values in the H_2O-free mixtures, particularly near the junction of second and third explosion limits. An opposite effect is caused by the temperature rise in rapid reaction noticeable near the third limit above the junction. The superposition of both effects explains the deviation of the actual explosion boundary from that predicted by the isothermal explosion condition for H_2O-free mixtures. In the range free from these influences, rates and explosion limits over wide ranges of all variables are well represented by the kinetic equations derived from the above mechanism after suitable numerical constants are introduced. A tentative equation of the course of the reaction in uncoated vessels assuming constant surface structure has been derived, which is similar to the empirical equation of Chirkov. The conclusion of Oldenberg and Sommers that the reaction is unbranched is shown to be invalid due to masking of branching by H_2O in their experiments. *Values of activation energies and rate coefficients of all reactions except 1 and 3 and concentrations of* HO_2 *and* H *are given.*

THE general features of the thermal reaction between hydrogen and oxygen have been well-established and described in earlier investigations. However, establishment of the reaction mechanism has been handicapped by lack of quantitative data. This is remedied in the present experimental investigation which, moreover, has brought out additional significant facts, and it is now possible to arrive at a comprehensive solution of the problem of the reaction mechanism.

I. APPARATUS AND EXPERIMENTAL PROCEDURE

The apparatus used (Fig. 1) was, with some modifications, the same as in a previous investigation.[4] Exclusively spherical quartz or Pyrex vessels were used, coated with various materials

[1] Published by permission of the Director, Bureau of Mines, U. S. Department of the Interior, and the Director, Coal Research Laboratory, Carnegie Institute of Technology.

[2] Coal Research Laboratory, Carnegie Institute of Technology, Pittsburgh, Pennsylvania.

[3] Senior Physical Chemist, Physical Chemistry Section, Central Experiment Station, Bureau of Mines, Pittsburgh, Pennsylvania.

[4] H. R. Heiple and B. Lewis, J. Chem. Phys. **9**, 584 (1941).

described below. They were placed in the center of a cylindrical furnace whose temperature was controlled to 0.1°–0.2°C. The temperature was measured with a chromel-alumel thermocouple made of Bureau of Standards calibrated wire, and frequently checked against the melting point of pure electrolytic zinc. The junction of the thermocouple was mounted close to the vessel in the plane of its center. The temperature dropped somewhat above this point. In vessels smaller than 10-cm diameter the temperature could be considered reasonably uniform. The bottom of the 10-cm vessel extended somewhat into a region 2° or 3°C below that registered by the thermocouple, which was a source of slight error in the explosion limit and rate determinations but was not considered important enough to warrant reconstruction of the furnace. Mixture compositions and reaction rates were corrected for the small dead space of the capillary inlet tube to the vessel, most of which was heated to prevent condensation of water. As a rule, the gases were admitted separately to the reaction vessel through special bellow-type stainless steel needle valves without packing. Between runs, the vessel was evacuated with a Hyvac pump and flushed with the first gas to be admitted in the next experiment. Separate admission of the gases is necessary because of the phenomenon of the low pressure explosion region. The pressure of the first gas to be admitted, usually hydrogen, must be so chosen that on subsequent admission of oxygen the pressure always exceeds the second explosion limits of all intermediate mixtures that are formed. To measure reaction rates, hydrogen was admitted to the desired pressure read on a mercury manometer to 0.1 mm; inert gases, when used, were similarly admitted; oxygen was then admitted as rapidly as possible, the total pressure being read by means of a sensitive quartz spiral differential manometer (9 spirals, 1.2-cm diameter) which was connected directly to the vessel. The movement of the pointer, etched to a fine point, was observed through a microscope against a scale of 100 divisions, readable to 0.1 division, one division corresponding to 0.466 mm Hg. After the desired pressure was attained (usually in 20 to 30 seconds) the vessel valve was closed, and the movement of the pointer caused by pressure decrease of the reacting mixture was

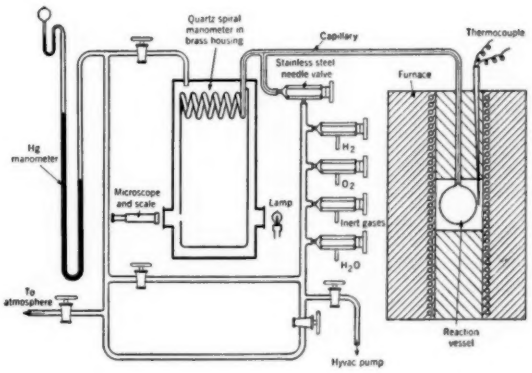

FIG. 1. Apparatus.

read in measured time intervals. All reaction rates in this paper are expressed as decrease of pressure in mm Hg per minute.[5] Second explosion limits were determined, whenever feasible, by the withdrawal method in which the gases were admitted as before and the evacuation observed with the quartz spiral manometer until a sudden kick of the pointer took place, followed by rapid movement of the latter toward lower pressure, corresponding in most cases to complete reaction. The explosion was audible, except at low pressures, and was accompanied by a flash of light. Explosion limits near the junction of first and second limits were determined largely by the heating method: A mixture was admitted at a temperature outside the explosion region and the vessel was heated until a sudden rapid pressure decrease occurred, indicative of explosion. This method gave the same results as the withdrawal method but was not feasible at higher temperatures because it was too slow to prevent inhibition of explosion by water formed in the rapid reaction close to the limit (Section IIIa); here, limits were determined with utmost speed by a modification of the withdrawal method: The mixture was made up within 3 or 4 seconds by admitting oxygen from a reservoir at a predetermined pressure and immediately connecting the reaction vessel to another reservoir at some set lower pressure. Depending on the latter pressure, explosion, manifested by a sharp click and

[5] Reaction between H_2 and Pyrex glass (cf. Williams and Ferguson, J. Am. Chem. Soc. **44**, 2160 (1922) and Roberts and Bittner, *ibid.*, **63**, 1513 (1941)) was found to be negligibly small under conditions of the present experiments. Also, the results were not affected by mercury vapor from the manometer.

a flash of light, did or did not occur. A series of such trials was required to determine the limit. The time between opening the oxygen valve and explosion was 10 to 14 seconds. At high temperature, even this procedure did not prevent the formation of some water sufficient to lower the second limit appreciably (Section IIIa). The third explosion limit was determined simply by admitting oxygen from the reservoir in the same manner and waiting for explosion. Here, too, a series of trials established the limit. Dynamic effects of the explosions were never sufficient to fracture the vessel or the quartz spiral.

TABLE I. Consecutive observations of reaction rates and second explosion limits in a clean quartz vessel. Vessel diameter, 3.9 cm; temperature, 520°C. Initial and peak rates in mm Hg pressure decrease per min. Gases admitted to vessel in order listed in columns 2 except run 6 second series, where O_2 was admitted first. The time (column 4) is taken from beginning of run (including about ½ minute for admission of O_2) to attainment of peak rate. Where run was not prolonged to peak rate the last rate taken and time of run are bracketed. Runs 1–4 second series are shown more completely in Fig. 2. After each run vessel was evacuated with Hyvac pump and flushed with first gas admitted. No flushing after runs 1, 7, and 9, second series. Runs 1, 7, 14, and 16, second series continued for about 12 hours. Several weeks elapsed between the two series.

Run No.	Initial partial pressures, mm Hg H_2O	H_2	N_2	O_2	Peak rate, $-dp/dt$, mm/min.	Time to peak rate, min.	Initial rate, $-dp/dt$, mm/min.
1st series							
1		150		150	0.8	78	0.15
2	3.5	150		150	1.5	14	0.64
3		150		150	1.7	47	0.11
4	3.7	150		150	1.7	18	0.47
5	14.3	150		150	2.7	7	1.6
2d series							
1		210		105	2.7	30	0.2
2	10	200		100	5.4	2.5	4.7
3	10	200	200	100	5.3	4.5	3.9
4	10	200		100	4.0	6.0	2.3
5		200		100	3.3	22	0.25
6		200		100	3.3	14	1.0
7		200		100	(1.9)	(21)	0.24
8	10	200		100	6.5	3	5.1
9	10	200		100	5.0	6	2.8
10	10	200		100	4.0	8	1.2
11		210		105	(1.3)	(20)	0.16
12		210	200	105	(2.1)	(20)	0.30
13		210		105	(0.31)	(37)	0.09
14		210		105			0.10
15	Second explosion limit for $2H_2+O_2$: 83 mm						
16		210		105			0.09
17		210		105			0.10
18	10	200		100	(0.27)	(121)	0.10
19	10	200	200	100			0.09
20	10	200		100			0.09
Vessel etched for ½ min. with 30 percent HF							
21	10	200		100	(0.19)	(14)	0.22
Vessel etched for 8 minutes with 30 percent HF							
22	10	200		100	6.7	5	3.5
23		210		105	7.5	4.9	1.5
24		210		105	8.3	4.6	1.4
25	10	200		100	(0.9)	(13)	0.4
26	Second Explosion Limit for $2H_2+O_2$: 91 mm						
27	10	200		100	(1.3)	(5.5)	0.80
28		210		105	(1.0)	(6.5)	0.60

The process of mixing was rapid, as was confirmed in the following manner. An outlet tube was affixed to the vessel opposite the inlet tube; the system was filled with hydrogen and a prepared mixture of hydrogen and oxygen was drawn through, the pressure during this operation being well above the second explosion limit; after sufficient flushing the pressure was reduced until explosion occurred. The results were identical with those obtained by the formerly described procedure and the most rapid manipulation, confirming the absence of inhomogeneities in the mixture a second or two after the admittance of oxygen. The attainment of temperature equilibrium after the admittance of gases was also a rapid process (of the order of 2 or 3 seconds), as was ascertained by a special test in which a thermocouple was sealed into the vessel. During admission of gas the temperature increased a little (1° or 2°C) above that of the furnace, showing that the gas had been effectively pre-heated in the capillary tubing and was further heated by compression; the temperature then decreased rapidly to that of the furnace.

Gas currents incidental to the admission of gas to the reaction vessel subsided rapidly, as shown by fine dust particles. Thermally induced convection currents hardly affect the rate of transport of chain carriers to the surface, even in rapid reaction, because temperature equilization is rapid and the average time of diffusion of a chain carrier from the center to the wall is only of the order of a second (Section VI).

Tank electrolytic hydrogen and oxygen were used. Hydrogen was passed through an outgassed charcoal trap in liquid air; oxygen was passed over heated platinum asbestos and dried over magnesium perchlorate. Tank nitrogen (99.7 percent) and tank argon (*ca.* 99 percent) were used; CO_2 was purified by discarding a large fraction of the contents of a full tank; these gases were also dried over magnesium perchlorate. Helium was treated in the same manner as hydrogen. Water vapor, at desired pressures up to saturation at room temperature, was admitted from a

reservoir before other gases. Chemicals used for coating the vessel were C.P. commercial products.

II. THE ROLE OF THE SURFACE OF THE VESSEL AND THE ELIMINATION OF THE NATURE OF THE SURFACE MATERIAL AS A VARIABLE BY COATING WITH VARIOUS SALTS (HIGH CHAIN-BREAKING EFFICIENCY)

The capricious behavior of the reaction in clean quartz or Pyrex vessels, which has been noted previously,[6] is shown in the series of observations in Table I and Fig. 2.

The reaction is seen to be self-accelerating until slowed, evidently by consumption of the reactants. Addition of water vapor sometimes appears to increase the initial rate and shorten the time to peak rate (first series; second series runs 1 and 2, 7 and 8, 10 and 11; cf. Prettre; Hinshelwood and Thompson);[6] sometimes the effect is not observed (17 and 18, 22 and 23, 24 and 25, 27 and 28). Rates may differ widely in runs of seemingly identical conditions (second series 1, 11, and 13, 8–10, and 18), no cause being apparent. After a series of high rates, the rates suddenly become low (13–20, 25) and fairly reproducible.[7] The former activity can be restored by etching the vessel with HF. Allowing the reaction to proceed over a long period (12 hours) had no effect (16 and 17; Oldenberg and Sommers once found a decrease of the rate). Notable is the absence of a significant inert-gas effect (second series, 3, 12, 19). Studies of vessel size effects are not feasible due to irreproducibility of the rates.[8]

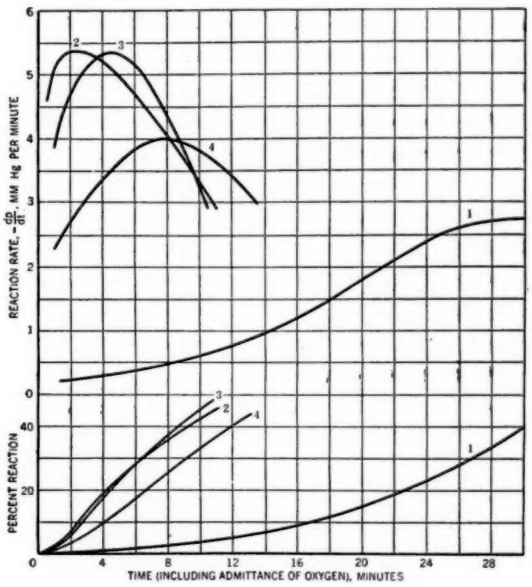

FIG. 2. Reaction rates in clean quartz vessel. Vessel diameter, 3.9 cm; 520°C.

		Initial pressures, mm Hg, in order of admission to vessel:			
		H_2O	H_2	N_2	O_2
Consecutive runs	1		210		105
	2	10	200		100
	3	10	200	200	100
	4	10	200		100

If the vessel is coated with any of a number of salts the rates are found to be, (a) as a rule, not self-accelerating[9] but constant until slowed down by consumption of reactants; (b) much slower[10] (1/100 to 1/1000 of rates in uncoated vessels); and (c) except at low pressures and temperatures, well-reproducible and identical for various chemically unrelated salts, such as potassium chloride, potassium tetraborate, potassium metaborate, barium chloride, and sodium tungstate. These facts are shown in Fig. 10. Furthermore, (d) the rates are strongly increased on adding inert gas[11,12] (Fig. 9) and by increase of vessel diameter (Fig. 10).

[6] Hinshelwood and Thompson, Proc. Roy. Soc. **A118**, 170 (1928); Pease, J. Am. Chem. Soc. **52**, 5106 (1930); Prettre, J. Chem. Phys. **33**, 189 (1936). Chirkov, Acta Phys. Chim. (U.S.S.R.) **6**, 915 (1937).

[7] This was also the experience of O. Oldenberg and H. S. Sommers, J. Chem. Phys. **9**, 432 (1941).

[8] Hinshelwood and Thompson, reference 6, found the rate to be suppressed by packing. Hinshelwood and Williamson, (*Reaction Between Hydrogen and Oxygen* (Oxford, 1934)) reported a series of rate measurements at 560°C for $2H_2+O_2$ mixtures at 600-mm pressure in silica bulbs of 1.7- to 7.7-cm diameter showing the rate to increase approximately with the square of the diameter. They also reported no difference in the rates in a clean and a KCl-coated silica bulb at 560°C, a result which was formerly quoted (B. Lewis and G. von Elbe, *Combustion, Flames and Explosions of Gases* (Cambridge, 1938), p. 41) to support the assumption that chain initiation changes with increasing temperature from a surface to a gas phase reaction, but which could not be confirmed by Heiple and Lewis (unpublished) in repeated trials; see also Prettre, reference 6, and Oldenberg and Sommers (J. Chem. Phys. **8**, 468 (1940)). It is possible that in H and W's experiments the KCl had distilled out of the vessel (see below) or that the uncoated bulb was accidentally covered with a film of some efficient chain-destroying material, or that much of the mixture had reacted in the uncoated vessel while admitting the oxygen. The vessel-size experiments were possibly also so affected because in an uncoated vessel of 7.7-cm diameter at 560°C and 600-mm pressure, one would expect a third-limit explosion instead of a rate, unless a considerable part of the gas reacted while admitting oxygen (cf. Section IVa).

[9] For exceptions, cf. Section IVc.

[10] This was first reported by Pease (reference 6).

[11] Except in small vessels at low temperatures and pressures (Table VII, Section IVd), and on addition of H_2O near the explosion limits (Section IVa).

[12] Gibson and Hinshelwood (Proc. Roy. Soc. **A119**, 591 (1928)) in Worcester porcelain vessel. Porcelain contains

The facts point to a chain reaction with destruction of chain carriers at the wall. Accordingly, in clean quartz vessels the chain-breaking efficiency ϵ (the fraction of destructive collisions to all collisions of chain carriers with the wall) is small compared with the ratio of mean free path to vessel diameter, λ/d; under these conditions, most chain carriers reaching the wall diffuse back into the gas phase and maintain an almost uniform concentration throughout the vessel,

$$n = n_0/[(3\epsilon\bar{v}/2d) - \alpha],^{13} \qquad (1)$$

where n_0 is the rate of chain initiation in the volume, $\bar{v}$ the average molecular velocity, and α the rate of chain branching. n is independent of inert gas like N_2 or A, except insofar as such addition affects n_0 and α,[14] ϵ presumably being unaffected. It is sensitive to changes of the surface-dependent quantity ϵ;[15] the erratic behavior of the rate, therefore, evidently reflects obscure changes of the surface. The self-acceleration of the rate suggests a progressive decrease of ϵ due to surface poisoning by water formed during the reaction. This effect predominates over two opposing effects, namely, consumption of the reactants and inhibition of chain branching by water (reaction 6, Section IIIa). The surface-poisoning effect of water is substantiated by the experiments with added water vapor, although it sometimes appears to be vitiated by superimposed obscure surface changes. In salt-coated vessels, on the other hand, $\epsilon \gg \lambda/d$, in which case most chain carriers that reach the wall are destroyed there and the rate is greatly reduced. As long as this condition is fulfilled, changes of ϵ such as may occur on substituting one salt coating for another do not appreciably affect the rate of chain destruction. The latter is governed by the rate of diffusion of chain carriers to the wall, the chain-carrier concentration being highest at the center of the vessel. The average chain-carrier concentration $\bar{n}$ is satisfactorily represented[16] by the equation

$$\bar{n} = 6n_0/\pi^2/[(4\pi^2 D/d^2) - \alpha], \qquad (2)$$

which contains no terms that depend on the nature of the surface and predicts an increase of the rate by addition of inert gas (the diffusion coefficient D decreases with increasing pressure) and by increase of vessel diameter.

Boric acid as a coating material behaves like clean silica or Pyrex. Potassium tetraborate behaves like other salts under conditions of rapid reaction (cf. Fig. 10) but yields larger rates than the other salts under conditions of slow reaction, though still much below the rates in uncoated vessels. Under the latter conditions, some self-acceleration and erratic variation are also found. Potassium tetraborate thus occupies an intermediate position where ϵ is of comparable magnitude to λ/d. If the alkali content of the coating is increased by flushing the vessel with KOH-solution and baking out, thus forming the metaborate and perhaps retaining some excess alkali, the coating behaves like other salts.

The chain carriers described later are distinguished from other molecules by the possession of a free valence. Their destruction is therefore accomplished only by reaction with themselves, in which free valences are neutralized. The surface facilitates this process by retaining chain carriers in the adsorbed state, the chance of reaction depending upon the surface concentration which is greater the higher the rate at which they arrive, that is, the more rapid the reaction rate, and the longer the average time between adsorption and desorption. If one ascribes to salts like KCl, $BaCl_2$, and Na_2WO_4 strong adsorptive forces, perhaps by formation of loose compounds, the surface concentration becomes large even for low reaction rates and the destruction of chain carriers at the surface highly probable. If a salt like $K_2B_4O_7$ has weak adsorptive forces, the probability of chain destruction is large only at high reaction rates, thus explaining the behavior of

potassium-aluminum and aluminum silicate. The rates in this vessel were almost identical with those in salt-coated vessels in the present investigation allowing for differences in shape and dimensions. They were increased by adding water vapor, apparently not more than corresponds to the inert gas effect.

Prettre (reference 6) in KCl-coated Pyrex. His rates were somewhat smaller than those found in the present investigation.

[13] B. Lewis and G. von Elbe, *Combustion, Flames and Explosions of Gases* (Cambridge, 1938), pp. 24–25.

[14] The mechanism developed in this paper admits of an increase of n_0 by reaction i and a decrease of α by reaction 6 on adding inert gas, which counteract each other to some extent. For further treatment see Section V.

[15] That the nature of the surface enters into the reaction through ϵ rather than the chain-initiation mechanism is shown by the effect of vessel surface on the second explosion limit (Table II, Section IIIa), which is independent of chain initiation (Section IIIa).

[16] Reference 13, p. 28.

such a coating at low reaction rates. B_2O_3 and SiO_2 appear, on this basis, to possess very weak adsorptive forces, possibly confined to sparsely distributed and unstable spots that are easily occupied by H_2O, thus explaining poisoning of the surface by H_2O.[17] Salt-coated surfaces are possibly also poisoned but evidently not sufficiently to change the relation $\epsilon \gg \lambda/d$. Only on a $K_2B_4O_7$ surface is the effect noticeable at low rates. The behavior of different salts, in particular, the improvement of the $K_2B_4O_7$ efficiency on adding more potassium ions, suggests that the retentive force is associated with the cation.

The use of nitrates and sulphates as coating materials was avoided because of possible formation of oxides of nitrogen and sulfur compounds. Carbonates and hydroxides are impractical on silica and Pyrex because they react to liberate CO_2 and H_2O. The use of chlorides appeared to be unobjectionable; no evidence of liberation of Cl_2 or HCl was found at the temperature of these experiments. KCl coating has the disadvantage of being noticeably volatile at temperatures above 550°C, tending, over a long period, to distill to the colder inlet tube.[18] All coatings were applied in heavy translucent layers. Loose particles were avoided because of the formation of dust suspensions on admitting the gases which affect the early stages of the reaction.

The elimination of the nature of the surface as a variable by coating the vessel permits quantitative investigation of the effect on the reaction of the other variables: pressure, temperature, mixture composition, and vessel diameter.

III. DETERMINATION OF THE INDIVIDUAL REACTIONS OF ATOMS, RADICALS, AND NEUTRAL MOLECULES THAT COMPRISE THE REACTION MECHANISM

(a) Determination of Chain Branching (Reactions 1, 2, and 3), Chain Continuation (Reaction 11), and Chain Destruction (Reaction 6 and Surface Reactions of H, O, OH, and HO_2) from Data of Second and First Explosion Limits

Between the reactants H_2 and O_2 and the chain carriers H, O, and OH only the following bimolecular reactions, except direct association, are possible.

1. $OH+H_2=H_2O+H$;
2. $H+O_2=OH+O$;
3. $O+H_2=OH+H$.

They constitute an intensely branched chain, the branching step being reaction 2 in which two new free valences are formed. If unchecked, reactions 1 to 3 would lead to explosion; but since mixtures of hydrogen and oxygen explode only in the limited range of temperatures and pressures between the first and second explosion limits (Fig. 3) and above the third explosion limit (Fig. 7), some inhibiting process must operate. For example, below the first limit, explosion might be inhibited by recombination of chain carriers in ternary collisions like $H+H+M=H_2+M$ where M is any third molecule. For a given mixture the chain-carrier concentration would then be independent of pressure, and the reaction rate would increase with the latter until thermal explosion took place. However, this mechanism conflicts, among other points, with the observations that inert gas lowers the first limit,[19] and that this limit is dependent on the nature of the surface[19] (Fig. 3); and it is wholly irreconcilable with the phenomenon of the second explosion limit. It must, therefore, be concluded that the explosion is inhibited not by recombinations of chain carriers in the gas phase but by other processes which check the growth of chain-carrier concentration long before recombinations become frequent. Recombinations may occur, but to an appreciable extent only when the chain-carrier concentration is so high that thermal explosion is unpreventable. Therefore, the inhibiting process must be first-order with respect to chain carriers: below the first limit it is the diffusion of H, O, and OH to the wall on which they are destroyed, in agreement with the experimental evidence; above the second limit it must be an association of a chain carrier and a reactant molecule in a collision with a third molecule to form a fairly inert complex in agreement with the inhibition of the second-limit explosion on adding inert gas or on increasing the partial pressure of either of the reactants. To determine the na-

[17] Prettre (reference 6) suggested a similar idea.

[18] The volatility of KCl has also been noted by Prettre (reference 6), Oldenberg and Sommers (reference 7), and Heiple and Lewis (reference 4).

[19] Hinshelwood and Moelwyn-Hughes, Proc. Roy. Soc. **A138**, 311 (1932). Semenova, Acta Phys. Chim. U.S.S.R. **6**, 25 (1937). Biron and Nalbandjan, *ibid.*, **6**, 43 (1937).

TABLE II. Second explosion limits in uncoated, B_2O_3-coated and salt-coated vessels (KCl, $BaCl_2$, Na_2WO_4, $K_2B_2O_4$). $2H_2+O_2$.

Temp., °C	P 2d limit, mm Hg Clean quartz	Clean Pyrex	B_2O_3 coating	Salt coating
$d=3.9$ cm				
500	64–68		—	41.8
520	83–91		—	61
530	—		111–115	74
540	110–124		—	89
$d=7.4$ cm				
530		94–102		85.6

ture of this association reaction, use is made of the requirement that branched chains can be broken only by destruction of the chain carrier capable of branching (in this case H) or by destruction of *all* chain carriers emerging from the branching reaction (in this case OH and O). The reaction

$$6.\quad H+O_2+M=HO_2+M,^{20}$$

appears to be the only imaginable association reaction for removing H, provided HO_2 does not react readily with H_2. Alternatively, O atoms may disappear by reactions $O+O_2+M=O_3+M$, and $O+H_2+M=H_2O+M$, and OH by $OH+H_2+O_2=H_2O+HO_2$, which is the only imaginable chain-breaking reaction for OH, so that HO_2 appears in the alternative scheme as well.

Reaction 6 is generally considered to be the first step in the formation of hydrogen peroxide from H and O_2. If HO_2 is assumed to be destroyed predominantly at the surface at low pressures but also capable, to some extent, of reaction

$$11.\quad HO_2+H_2=H_2O_2+H,$$

then it becomes the principal chain carrier in the reaction above the second explosion limit.[21] For a surface where $\epsilon \ll \lambda/d$, the lifetime of HO_2 becomes large, and reaction 11 should become noticeable already at second-limit pressures; that is, some of the chains are continued and the pressure required to inhibit the explosion should be larger than for a surface where $\epsilon \gg \lambda/d$. Thus, the second explosion limit should be higher in uncoated silica or Pyrex vessels or vessels coated with boric acid than in salt-coated vessels, and subject to erratic changes. This is found to be the case (Table II).[22]

Since reactions 1, 2, 3, and 6 are of the same, namely first, order with respect to the chain carriers, they provide a formal relation for the explosion limit by equating the rates of formation and destruction of each chain carrier regardless of considerations of temperature equilibrium (isothermal branched chain theory). The explosion condition is:

$$k_6(M)_e=2k_2, \tag{3}$$

where subscript e refers to the explosion limit. Since $k_6(M)$ represents

$$k_{6,H_2}(H_2)+k_{6,O_2}(O_2)+k_{6,X}(X),$$

$$k_6=k_{6,H_2}f_{H_2}+k_{6,O_2}f_{O_2}+k_{6,X}f_X \tag{4}$$

where f_{H_2}, etc., are mole fractions and X is an inert molecule. Rewriting,

$$(M)_e=\frac{2k_2}{k_{6,H_2}\left(f_{H_2}+\frac{k_{6,O_2}}{k_{6,H_2}}f_{O_2}+\frac{k_{6,X}}{k_{6,H_2}}f_X\right)}. \tag{5}$$

For constant temperature

$$\frac{(M_2)_e}{(M_1)_e}=\frac{P_2}{P_1}=\frac{f_{1,H_2}+\frac{k_{6,O_2}}{k_{6,H_2}}f_{1,O_2}+\frac{k_{6,X}}{k_{6,H_2}}f_{1,X}}{f_{2,H_2}+\frac{k_{6,O_2}}{k_{6,H_2}}f_{2,O_2}+\frac{k_{6,X}}{k_{6,H_2}}f_{2,X}}, \tag{6}$$

where P is the second limit pressure.

Experimental results of second explosion limits for various mixture compositions are given in

[20] Reaction numbers 1, 2, 3, 6, 11, and 12 follow an earlier treatment (reference 13).

[21] Jost (*Explosions- und Verbrennungsvorgänge in Gasen* (Berlin, 1938), p. 322) criticizes the view that reaction 11 does not seriously compete with the surface destruction of HO_2 under second limit conditions on the basis of photochemical evidence that HO_2 and H_2 react with each other even at room temperature. However, there is no evidence that this latter reaction occurs in the gas phase (cf. reference 37) and as pointed out earlier (von Elbe and Lewis, J. Chem. Phys. **7**, 710 (1939)) the photochemical evidence is well interpreted on the basis of heterogeneous reaction between HO_2 and H_2 (cf. Oldenberg and Sommers, J. Chem. Phys. **9**, 573 (1941)); the question raised by these authors why Taylor and Salley should have found an induction period even at temperatures where the homogeneous reaction becomes noticeable is perhaps answered by the fact that in only one out of their 52 experiments was the heterogeneous contribution negligible and that the occurrence of induction periods was mentioned only in a general statement for the entire investigation.

[22] Compare also, Kimata, Aomi, and Goto (Rev. Phys. Chem. Japan **15**, 42 (1941)) in Pyrex tubes uncoated and coated with various salts.

Table III. Using for P_1 the second limit for the stoichiometric mixture, values of $k_{6,O_2}/k_{6,H_2}$, etc., have been calculated from Eq. (6).

The constancy of the k_6 ratios (last column Table III) over a wide range of mixture compositions confirms the correctness of the general second-limit mechanism. It does not by itself prove the specific scheme 1, 2, 3, 6 since corresponding relations follow from other schemes discussed below. The k_6 ratios for O_2, N_2, A, and He agree, on the whole, reasonably well with those calculated from second-limit data of other investigators.[23] On comparing the k_6 ratios of O_2 and various inert gases, one notes a particularly large ratio for H_2O. This means that even a small

TABLE III. Dependence of second explosion limit on mixture composition. d = 7.4-cm KCl-coated Pyrex vessel.

Temperature = 530°C

f_{H_2}	f_{O_2}	P 2d limit mm Hg
0.667	0.333	85.6±0.5 mm (from numerous determinations)

Oxygen experiments

f_{H_2}	f_{O_2}	P 2d limit mm Hg	$k_{6,O_2}/k_{6,H_2}$
0.500	0.500	99.4	0.35
.500	.500	99.3	.35
.334	.666	118.6	.35
.334	.666	117.9	.35
.334	.666	119.4	.34
.333	.667	117.3	.36
.334	.666	119.3	.34
.334	.666	117.9	.35
.200	.800	138.4	.37
.201	.799	136.8	.37
.200	.800	136.8	.37
		Average	0.35

Nitrogen experiments

f_{H_2}	f_{O_2}	f_{N_2}	P 2d limit mm Hg	$k_{6,N_2}/k_{6,H_2}$
0.538	0.269	0.193	94.5	0.40
.325	.163	.512	108.8	.46
.199	.097	.704	125.7	.43
.200	.100	.700	123.2	.44
			Average	0.43

Carbon dioxide experiments

f_{H_2}	f_{O_2}	f_{CO_2}	P 2d limit mm Hg	$k_{6,CO_2}/k_{6,H_2}$
0.532	0.266	0.202	72.8	1.47
.321	.167	.512	60.7	1.42
.202	.101	.697	52.1	1.51
			Average	1.47

Water-vapor experiments

f_{H_2}	f_{O_2}	f_{H_2O}	P 2d limit mm Hg	$k_{6,H_2O}/k_{6,H_2}$
0.647	0.323	0.0298	55.2	15.1
.645	.323	0.0321	54.3	15.0
.644	.322	.0335	54.9	13.7
.627	.314	.0587	42.8	14.0
.624	.312	.0637	41.8	13.8
.601	.301	.0978	32.7	13.7
.600	.299	.1011	30.1	14.7
.596	.301	.1033	31.5	13.8
.593	.297	.1103	29.4	14.5
			Average	14.3

TABLE III.—*Continued.*

Helium experiments

f_{H_2}	f_{O_2}	f_{He}	P 2d limit mm Hg	$k_{6,He}/k_{6,H_2}$
0.533	0.266	0.201	95.3	0.39
.531	.265	.204	97.4	.32
.329	.163	.508	118.7	.35
.211	.105	.684	131.9	.38
			Average	0.36

Argon experiments

f_{H_2}	f_{O_2}	f_A	P 2d limit mm Hg	$k_{6,A}/k_{6,H_2}$
0.534	0.267	0.199	100.2	0.21
.305	.152	.543	139.9	.22
.206	.103	.691	182.0	.18
.203	.102	.695	185.6	.18
			Average	0.20

Temperature = 480°C

f_{H_2}	f_{O_2}	P 2d limit mm Hg
0.667	0.333	33.0

Water-vapor experiments

f_{H_2}	f_{O_2}	f_{H_2O}	P 2d limit mm Hg	$k_{6,H_2O}/k_{6,H_2}$
0.646	0.324	0.0303	24.1	10.5
.628	.314	.058	19.3	10.1
.584	.291	.125	13.0	10.6
			Average	10.4

Temperature = 570°C

f_{H_2}	f_{O_2}	P 2d limit mm Hg	Remarks
0.667	0.333	186.5	Rapid withdrawal, trial method

Water-vapor experiments

f_{H_2}	f_{O_2}	f_{H_2O}	P 2d limit mm Hg	$k_{6,H_2O}/k_{6,H_2}$
0.635	0.318	0.0469	102.0	14.6

[23] Grant and Hinshelwood, Proc. Roy. Soc. **A141**, 29 (1933); Frost and Alyea, J. Am. Chem. Soc. **55**, 3227 (1933). Frost and Alyea's experiments were made in a KCl-coated cylindrical Pyrex vessel, 2-cm diameter, 20 cm long. Their absolute second-limit pressures agree closely with those in the present paper, allowing for mixture composition and vessel size. Grant and Hinshelwood's experiments were made in uncoated silica and alumina vessels and their second limit values as well as those of Thompson and Hinshelwood (Proc. Roy. Soc. **A122**, 610 (1929)) in uncoated silica and Worcester porcelain vessels are consistently lower. Possibly they underestimated the powerful effect of water (see below). Garstang and Hinshelwood (Proc. Roy. Soc. **A130**, 640 (1931)) reported a few second-limit pressures in Worcester porcelain which are almost identical with those in the present paper. They suggested that the discrepancy between their and Thompson and Hinshelwood's values was due to an error in temperature calibration.

amount of water vapor markedly lowers the second-limit pressure[24] and that the formation of H_2O during the manipulation period may be a source of error.[25] Below 530°C the formation of H_2O during this period is too small to be of consequence. Toward higher temperatures the reaction rate increases markedly and the manipulation time must be made as short as possible. It is rather likely, in view of the magnitude of reaction rates (see below), that the 570°C limit values given in the table are both too low, even though this time was only about 14 seconds.[26] Since the k_{6,H_2O} values remain constant over a large range of H_2O percentage, there is no reason to attribute the inhibiting role of H_2O to any other effect than that of an efficient third body in reaction 6. The data at 480°C suggest that the effect decreases with temperature.

Grant and Hinshelwood[23] have shown the agreement of the ratios $k_{6,He}/k_{6,A}$ and $k_{6,O_2}/k_{6,H_2}$ with ratios calculated from gas kinetic theory, assuming that in the chain-breaking reaction a fairly long-lived collision complex (in the present theory HO_2) is stabilized by collision with another molecule. Under this assumption, collisions of the molecule with the complex are proportional to the square of the molecular diameter σ, averaged over the complex and the colliding molecule, and inversely proportional to the square root of the reduced mass, $m_1m_2/(m_1+m_2)$. Table IV shows this agreement, using the present data. The following values of $\sigma\times10^8$ cm are taken from Tolman's[27] tabulation: $H_2=2.36$, $O_2=2.93$, $N_2=3.10$, $He=1.89$, $A=2.84$, $CO_2=3.23$. For H_2O, a value of 3.5 to 5.0 and for HO_2, the O_2 values are used. Agreement is found for similar molecules like He and A, or O_2, N_2, and H_2. For H_2O and, to a lesser degree CO_2, specific interactions are indicated.

The other reaction schemes that yield a relation of the form of Eq. (3), $(M)_e=$const., all involve implausible assumptions. By assuming that the rate of reaction 3 is negligible compared to the rate of (a) $O+H_2+O_2=HO_2+OH$, one obtains with reactions 1, 2, and 6, $(M)_e=k_2/k_6$; or if the rate of reaction 1 is assumed to be negligible compared to the rates of (b) $OH+H_2+O_2=H_2O+OH+O$ and (c) $OH+H_2+O_2=H_2O+HO_2$, one obtains with reactions 2, 3, and 6, $(M)_e=2k_2k_b/k_6(k_c-k_b)$. (The association reaction $O+O_2+M=O_3+M$ does not permit a solution.) Using reactions (c) and (d) $O+H_2+M=H_2O+M$ mentioned earlier as alternatives to reaction 6, one obtains with reactions 1, 2, and (a), $(M)_e=k_1ka/k_dk_c$ for $ka\ll kd$, which again requires the assumption of negligible reaction 3 compared to reaction (a); or one may again assume that reaction 1 is negligible compared to reaction (b) which with 2, 3, (c), and (d) gives $(M)_e=2k_bk_3/k_dk_c$. This exhausts the possibilities of obtaining the desired expression by means of ternary reactions. Additional imaginable ternary reactions may be added to the above schemes which add more

TABLE IV. Comparison of k_6 values with gas kinetic theory.

	Experimental	Calculated
$k_{6,He}/k_{6,A}$	1.80	1.60
$k_{6,O_2}/k_{6,H_2}$	0.35	0.42
$k_{6,N_2}/k_{6,H_2}$	0.43	0.46
$k_{6,CO_2}/k_{6,H_2}$	1.47	0.43
$k_{6,H_2O}/k_{6,H_2}$	14.3	0.6 to 0.9

[24] This effect was reported by Garstang and Hinshelwood (reference 23). The data are erratic and do not show its actual magnitude. Further data in uncoated Pyrex vessels were published recently by Kimata, Aomi, and Goto (reference 22).

[25] This explains the lowering and even suppression of the second limit in aluminum vessels found by Garstang and Hinshelwood (reference 23), aluminum strongly catalyzing the formation of H_2O. The same effect is found with other catalytic materials (metals and metal oxides). It will be recalled that Alyea and Haber (Zeits. f. physik. Chemie **B10**, 193 (1930)) found that crossed streams of hydrogen and oxygen in a nitrogen atmosphere under conditions of the low pressure explosion, while not igniting by themselves, did so on interposing a silica rod. An aluminum rod proved ineffectual. The reason for the latter seems clear from the above. The effectiveness of silica may be seen in the decrease of the ratio of induction period to the time available for dilution of the mixture with nitrogen, probably caused by slowing of the streams and also by formation of additional chain carriers by surface reaction (cf. N. Semenoff, *Chain Reactions* (Oxford, 1935), p. 260). Short induction periods of the order 1 second have actually been observed in the present investigation of second limits, particularly in diluted mixtures at low temperatures.

[26] In this way, certain results of Oldenberg and Sommers (J. Chem. Phys. **8**, 468 (1940)) find explanation. With rapid manipulation they found a second-limit pressure of 182 mm for $fH_2=0.667$ at 568°C. In the succeeding experiment they waited for several minutes at a pressure slightly above (184 mm), until a pressure decrease corresponding to 4-percent reaction had occurred, and then found the limit at 120 mm. This shift is in quantitative agreement with the above value of $k_{6,H_2O}/k_{6,H_2}$. The higher second-limit pressures found by them in a KCl-coated vessel, as compared with an uncoated vessel, as well as the declining slope of their second-limit curves toward high temperatures, are also accountable by water inhibition.

[27] Tolman, *Statistical Mechanics* (Chemical Catalogue Company, 1927), p. 327.

constant terms to the results but this only increases the number of implausible assumptions.

Kassel and Storch[28] developed a scheme which consists essentially of reactions 1 and 6 and the reactions

(e) $H+O_2=HO_2^*$ and (f) $HO_2^*+H_2=H+2OH$,

whence $(M)_e=2k_e/k_6$. The success of this scheme, however, rests on the assumption that the rate of reaction (f) is large compared to the rate of deactivation of HO_2^* by collisions with other molecules. Similarly, Semenoff[29] suggested the scheme

(g) $O+H_2=H_2O^*$, (h) $H_2O^*+O_2=H_2O+O+O$,

and (d), whence $(M)_e=k_g/k_d$, the success of which rests on a similar assumption concerning H_2O^*. The Kassel and Storch scheme can function concurrently with the mechanism 1, 2, 3, 6, whereas the Semenoff scheme and 1, 2, 3, 6 are mutually exclusive.

Thus, considerations of probability compel the acceptance of 1, 2, 3, 6.

The first explosion limit is obtained by the addition of the surface destruction of H, O, and OH to these reactions. The numerous complexities of this seemingly simple mechanism are brought out by a number of investigations. Kowalsky[30] has shown that if a mixture is admitted to a heated vessel at pressures corresponding to or even considerably above the first explosion limit, the reaction, though initially rapid and self-accelerating, subsides within a fraction of a second without going to completion. This has been confirmed in the present investigation using the heating method: The mixture was admitted to the vessel at some temperature below the limit where no reaction was noticeable; the temperature was then raised until a sudden pressure decrease occurred which corresponded to an explosively fast rate, but subsided after only a fraction of the mixture had reacted. This fraction was larger the higher the temperature had been raised. Threshold temperatures were fairly well observable in the pressure and temperature range where the first and second limits join (cf. Fig. 3) but were increasingly difficult to observe from the junction on toward lower pressures and higher temperatures. For this reason, observations were limited to the neighborhood of the junction. Subsidence of the explosion may be due in part to the fact that the pressure has dropped below the limit coupled with rapid heat loss, as was suggested by Semenoff,[30] and probably in a large measure to the quenching effect of H_2O by reaction 6.

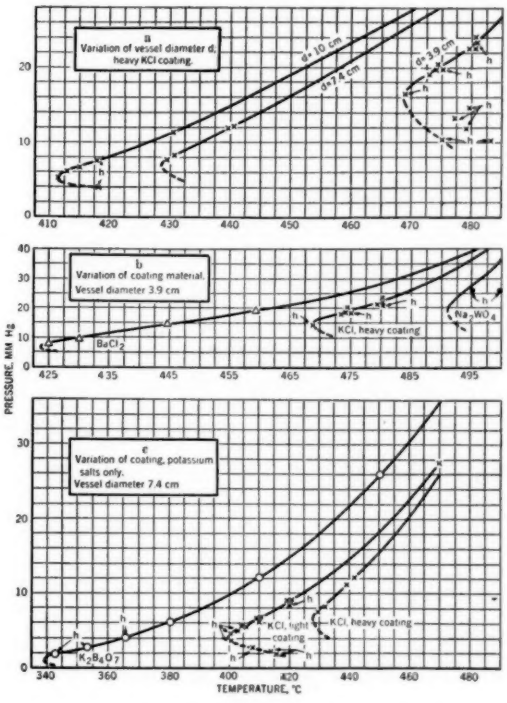

FIG. 3. Junctions of first and second explosion limits. Experimental points marked h=heating method. Others, withdrawal method. Position of tips determined by withdrawal method.

Figure 3a shows three junctions of first and second limits for uniformly KCl-coated vessels of different diameters, determined both by the heating and withdrawal methods. As is to be expected from the chain-breaking diffusion mechanism operative at the first limit, the junctions shift to higher temperatures and pressures with decreasing diameter. The sensitivity to coating materials is shown in Figs. 3b and 3c. Figure 3c also shows the effect of attenuating a KCl-coating (curve marked "KCl, light coating"), which was obtained by removing some of the KCl by evaporation at high temperature. The results indicate that the reflectivity for H, or O, or OH, or all three, decreases in the order $K_2B_4O_7$,

[28] Kassel and Storch, J. Am. Chem. Soc. **57**, 672 (1935).
[29] Reference 25, p. 248.
[30] Kowalsky, Physik. Zeits. U.S.S.R. **1**, 595 (1932); **4**, 723 (1933); cf. N. Semenoff, reference 25, pp. 217–225.

$BaCl_2$, KCl, Na_2WO_4. Clean silica, Pyrex, and B_2O_3 are probably even more reflective than $K_2B_4O_7$ (the pressures were too low to verify this point), and $K_2B_2O_4$ (not included in the figure) is of the same order as KCl.

The quantitative theory of the first explosion limit was studied by Kassel.[31] It involves simultaneous consideration of the diffusions and gas-phase reactions of all three chain carriers H, O, and OH and the assignment of individual chain-breaking efficiencies. Depending upon the latter, that is, the nature of the surface, widely different relations between limit pressure and mixture composition are possible. This was found in the earlier experimental work of Frost and Alyea[23] in KCl-coated vessels and Hinshelwood and Moelwyn-Hughes[19] in quartz vessels. An inert gas effect, indicating the destruction of at least one of the chain carriers with high efficiency, and the effect of vessel size[19] were also found. Because of the experimental procedure, the actual limits were probably exceeded in both investigations; this and lack of good reproducibility prevent the quantitative application of the theory to their data. Recently, Semenova[19] and Biron and Nalbandjan[19] studied the first limit by means of a very sensitive membrane manometer in newly fused Pyrex cylinders, where good reproducibility could be obtained. The limit pressures were very low (a fraction of a millimeter), and inert gas had no effect; that is, the efficiency of destruction of all chain carriers was low. From a plot of the logarithm of the limit pressure *vs.* $1/T$ an "activation energy" of about 11 kcal. was obtained. For the case of low chain-breaking efficiency this value should represent the difference between the activation energy of reaction 2 ($E_2=17$ kcal.—Section IVb), and the corresponding quantity calculated from the temperature coefficient of the chain-breaking efficiency. Semenova's interpretation of the 11-kcal. value, based upon a first-limit relation for high chain-breaking efficiency and an earlier value of E_2 of about 22 kcal., appears to be incorrect. Biron and Nalbandjan studied the effect of mixture composition in a freshly fused Pyrex vessel and obtained satisfactory correlation with theory. They also found the usual inert gas effect and much higher limits in ordinary quartz vessels.

[31] Kassel, Chem. Rev. **21**, 331 (1937).

(b) Completion of the Reaction Mechanism (Reactions Involving H_2O_2) and the Development of the Kinetic Equation of Explosion Limits and Reaction Rates for High Chain-Breaking Efficiency

In the non-explosive region between second and third limits, chains are continued by reaction 11 (Section IIIa) and broken at the surface (Section II), most probably by reaction

$$12.\quad 2HO_2=H_2O_2+O_2.$$

For the initiation of chains, earlier data suggested the thermal dissociation of H_2[32] because of the hydrogen dependence of the reaction rate. However, the temperature coefficient of the reaction in a range uninfluenced by explosion limits gives an over-all activation energy of the order of only 100 kcal.; since this represents the sum of the activation energies of the chain-initiating and chain-continuing reactions there is insufficient energy for H_2 dissociation. The only compound of hydrogen and oxygen in the system of sufficiently low dissociation energy is H_2O_2, which according to energy data presented in Section VI may dissociate into H_2O+O (34 kcal.) or 2 OH (51 kcal.), so that the initiating reaction may be written

$$\text{i.}\quad H_2O_2+M=M+H_2O+O \quad \text{or} \quad 2\,OH.$$

Since in salt-coated vessels the reaction reaches a steady state (Section II), the H_2O_2 concentration must also reach a steady state if it takes part in the mechanism. This will be the case if H_2O_2 is destroyed by a chain carrier in the gas phase. In particular, if this reaction is

$$7.\quad HO_2+H_2O_2=H_2O+O_2+OH,$$

then the H_2O_2 concentration becomes, at high pressures, where it is predominantly formed and destroyed by reactions 11 and 7, equal to $k_{11}(H_2)/k_7$ and thus proportional to the H_2 concentration.[33]

[32] Reference 13, p. 39.

[33] This relation is independent of the nature of the surface and therefore not limited to salt-coated vessels. Indeed, Pease (reference 6) found on passing H_2 and O_2 at 1 atmosphere pressure through a clean Pyrex tube heated from 530° to 550°C that H_2O_2 attained an approximate steady-state concentration though the reaction, as far as H_2O formation was concerned, was clearly self-accelerated. This steady-state concentration increased approximately proportional to the hydrogen concentration. In salt-coated tubes the H_2O_2 concentration was generally lower, suggesting heterogeneous decomposition by reaction 13 (see below).

It is known[34] that H_2O_2 decomposes heterogeneously, hence the additional reaction,

$$13.\quad H_2O_2 \xrightarrow{\text{surface}} H_2O+\tfrac{1}{2}O_2,$$

must be considered. Finally, there must be some spontaneous reaction in the system supplying species for the first brief stage of the reaction preceding the establishment of the various steady-state concentrations. This may involve heterogeneous catalysis or thermal dissociation in the gas phase, forming atoms which react via reactions 6, 12, and 11 to form H_2O_2. Without specifying this reaction further one may write

$$14.\quad H_2+O_2=H_2O_2.$$

By reactions 12 and 7, 1 H is recovered out of every 3 H entering reaction 6,[35] and it is easily shown that the condition for the second explosion limit is now $k_6(M)_e/k_2=3$ instead of 2, as in Eq. (3). This leaves Eq. (6) and the values of k_6 in Table II unchanged. If some of the H_2O_2 formed at the surface in reaction 12 is decomposed there catalytically, this ratio assumes values between 2 and 3, depending on the nature of the surface. This can explain occasionally observed small shifts of the second limit to lower pressures. For example, in a large number of determinations the limit at 530°C for a stoichiometric mixture in a 7.4-cm vessel coated with different salts was found to vary between 86 and 84 mm; in a 10-cm vessel it ranged between 88 and 86 mm; an 8-cm silica vessel coated with KCl once yielded a value as low as 79 cm and at the same time abnormally low reaction rates (cf. Section IVc). Normal limits and rates were restored in the latter vessel on recoating with $BaCl_2$.

The HO_2 concentration decreases with decreasing vessel diameter, whereas the concentrations of H, O, and OH remain constant since the pressures are much above the first explosion limit. If H_2O_2 is destroyed by other chain carriers besides HO_2, reaction 7 meets increasing competition from these other reactions as the vessel diameter is decreased. It follows that $k_6(M)_e/k_2$ is about 3 only in large vessels where reaction 7 predominates and falls below this value on decreasing the size of the vessel. It reaches a limit of 2 provided none of the other chain carriers is permanently destroyed in reactions with H_2O_2. Under this condition, the second-limit pressure should be approximately independent of the vessel size in large vessels and should approach to within $\frac{2}{3}$ of the large-vessel value as the size of the vessel is decreased. A diameter dependence of the second limit of this type is shown by the following data: In 10-cm and 7.4-cm vessels, the second limits at 530°C for $2H_2+O_2$ were found to be 88 mm and 85 to 86 mm, respectively; in a 3.9-cm vessel the limit was found not larger than 74 mm in a great many determinations with various coating materials; in a 1.8-cm vessel the limit was somewhat erratic and depended considerably on the coating material—$BaCl_2$, 74 to 70 mm, KCl, 68 to 67 mm, Na_2WO_4, 62 to 57 mm. The alternative explanations of a diameter dependence, namely, (a) not negligible contribution of HO_2 chains (i.e., B in Eq. (16) not small compared to 1), and (b) partial destruction of H, O, and OH at the wall, that is a residual influence of the first limit, are inconsistent with the data. (a) would demand that the difference between the limit pressures in the 7.4- and 10-cm vessels should be more than twice the difference found between the 3.9- and 7.4-cm vessels, while (b) would demand total suppression of explosion in the 1.8-cm vessel. In reality, as shown by the data on reaction rates and third explosion limits, $B \ll 1$ under the above conditions, and furthermore, the first explosion limit is too remote to affect the second limit, being of the order of a few millimeters.

The reaction

$$5.\quad H+O_2+H_2O_2=H_2O+O_2+OH$$

is chosen as the chain-carrier reaction competing with reaction 7. This choice will be justified later. Reaction 5 may be interpreted chemically as involving a primary association of H and O_2 and subsequent reaction, as in reaction 7, within the collision complex before redistribution of the available energy.

[34] Elder and Rideal, Trans. Faraday Soc. **23**, 545 (1927).

[35] The number recovered would be larger if adsorbed HO_2 and H_2 reacted to form H_2O_2 and an adsorbed H. While it has been suggested that this reaction occurs (G. von Elbe and B. Lewis, J. Phys. Chem. **7**, 710 (1939)) considerations put forward in Section II suggest that on salt surfaces the number of HO_2 in activated adsorption is a function only of the extent of the surface and is not dependent on the rate of HO_2 production in the gas phase. Thus, the above heterogeneous reaction is only contributory to reaction 14 and does not influence the explosion limit.

The complete reaction scheme applicable to the second and third limits and the non-explosive region between them is summarized for kinetic purposes in the following manner, recalling that every OH yields H_2O and H by reaction 1 and every O yields OH and H by reaction 3.

i. $H_2O_2+M\rightarrow 2H_2O+2H$
2. $H+O_2\rightarrow 2H_2O+3H$
6. $H+O_2+M=HO_2+M$
11. $HO_2+H_2=H_2O_2+H$
12. $HO_2 \xrightarrow{\text{surface}} 0.5\gamma\ H_2O_2$
5. $H+O_2+H_2O_2\rightarrow 2H_2O+O_2+H$
7. $HO_2+H_2O_2\rightarrow 2H_2O+O_2+H$
13. $H_2O_2 \xrightarrow{\text{surface}} H_2O+\frac{1}{2}\ O_2$
14. spontaneous formation of H_2O_2

The formulation of reaction i is consistent with either of the two H_2O_2 dissociations given above. γ denotes the fraction of H_2O_2 that escapes undecomposed into the gas phase.

For the development of the kinetic expressions, the diffusion problem is approximated[36] by taking the rate of reaction 12 equal to $K_{12}(HO_2)$, where, for $\epsilon \gg \lambda/d$ (cf. Eq. (2))

$$K_{12}=4\pi^2 D/d^2=k_{12}/(M)d^2. \tag{7}$$

At low pressures H_2O_2 is formed principally by reaction 12 at the surface, whence it diffuses into the gas phase. It is, therefore, not distributed uniformly throughout the vessel, as is assumed in the treatment. It is difficult to analyze the effect of this complication, but it is believed to introduce only insignificant corrections.

In the steady state the equations for HO_2, H, and H_2O_2 are

$$k_6(O_2)(M)(H)=k_7(H_2O_2)(HO_2)+k_{11}(H_2)(HO_2)+K_{12}(HO_2), \tag{8}$$

$$2k_i(M)(H_2O_2)+2k_2(O_2)(H)+k_{11}(H_2)(HO_2)+k_7(H_2O_2)(HO_2)=k_6(O_2)(M)(H), \tag{9}$$

and

$$0.5\gamma K_{12}(HO_2)+k_{11}(H_2)(HO_2)+K_{14}=k_7(HO_2)(H_2O_2)+k_5(O_2)(H)(H_2O_2)+k_i(M)(H_2O_2)+K_{13}(H_2O_2). \tag{10}$$

[36] Reference 13, p. 41. For justification of this approximation, cf. Kassel, reference 31.

Let

$$2k_2/k_6(M)=a, \quad k_{11}(H_2)/K_{12}=b,$$
$$k_5K_{12}/k_7k_2=c, \quad K_{13}/k_i(M)=u,$$
$$k_7K_{14}/k_i(M)K_{12}=s, \quad k_7(H_2O_2)/K_{12}=x,$$
$$k_i(M)K_{12}/k_7=I.$$

These quantities are dimensionless except I, which has the dimension of a rate. Adding (8) and (9), and since $k_i(M)(HO_2)=Ix$,

$$(H)=[K_{12}(HO_2)-2Ix]/2k_2(O_2). \tag{11}$$

Substituting (H) in (8), dividing by K_{12}, and transposing

$$(HO_2)=2Ix/K_{12}[1-a(1+x+b)]. \tag{12}$$

Water is formed at the rate

$$R=2k_i(M)(H_2O_2)+K_{13}(H_2O_2)+2k_2(O_2)(H)+2k_5(O_2)(H_2O_2)(H)+2k_7(H_2O_2)(HO_2), \tag{13}$$

or

$$R=2Ix\left[1+0.5u+\frac{a(1+x+b)(1+cx)+2x}{1-a(1+x+b)}\right]. \tag{14}$$

This is to be divided by 2 if the rate is expressed in terms of pressure decrease of the system.

x is obtained from Eq. (10) which, after dividing by $K_{12}(HO_2)$, may be written

$$0.5\gamma+b+s[1-a(1+x+b)]/2x=x+0.5cxa(1+x+b)+0.5[1-a(1+x+b)](1+u). \tag{15}$$

Denoting the variables at the explosion limit by capital letters, the explosion condition is given by

$$1-A(1+X+B)=0. \tag{16}$$

From Eqs. (15) and (16),

$$X=(0.5\gamma+B)/(1+0.5C). \tag{17}$$

Hence

$$1/A=k_6(M)_e/2k_2=[1+0.5\gamma+0.5C+(2+0.5C)B]/1+0.5\text{C}. \tag{18}$$

At the second limit, B is small. γ depends on the nature of the surface, so that Eq. (18) formally accounts for small, erratic changes of the limit from this source. Taking $\gamma=1$, then for large vessel diameter ($c\rightarrow 0$)

$$k_6(M)_e/k_2=3, \tag{19}$$

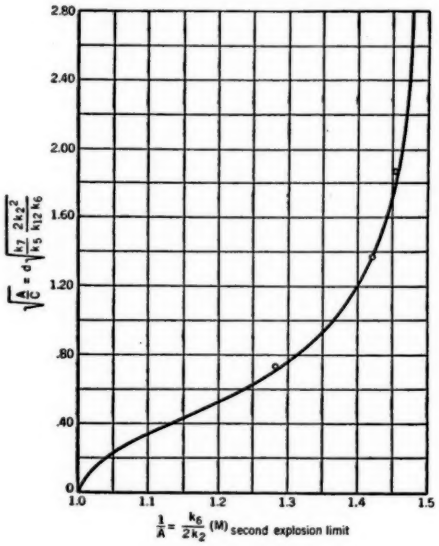

FIG. 4. Plot of $1/A$ *vs.* $(A/C)^{\frac{1}{2}}$.

and for small vessel diameter $(c \rightarrow \infty)$

$$k_6(M)_e/k_2 = 2. \tag{20}$$

Figure 4 is a plot of $1/A$ *vs.* $(A/C)^{\frac{1}{2}}$, the former quantity being proportional to the second-limit pressure and the latter to the vessel diameter. At 530°C for stoichiometric mixture, the experimental second limits are 88 mm for $d=10$ cm, 85 mm for $d=7.4$ cm, 74 mm for $d=3.9$ cm. Corrected for the contribution of the B term these become 86 mm, 84 mm, and 74 mm, respectively. If the value for the 7.4-cm vessel is suitably located at the beginning of the steep part of the curve, namely at about $1/A=1.44$, the other points take the positions shown. From this the limit in the 1.8-cm vessel (not shown) would be at 64 mm, which is consistent with values reported above.

Concerning the justification of reaction 5: if the binary reaction $H+H_2O_2=H_2O+OH$ is substituted for it, C becomes $k_5K_{12}/k_7k_2(O_2)$, that is, inversely proportional to the O_2 concentration. Hence, an increase of f_{O_2} should cause a larger increase of the limit in a smaller vessel than in a larger vessel: for example, in the 3.9-cm vessel the ratio $k_6(M)_e/2k_2$ should rise above 1.28 (Fig. 4). Equation (6) would then no longer be applicable. In the 3.9-cm vessel, the limit for $f_{H_2}=0.2$ was found to be 121.9 mm, from which Eq. (6) yields a value of 0.345 for $k_{6,O_2}/k_{6,H_2}$ in close agreement with 0.35 obtained in the 7.4-cm vessel. This result is inconsistent with an inverse (O_2) factor in C. There appears to be no other way of eliminating the (O_2) factor than by formulating reaction 5 as given. All imaginable binary reactions between H_2O_2 and the other chain carriers O or OH lead to completely wrong diameter and mixture composition dependence of the limit. Only the two ternary reactions, $OH+H_2+H_2O_2=2H_2O+OH$ and $O+H_2+H_2O_2=H_2O+2OH$, yield the required relations, although the latter reaction gives a decidedly poor representation of the diameter dependence. Reaction 5 appears to be more plausible than either of these reactions, considering among other reasons the high rates of the competing reactions 1 and 3.[37]

[37] Geib (Zeits. f. physik. Chemie **A169**, 161 (1934)) observed destruction of H_2O_2 and formation of free O_2 (in the ratio of about 1 O_2 to 4–20 H_2O_2 destroyed) by mixing streams of H atoms and H_2O_2 vapor at room temperature and total pressure of about 0.5 mm, the former entering at the top of a 1-liter cylindrical phosphoric acid-covered glass vessel and the latter emerging from a central tube with its outlet near the top of the vessel. The gases passed directly from the vessel to a freezing trap. Geib suggested the following mechanism

(a) $H+H_2O_2=H_2O+OH$,
$2\,OH=H_2O+O$,
$2\,O+M=O_2+M$,

some of the O_2 reacting further with H. From the reaction time and H_2O_2 recovered he estimated an activation energy for reaction (a) of about 5.8 kcal. assuming a steric factor of 1. If this were so, this reaction would entirely displace reactions 5 and 7 in the present mechanism and it would be impossible to describe the vessel dependence of the second limit and the effect of pressure and mixture composition on the rate. Alternatively, the rate coefficient k_a must be assumed smaller than $k_5(O_2)$, or, at 530°C, smaller than 2.3×10^{-17} cm^3 sec.$^{-1}$ (from value of k_5 (Section V) and second-limit pressure equal to 84 mm), requiring an activation energy of 26.0 kcal. with a steric factor of 1, or 15.0 kcal. with a steric factor of 10^{-3}. It appears to the authors that the facts of the thermal reaction between H_2 and O_2 limit the choice of elementary reactions far more stringently than the various experiments performed at room temperature with free atoms and radicals. In particular one may suspect surface reactions to play an important role there. Evidences of heterogeneous character are available in some cases whereas in no instance has the exclusive homogeneous character been established. (Cf. G. von Elbe and B. Lewis, J. Chem. Phys. **7**, 710 (1939)). Under the conditions of Geib's experiments, a molecule of H_2O_2 strikes the surface some 100 times before entering the freezing trap, where further reactions are possible. Thus, considering that absorption and desorption take place on the phosphoric acid surface the reaction may occur according to Geib's mechanism with reaction (a) as a surface reaction of low activation energy. An alternative mechanism involving branched chains may be suggested as follows:

(b) $OH+H_2O_2=H_2O+HO_2^*$,
(7) $HO_2^*+H_2O_2=H_2O+O_2+OH$,
(c) $HO_2^*+H=2\,OH$,

where the initial OH could be formed in reaction (a) or in

IV. QUANTITATIVE APPLICATION OF THE KINETIC EQUATION FOR HIGH CHAIN-BREAKING EFFICIENCY TO THE EXPERIMENTAL DATA IN SALT-COATED VESSELS

(a) Limitations of Quantitative Application in the Vicinity of the Third Explosion Limit (Thermal and Water Vapor Effects)

Since B $(=k_{11}f_{H_2}(M)_e{}^2d^2/k_{12})$ is proportional to the square of the pressure, Eq. (18) has another root at higher pressures approximately given by $(M)_e=k_6k_{12}/4k_2k_{11}f_{H_2}d^2$, which should represent the third explosion limit. Thus, the latter is expected to decrease with increasing diameter, to change with mixture composition as it affects f_{H_2}, k_6, and k_{12}, and to be independent of the nature of the surface if it is heavily coated with any of the previously mentioned salts (Section II). This has been verified.[38] If the vessel is covered with only a thin invisible coating (formed by rinsing with salt solution and distilled water) the limit is lowered;[4] in uncoated silica or Pyrex vessels the limit is lowered still more and becomes very erratic. The third limit is preceded by an induction period that is small near its junction with the second limit and increases toward lower temperatures (cf. Fig. 7). Figure 5 illustrates the effect of temperature and pressure on the induction period. In these experiments oxygen was admitted rapidly from a reservoir to the reaction vessel which contained hydrogen, the time being counted from the instant the valve was opened. Pressure equalization required about 3 sec., although the bulk of the O_2 entered in a considerably shorter time. As the pressure is increased beyond that required for explosion, the induction period becomes progressively shorter. The curves are asymptotic, and evidently it is not possible to extrapolate to zero induction period, which is in contrast to the results of Oldenberg and Sommers[38] who have published zero-induction-period explosion pressures obtained by extrapolation.

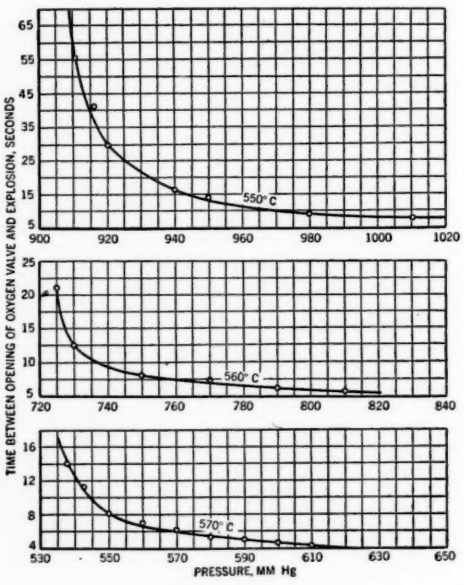

FIG. 5. Ignition lags of third-limit explosions. Vessel diameter, 7.4 cm; Na_2WO_4 coating; $2H_2+O_2$.

During the induction period a rapid reaction occurs, and a rise in temperature can readily be observed. Just below the explosion limit, reaction rates as high as 80 to 100 mm H_2O per minute have been observed. If the process were adiabatic then, for example, at a pressure of 600 mm, the temperature would rise at a rate of 25° to 30°C per second. This indicates that a strong thermal influence is superimposed on the explosion condition, Eq. (18), tending to displace the third limit to lower pressures. The thermal effect is counteracted by the formation of H_2O, which raises the third limit for the same reason that it depresses the second limit (Section IIIa). H_2O also causes self-inhibition of reaction rates close to the explosion limits[39] where the rates become very sensitive to small changes of a, that is, k_6, due to the fact that the denominator in the rate expression (14), namely $1-a(1+x+b)$ is small compared to 1 and doubles or triples for

some other manner. In reaction (b), excitation energy arises from the larger bond energy of H−OH over H−O_2H (at least 40 kcal.) and is available for reaction without having to survive many collisions with inert molecules because of the high percentage of H_2O_2 and H. This mechanism may be further elaborated as the experimental results warrant.

[38] Diameter influence, Oldenberg and Sommers, J. Chem. Phys. **9**, 114 (1941); Heiple and Lewis (reference 4) and present experiments. Mixture composition influence, Heiple and Lewis (reference 4). Effect of salt surfaces, KCl, $BaCl_2$, $K_2B_4O_7$, Na_2WO_4, present experiments.

[39] Self-inhibition by H_2O explains the failure of Oldenberg and Sommers (reference 8) to observe an increase of the reaction rate on approaching the second limit because in their procedure the brief initial stages of the reaction were not observed. This increase has been definitely established in the present work (cf. Fig. 10, also G. von Elbe and B. Lewis, J. Chem. Phys. **9**, 194 (1941)) as well as by Chirkov (reference 6).

relatively small changes of a. This self-inhibition is illustrated by two examples in Fig. 6, one near the second limit at lower temperatures and the other near the junction of second and third limits. As to thermal effects at the second limit, it is noted that as one approaches the limit from higher pressures the reaction rate increases to values capable of producing a noticeable thermal effect only after it has become very sensitive to H_2O-inhibition. For example, if in the absence of water the value of $a(1+x+b)$ is 0.98, corresponding to pressures of 1 to 3 mm above the limit, then only 0.1 percent H_2O need be formed to decrease this to 0.96 and halve the rate. Thus, even if the reaction is rapid without H_2O it is quickly inhibited, and the thermal effect is overshadowed by the H_2O effect. This remains so all along the second-limit curve, including the region around the junction of second and third limits. The H_2O effect does not disturb second-limit determinations at temperatures sufficiently below the junction if the manipulation is reasonably rapid, because reaction rates are small even in the close vicinity of the limit; near the junction, however, the initial rates are rapid, and even the most rapid manipulation cannot prevent the limits from being depressed. A different situation prevails on approaching the third limit from lower pressures at temperatures well below the junction. Here reaction rates increase strongly, not only because $1-a(1+x+b)$ decreases with increasing pressure but to a large extent because the numerator of the rate expression (14) increases with a high order of pressure. Thus, reaction rates capable of unbalancing thermal equilibrium are reached before $1-a(1+x+b)$ has become very sensitive to H_2O, and the thermal effect predominates. From these considerations, which are further discussed below (Fig. 11, Section IVc), it may be concluded that experimental third limits should fall below the theoretical isothermal third limits (Eq. (18)) at low temperatures but as the temperature increases they should approach and finally cross each other, and that experimental second and third limits should join at a higher temperature than the theoretical.

Because of the disturbing thermal and H_2O effects third-limit data cannot be used to determine values of rate coefficients in Eq. (18). These can be obtained from second-limit data.

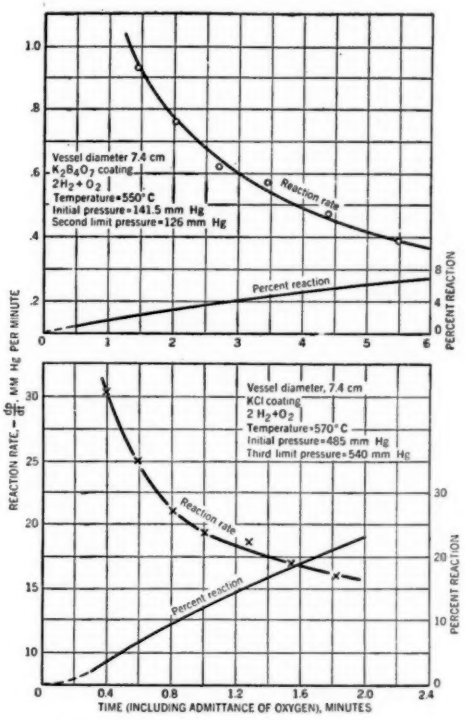

FIG. 6. Self-inhibition of reaction rates near explosion limits.

(b) Numerical Values of Coefficients a, b, and c from Second Explosion Limit Data. Comparison of Experimental and Calculated Explosion Limits of Stoichiometric Mixtures as Function of Temperature and Vessel Diameter

Denoting by a_0, b_0, and c_0 the values of these quantities at some reference temperature T_0, pressure p_0 and vessel diameter d_0, and using the Arrhenius equation,

$$a=a_0\frac{p_0}{p}\frac{T}{T_0}\exp-\left(\frac{E_2}{RT_0}\right)\left(\frac{T_0}{T}-1\right), \tag{21}$$

$$b=b_0\left(\frac{p}{p_0}\frac{T_0}{T}\frac{d}{d_0}\right)^2\exp-\left(\frac{E_{11}}{RT_0}\right)\left(\frac{T_0}{T}-1\right), \tag{22}$$

$$c=c_0\frac{p_0}{p}\frac{T}{T_0}\frac{d_0^2}{d^2}\exp-\left[\frac{(E_5-E_7-E_2)}{RT_0}\right]\times\left(\frac{T_0}{T}-1\right), \tag{23}$$

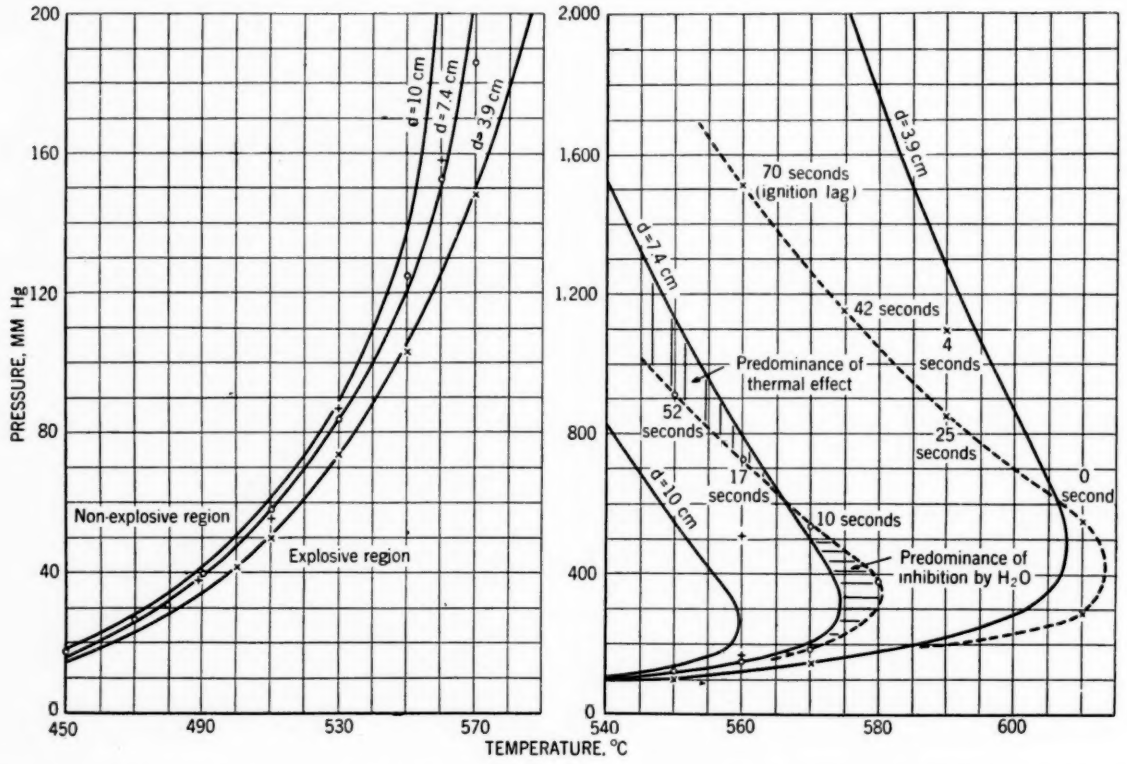

FIG. 7. Second and third explosion limits for mixtures of $2H_2+O_2$ in salt-coated vessels. —— Calculated curves for vessels of diameter d (Eqs. 18, 21a to 23a). Experimental limits: + $d=10$ cm; ○ $d=7.4$ cm; × $d=3.9$ cm.

for constant mixture composition, where E_2, etc., is the activation energy of reaction 2, etc., and E_6 is assumed to be zero.

Using Eq. (18) ($\gamma=1$), c and a are estimated from the diameter dependence of the second limit below 530°C. Toward higher temperatures, c vanishes, thus allowing an estimate of b and a. By trial the following values, referring to stoichiometric mixtures, are found to represent the experimental results satisfactorily. Some variation of the numerical constants is possible but least of all of E_2.[40]

$$a=0.679\frac{84}{p}\frac{T}{803}\exp-\left[\frac{17000}{803R}\left(\frac{803}{T}-1\right)\right], \quad (21a)$$

$$b=0.141\left(\frac{p}{151}\frac{833}{T}\frac{d}{7.4}\right)^2 \times\exp-\left[\frac{24000}{833R}\left(\frac{833}{T}-1\right)\right], \quad (22a)$$

$$c=0.36\frac{84}{P}\frac{T}{803}\left(\frac{7.4}{d}\right)^2 \times\exp+\left[\frac{31000}{803R}\left(\frac{803}{T}-1\right)\right]. \quad (23a)$$

All pressures are expressed in mm Hg. Figure 7 shows calculated and experimental second and third explosion limits in three different size vessels.[41] The positions of the third limits and

[40] The value of $E_2=17{,}000$ cal. determined from the second-limit curve is consistent with the thermochemical value of $-16{,}700$ cal. for reaction 2, determined from $2H=H_2+102.5$ kcal., $2O=O_2+117.3$ kcal., $H_2+\frac{1}{2}O_2=H_2O+57.1$ kcal. (cf. reference 13, p. 382) and $H+OH=H_2O+117.6$ kcal. (Dwyer, Phys. Rev. **59**, 928A (1941)).

[41] Oldenberg and Sommers (reference 8) also reported an increase of the second limit with vessel diameter in KCl-coated vessels, although no data were given. Kimata, Aomi, and Gota (reference 22) reported an increasing second limit with decreasing vessel size in uncoated Pyrex tubes. Their result is evidently due to the relatively larger amount of water formed in the larger vessels during the rather long manipulation periods.

the junctions of second and third limits in experiment and theory correspond to the description given in Section IVa.

Second-limit values in the 7.4 cm $K_2B_4O_7$ coated vessel are of special interest. As discussed in Section II, ϵ in this vessel becomes comparable with λ/d at low temperatures where reaction rates are small, and therefore K_{12} becomes smaller than its normal value for $\epsilon \gg \lambda/d$. The decrease of K_{12} may be estimated from the reaction rates for coatings of $K_2B_4O_7$ and other salts. Already at 530°C at pressures near the second explosion limit, the rates for $K_2B_4O_7$ are 3 to 5 times larger, and the ratio increases toward lower temperatures. This means that K_{12} is reduced to $\frac{1}{3}$ to $\frac{1}{5}$ and less of its value for other salts from 530°C downward. It follows that C is almost negligibly small while B, though larger than for other salts, is still rather small, even at 530°C. Therefore, according to Eq. (18), the second limit is given by $(M)_e = 3k_2/k_6$ from 530°C downward, and E_2 can be obtained directly from the ratio of second-limit pressures at two temperatures by means of the Arrhenius equation. From the data, 86 mm at 530°C and 6.0 mm at 380°C, E_2 is found to be 17,000 cal., in excellent agreement with the value in Eq. (21a). Below 530°C, second limits are higher for $K_2B_4O_7$ than for other salts (Fig. 3c) because of the smallness of C. Above this temperature they coincide, K_{12} for $K_2B_4O_7$ approaching the normal value as described in Section II (compare the following $K_2B_4O_7$ limits with Fig. 7: 86 mm at 530°C, 126 mm at 550°C, 186 mm at 570°C).

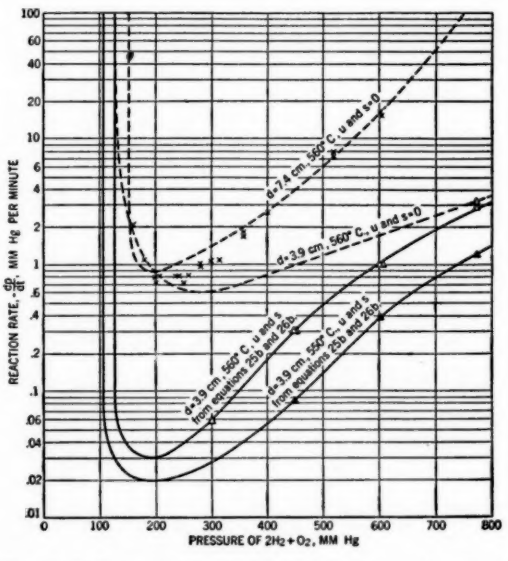
REACTION RATE, -dp/dt MM Hg PER MINUTE
PRESSURE OF 2H2+O2, MM Hg
d=7.4 cm, 560° C, u and s=0
d=3.9 cm, 560° C, u and s=0
d=3.9 cm, 560° C, u and s from equations 25b and 26b
d=3.9 cm, 550° C, u and s from equations 25b and 26b

FIG. 8. Influence of reactions 13 and 14 on the reaction rate. Calculated curves —— and – – –. Experimental rates: × 7.4-cm Pyrex vessel, KCl coating, 560°C; △ 3.9-cm quartz vessel, $BaCl_2$ coating, 560°C; ▲ 3.9-cm quartz vessel, $BaCl_2$ coating, 550°C.

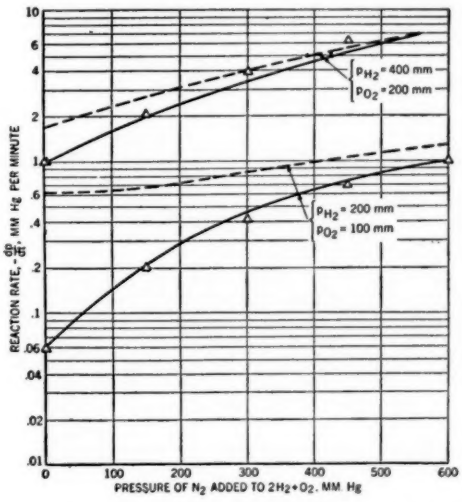

FIG. 9. Effect of nitrogen on reaction rate. – – – Calculated curves, u and $s=0$. —— Calculated curves, u and s from Eqs. (25b), (26b), (31), (32), (39), (40); 3.9-cm quartz vessel, $BaCl_2$ coating, 560°C; △ experimental rates.

In an uncoated or boric acid-coated vessel K_{12} is so small that not only is C suppressed, but B makes a substantial contribution to the limits even at low temperatures, and $(M)_e > 3k_2/k_6$. The data in Table II and Fig. 7 show that in a 3.9-cm uncoated quartz vessel the limit is even higher than in a 10-cm salt-coated vessel.

(c) Numerical Values of the Coefficients I, u, and s from Reaction Rate Data. Comparison of Experimental and Calculated Rates of Stoichiometric Mixtures as Function of Temperature, Pressure, and Vessel Diameter

Coefficient I has the dimension of reaction rate. Analogous to the previous section and expressing I as rate of change of pressure,

$$I = I_0(T/T_0)^{\frac{1}{2}}(d_0/d)^2 \times \exp -\left[\frac{E_i - E_7}{RT_0}\left(\frac{T_0}{T} - 1\right)\right], \quad (24)$$

for constant mixture composition.

Neglecting u and s, the experimental rates are rather well described in large vessels at high temperatures and pressures by putting, for stoichiometric mixtures,

$$I=0.154(T/833)^{\frac{1}{2}}(7.4/d)^2 \times\exp-\left[\frac{31500}{833R}\left(\frac{833}{T}-1\right)\right]. \quad (24a)$$

This is illustrated in Fig. 8 for $d=7.4$ cm and $T=560$°C. It is seen that for $d=3.9$ cm, the data tend to agree only toward high pressures. Toward lower pressures the experimental rates are much lower, the discrepancy becoming so large that no choice of a, b, c, and I can describe the experimental trend. This is remedied by the inclusion of reactions 13 and 14 in the scheme, that is, introduction of terms u and s (cf., solid curves). Qualitatively the effect of u is readily seen if $a(1+x+b)$ in Eq. (15) is assumed to be small and the s term neglected. The equation reduces to

$$1-0.5u/b=x/b,$$

and the rate drops to zero if $0.5u=b$. On the other hand, since u is an inverse function of pressure and diameter and $b\sim p^2d^2$, the ratio $0.5u/b$ vanishes toward higher pressures and diameters with a high order of these variables and the rate becomes independent of u. This serves to explain the conditions described in Fig. 8. That the reaction rate does not fade out completely toward low pressures is due to the small but finite s term. The effect of pressure in suppressing the u term is demonstrated independently by addition of nitrogen (Fig. 9). It is seen that as nitrogen is added to the mixture the discrepancy between experimental and calculated rates for u and s equal to zero (dotted curves; for calculation, cf. Section IVd) decreases. Under conditions where the u term is important, the first additions of inert gas produce a disproportionately large rate increase (cf. Fig. 9; rates for 300-mm stoichiometric mixture). This explains similar observations by Gibson and Hinshelwood[12] at 559°C. with inert gas. At a higher temperature, 569°C, no pronounced initial effect was found, which is consistent with the foregoing because the effect of the u term vanishes with increasing temperature.

For the coefficient K_{13}, similar considerations apply as for K_{12}. Denoting the H_2O_2 destroying efficiency of the surface by ϵ', K_{13} can be approximated by either $3\epsilon'\bar{v}/2d$ or $4\pi^2D/d^2$, depending upon whether $\epsilon'\ll\lambda/d$ or $\epsilon'\gg\lambda/d$. The first of these expressions applies since, as estimated from values of u (Section VI), K_{13} is only about 1/1000 of $4\pi^2D/d^2$. This explains some residual surface effects observable even with heavy salt coatings—at high temperatures and pressures it is slight, but at low temperatures and pressures, particularly in smaller vessels where the u term comes into prominence, the rate varies erratically from experiment to experiment and depends somewhat on the vessel coating. It is notable that the rates were somewhat lower in a 3.9-cm KCl-coated quartz vessel than in a 3.9-cm KCl-coated Pyrex vessel. On coating the quartz vessel with $BaCl_2$ or Na_2WO_4, the rates became larger, approaching those of the KCl-coated Pyrex vessel. The interpretation is not unambiguous, because this effect may also have been caused by the surface-dependent reaction 14. However, it was occasionally observed that in an 8-cm KCl-coated quartz vessel at 530°C and at a pressure of 1 atmosphere or more, the rate in a given run started abnormally low and increased slowly to its normal value. This also happened in a 7.4-cm Pyrex vessel which had previously been etched with molten KOH, thoroughly washed, and then coated with KCl. Since at these pressures and vessel diameters the s term is insignificant, this points to an abnormally large ϵ' at the beginning of the reaction, which subsequently decreases, possibly due to poisoning of the surface by H_2O. In agreement with this interpretation is the observation that the second explosion limit determined at the same time in the above 8-cm quartz vessel was abnormally low, corresponding to increased destructiveness of the surface for H_2O_2 (cf. Section IIIa), that is, abnormally large ϵ'.

Assuming reasonably constant surface conditions, one may write

$$u=u_0\frac{p_0}{p}\frac{T}{T_0}\frac{d_0}{d}\exp-\left[\frac{E_{13}-E_i}{RT_0}\left(\frac{T_0}{T}-1\right)\right]. \quad (25)$$

E_{13} determines the temperature coefficient of surface destruction of H_2O_2.

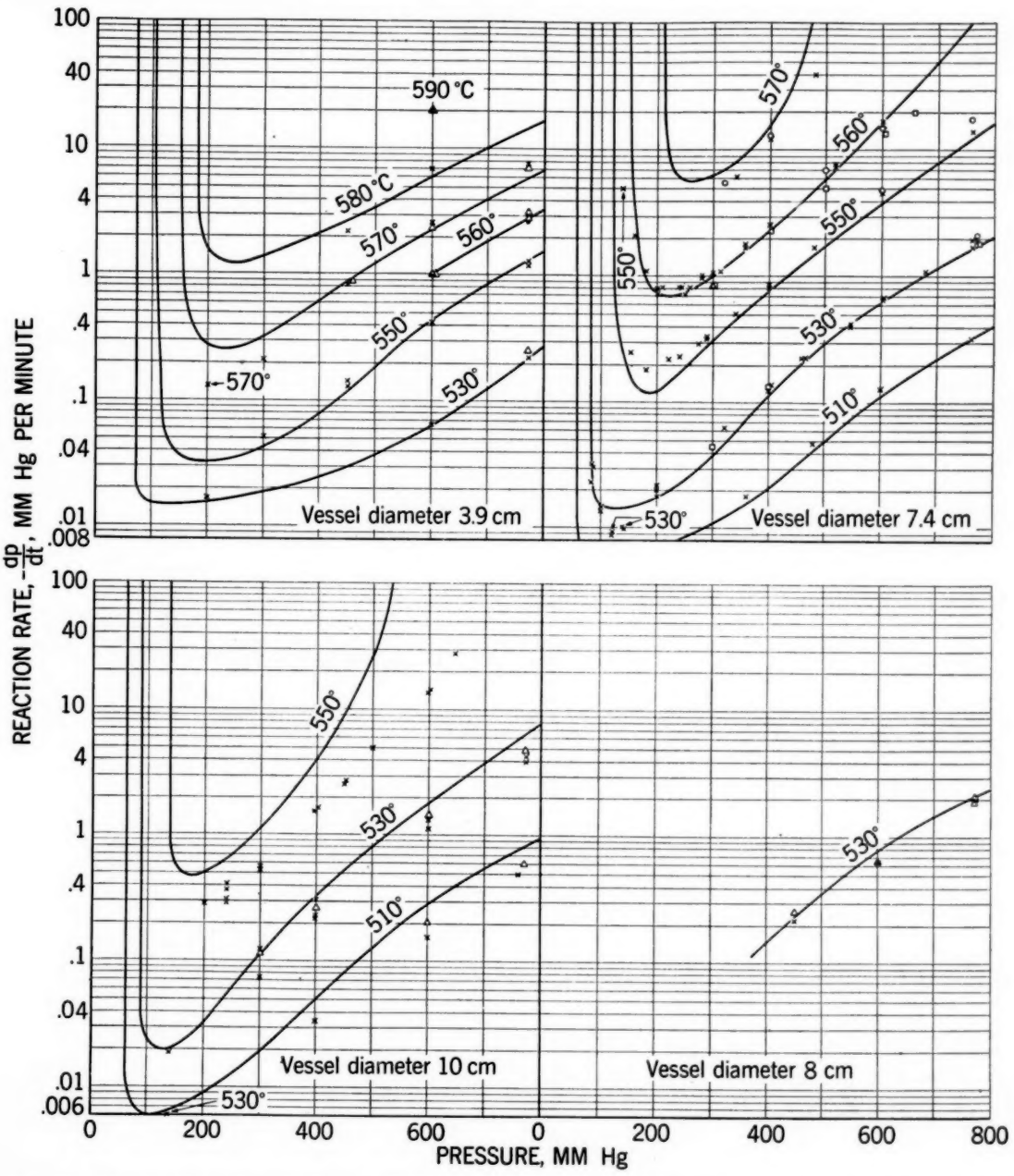

FIG. 10. Initial reaction rates of mixtures of $2H_2+O_2$. Curves calculated from Eqs. (14), (15), (21a)–(26a). Experimental rates: × vessel coated with KCl; △ vessel coated with $BaCl_2$; ○ vessel coated with $K_2B_4O_7$; □ vessel coated with $K_2B_2O_4$ + KOH; ● vessel coated with Na_2WO_4. The 8-cm vessel and the 3.9-cm $BaCl_2$- and Na_2WO_4-coated vessels were quartz. All the other vessels were Pyrex.

If reaction 14 is a surface reaction and is independent of concentrations of reactants,[42] s may be written

$$s=s_0\frac{d}{d_0}\exp-\left[\frac{E_7+E_{14}-E_i}{RT_0}\left(\frac{T_0}{T}-1\right)\right] \quad (26)$$

[42] Gibson and Hinshelwood observed a zero-order surface reaction with a small temperature coefficient in a packed Worcester porcelain vessel. In the present investigation a very low order was observed in a 3.9-cm vessel at 530°C. (Cf. Fig. 10). Additional data obtained in a 3.9-cm KCl-coated quartz vessel also indicated a small temperature coefficient below 530°C.

since K_{14} is proportional to the ratio of surface to volume. This form of the s expression is uncertain, but because of the smallness of its contribution to the rate its exact form is unimportant.

In extending rate calculations to regions where the u and s terms become prominent, one should confine comparisons to data obtained in vessels of equal surface conditions. Although this can hardly be accomplished with precision, even for the same coating material (that is, the small rates are somewhat erratic), generally satisfactory results have been obtained in three Pyrex vessels of 3.9-cm, 7.4-cm, and 10-cm diameters coated with KCl. For these conditions, u and s for stoichiometric mixtures are taken as

$$u=\frac{490}{p}\frac{T}{823}\frac{3.9}{d}\exp+\left[\frac{33800}{823R}\left(\frac{823}{T}-1\right)\right], \quad (25a)$$

and

$$s=0.04\frac{d}{3.9}\exp+\left[\frac{27700}{823R}\left(\frac{823}{T}-1\right)\right]. \quad (26a)$$

Figure 10 shows experimental initial reaction rates and curves calculated from Eqs. (14), (15), and (21a) to (26a). Experimental points obtained with other coating materials at higher temperatures and pressures (where the u and s terms are less important) are included, as well as a few results in an 8.0-cm silica vessel. On the whole, the experiments are well represented. Some variation of the numerical constants used, particularly in the functions u and s, is admissible without seriously affecting the results. At high temperatures, that is, 550°C in the 10-cm vessel and 570°C in the 7.4-cm vessel, the difference $1-a(1+x+b)$ is small over the whole range, and consequently the rate is markedly inhibited by water vapor formed during the period between admitting the gases and the first reading. It is generally not possible to extrapolate the experimental data close to the explosion limit to the H_2O-free rates for zero time because of the extreme decrease of the rate caused by the first traces of H_2O; therefore, the experimental points fall below the curves in Fig. 10 which are calculated on the H_2O-free basis. One may, however, estimate the amount of water formed during the manipulation period and recalculate the rate for the new mixture, using Eq. (4) and $k_{6,H_2O}/k_{6,H_2}=14.3$. This has been done in a few instances (Table V) and the agreement is good. In the 10-cm vessel the rates are also slightly low because of the temperature gradient in the furnace (Section I).

TABLE V. Comparison of experimental and calculated rates, corrected for H_2O formed during manipulation period.

$d=10$ cm KCl-Pyrex $T=550$°C $2H_2+O_2$

Pressure, mm Hg	Manipulation time, minutes	H_2O formed, mm Hg	Reaction rate, mm/min. Calculated without H_2O correction	Calculated with H_2O correction	Experimental
300	1.5	1.4	1.15	0.8	0.55
500	0.6	6.0	26.6	5.3	5.0

$d=7.4$ cm $BaCl_2$-Pyrex $T=560$°C Nitrogen mixtures

Partial pressures, mm Hg p_{H_2}	p_{O_2}	p_{N_2}	Manipulation time, min.	H_2O formed mm Hg	Reaction rate, mm/min. Calculated without H_2O correction	Calculated with H_2O correction	Experimental
200	100	150	1.4	3.6	6.84	2.2	2.6
200	100	300	0.66	4.6	explosion	7.5	7.0

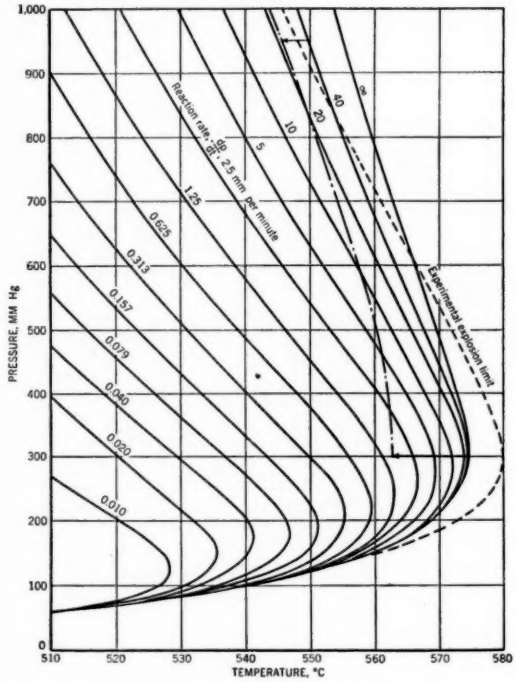

FIG. 11. Curves of equal reaction rates. $2H_2+O_2$ in 7.4-cm KCl, Pyrex vessel. ——– – ——– (see text for explanation).

Figure 11, which is based upon the data of Figs. 7 and 10 for the 7.4-cm vessel, represents curves of equal reaction rates in the temperature and pressure range between the second and third limits. It illustrates conditions near the explo-

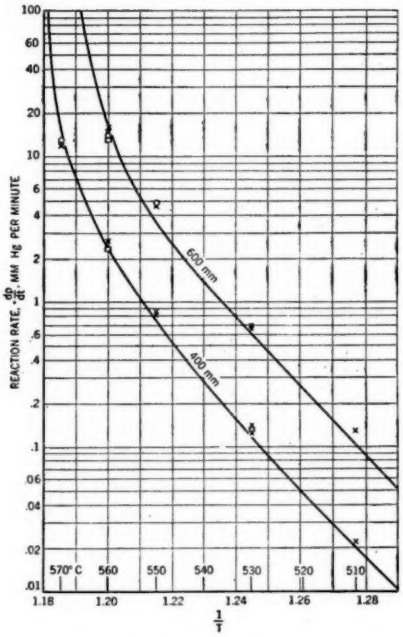

FIG. 12. Reaction rate *vs.* $1/T$ at constant pressure. $2H_2+O_2$, 7.4-cm vessel, salt coated. —— calculated curves. Experimental rates: × KCl coating; ○ $K_2B_4O_7$ coating; □ $K_2B_2O_4$+KOH coating (data from Fig. 10).

sion limit described in Section IVa. Let us assume that a reaction rate of 40 mm/minute normally leads to thermal explosion and that an attempt is made to prepare mixtures at temperatures and pressures along the 40-mm/min. curve in the figure. If 10 mm H_2O are formed during the manipulation time of about 7 seconds, the rates that one would observe under isothermal conditions are given by the intersections of the dot-dashed curve with the solid curves. Thus, at 550°C and 950 mm of $2H_2+O_2$, the observed initial rate would be 22.5 mm/minute instead of 40 provided the temperature remained at 550°C. However, at this rate isothermal conditions would certainly not be maintained; an increase of only 4° would restore the 40 mm/minute rate; and explosion would follow after an induction period. On the other hand, at 574°C and 300-mm pressure, the observed initial rate would be only 1.5 mm/min., which is too small to disturb seriously isothermal conditions. To obtain explosion in this case the temperature must be raised considerably above the ideal isothermal explosion temperature (as shown in Figs. 7 and 11), and the induction period would be very short.

The water-vapor effect may explain the failure of Oldenberg and Sommers[7] to observe the effect of chain branching in curves of log R *vs.* $1/T$. These curves should exhibit an increasing slope on approaching the explosion temperature. Instead, these authors obtained only "reasonably straight lines." The present results do not confirm this. Figure 12 shows theoretical curves and experimental points taken from Fig. 10 for approximately the same conditions as those of Oldenberg and Sommers, namely 400 and 600 mm of stoichiometric mixture in a 7.4-cm KCl-coated vessel. It is seen that the slopes increase toward high temperature corresponding to chain branching and that the experimental points follow the curve closely. But for the highest temperatures, the curves approximate straight lines, and since the experimental points at the highest temperatures are influenced by the H_2O and thermal effects, the reason for the results of Oldenberg and Sommers is clear. For the relative magnitudes of the disturbing effects in the present experiments Fig. 11 may serve as guide. At 600 mm the experimental third limit coincides with the isothermal third limit, that is, thermal and water vapor effects approximately neutralize each other; in conformity with this the observed rates at 600 mm and 560°C are nearly constant over the first period (Table VI). At 400 mm and 570°C the water-vapor effect, according to Fig. 11, predominates, and the rate decreases with time (Table VI). Extrapolation to zero time gives, with some uncertainty, a rate of about 12 mm per minute, as plotted in Figs. 10

TABLE VI. Change of reaction rate with time at high temperatures.

Pressure, 600 mm $2H_2+O_2$ T =560°C d =7.4 cm. $K_2B_4O_7$ coating							
Time (including admittance of oxygen), min.	0.62	.93	1.25	1.57	1.90	2.23	2.57
Rate, mm/min.	14.7	15.1	14.4	14.7	14.4	14.0	13.7
% reaction	3.3	5.6	7.9	10.3	12.6	14.9	17.2
KCl coating							
Time, min.	0.52	.68	.96	1.23	1.50	1.78	2.07
Rate, mm/min.	15.5	14.8	16.5	17.5	16.9	16.5	16.5
% reaction	1.9	3.0	5.4	7.7	10.0	12.3	14.6
Pressure, 400 mm $2H_2+O_2$ T =570°C d =7.4 cm $K_2B_4O_7$ coating							
Time, min.	0.92	1.47	2.1	2.75	3.45		
Rate, mm/min.	9.5	8.5	7.4	7.2	6.7		
% reaction	8.1	11.9	15.2	18.6	22.1		
KCl coating							
Time, min.	1.15	1.45	1.77	2.25	2.43	2.80	
Rate, mm/min.	8.7	8.1	7.3	7.2	6.8	6.4	
% reaction	15.8	21.0	22.8	24.6	26.4	28.2	

and 12. It is noted, however, that even without extrapolation the first-observed rates lie above the straight line through the points at lower temperatures.[43]

(d) The Change of Reaction Rate with Mixture Composition. Comparison of Experiment and Calculation

The above values of a, b, c, I, u, and s, determined for mixtures of the composition $2H_2+O_2$, change if the ratio of H_2 : O_2 is changed or inert gases are admixed. Of the latter, only nitrogen will be considered here. Denoting by the subscript st the values of a, etc., for the mixture composition $2H_2+O_2$, then

$$a/a_{st}=k_{6st}/k_6 =0.784/(f_{H_2}+0.35f_{O_2}+0.43f_{N_2}) \quad \text{(Eq. (4))}, \quad (27)$$

$$b/b_{st}=(f_{H_2}/0.667)(k_{12st}/k_{12}), \quad (28)$$

$$c/c_{st}=k_{12}/k_{12st}, \quad (29)$$

$$I/I_{st}=(k_{12}/k_{12st})(k_i/k_{i,st}), \quad (30)$$

$$u/u_{st}=k_{i,st}/k_i, \quad (31)$$

$$s/s_{st}=I_{st}/I, \quad (32)$$

where $k_{12}=K_{12}(M)d^2=4\pi^2D(M)$ (Eq. (7)). The diffusion coefficient D, for very small concentrations of HO_2, may be written[44]

$$D=\lambda_e\bar{v}_{HO_2}/3, \quad (33)$$

where $\bar{v}_{HO_2}$ is the average molecular velocity of HO_2 and λ_e its effective mean free path. If HO_2 diffuses through pure gas of approximately equal mass like O_2, λ_e equals the ordinary mean free path[44]

$$\lambda=1/\pi(O_2)\sigma^2_{HO_2,O_2}(1+33/32)^{\frac{1}{2}}. \quad (34)$$

If HO_2 diffuses through a much lighter gas like H_2, the persistence of velocity of HO_2 in collisions with the light gas causes λ_e to be larger than λ, the relation being approximately[44,45]

$$\lambda_e=(33/2)\lambda =(33/2)/\pi(H_2)\sigma^2_{HO_2,H_2}(1+33/2)^{\frac{1}{2}}. \quad (35)$$

The effective mean free path in a mixture of gases is computed in the same way as the ordinary mean free path[46] that is,

$$1/\lambda_e=1/\lambda_{e,H_2}+1/\lambda_{e,O_2}+1/\lambda_{e,N_2}. \quad (36)$$

k_{12} then becomes

$$k_{12}=\frac{4}{3}\frac{\pi\bar{v}_{HO_2}}{f_{H_2}\sigma^2_{HO_2,H_2}(2/33)(1+33/2)^{\frac{1}{2}}+f_{O_2}\sigma^2_{HO_2,O_2}(1+33/32)^{\frac{1}{2}}+f_{N_2}\sigma^2_{HO_2,N_2}(1+33/28)^{\frac{1}{2}}}. \quad (37)$$

The effect of mixture composition on reaction i will be assumed to involve only the change in collision frequency due to differences in molecular mass and diameter and not any other specific properties. Hence, k_i is given by

$$k_i/k_{i,st}=\frac{f_{H_2}\sigma^2_{H_2O_2,H_2}(1/34+1/2)^{\frac{1}{2}}+f_{O_2}\sigma^2_{H_2O_2,O_2}(1/34+1/32)^{\frac{1}{2}}+f_{N_2}\sigma^2_{H_2O_2,N_2}(1/34+1/28)^{\frac{1}{2}}}{0.667\sigma^2_{H_2O_2,H_2}(1/34+1/2)^{\frac{1}{2}}+0.333\sigma^2_{H_2O_2,O_2}(1/33+1/32)^{\frac{1}{2}}}. \quad (38)$$

Using values of the molecular diameters of H_2, O_2, N_2, and HO_2 given in Section III and assuming $\sigma_{H_2O_2}=3.0\times10^{-8}$ cm,

$$k_{12}/k_{12st}=\frac{2.96}{f_{H_2}+6.88f_{O_2}+7.84f_{N_2}}, \quad (39)$$

and

$$k_i/k_{i,st}=\frac{f_{H_2}+0.414f_{O_2}+0.454f_{N_2}}{0.805}. \quad (40)$$

Figure 13 shows the close agreement of experimental and calculated rates for various mixtures of hydrogen and oxygen. Both in experiment and theory the rates in mixtures containing 80 and 66.7 percent H_2 are practically identical.

[43] Prettre (reference 6) obtained curvatures similar to Fig. 12 on plotting the logarithm of time for half reaction in a KCl-coated vessel *vs.* $1/T$ even though the high temperature rates must have been lowered by H_2O.

[44] Cf. Sir James Jeans, *Dynamical Theory of Gases*, third edition (1921), p. 314.

[45] Jeans gives a factor due to persistence of velocity of 33/2.7. The factor 33/2 (Eq. (35)) is used following the treatment of Townsend (*Electricity in Gases* (Oxford, 1915), p. 92). In the present calculations this difference is unimportant.

[46] Cf. reference 44, p. 252.

The experiments with nitrogen were carried out in a 3.9-cm $BaCl_2$-coated quartz vessel; and it was necessary, before calculating the curves of Fig. 9, to determine the functions u and s for this coating. This was obtained from the series of experimental rates of stoichiometric mixtures shown in Fig. 8. The functions u_{st} and s_{st} are

$$u_{st}=\frac{512}{p}\frac{T}{823}\exp+\left[\frac{33800}{823R}\left(\frac{823}{T}-1\right)\right], \quad (25b)$$

$$s_{st}=0.027\exp+\left[\frac{27700}{823R}\left(\frac{823}{T}-1\right)\right]. \quad (26b)$$

They provide the close agreement between experiment and calculation shown in Figs. 8 and 9.

In small vessels at low temperature the inert-gas effect vanishes, as is indicated by theory and confirmed by experiment (Table VII). The good agreement shows that the functions of u_{st} and s_{st} (Eqs. (25b) and (26b)) are applicable over a large temperature range.

The foregoing treatment of the effect of mixture composition on the rates supersedes similar previous ones[47,48] because of better knowledge of the reaction mechanism. It is not feasible to recalculate[48] the data of Gibson and Hinshelwood[12] on the relative rates of different mixtures because of lack of knowledge of vessel factors in their experiments. However, since most of their experiments were performed at rather high temperatures where the influence of u and s is small and since the calculated relative rates are not very sensitive to the specific mechanism of the initiating reaction and the other new reactions introduced in this paper, the former calculation,[48] which described Gibson and Hinshelwood's results reasonably well, may be considered to retain approximate validity.

TABLE VII. Effect of inert gas on reaction rate in small vessels at low temperature.

d = 3.9 cm		$BaCl_2$ Pyrex	T = 530°C	
Partial pressures, mm Hg			Reaction rates, mm/min.	
p_{H_2}	p_{O_2}	p_{N_2}	Calc.	Exp.
133	67	—	0.011	0.013
133	67	300	.014	.014

[47] Semenoff, Zeits. f. physik. Chemie **B2**, 169 (1929).
[48] Reference 13, p. 49.

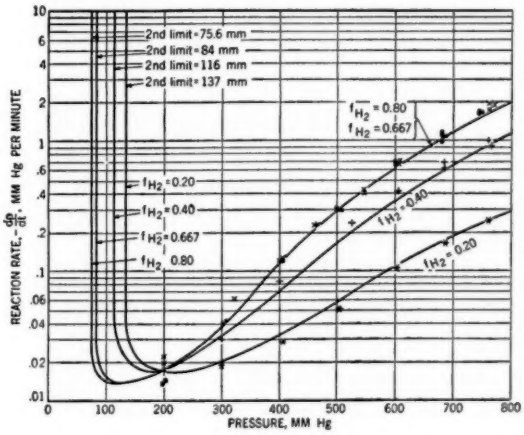

FIG. 13. Initial reaction rates for various ratios of hydrogen and oxygen. —— calculated curves. Experimental rates: ● $f_{H_2}=0.80$, + $f_{H_2}=0.40$; × $f_{H_2}=0.667$, * $f_{H_2}=0.20$. 7.4-cm Pyrex vessel, KCl coating, $T=530$°C.

V. QUANTITATIVE TREATMENT OF THE REACTION IN VESSELS OF LOW CHAIN-BREAKING EFFICIENCY (QUARTZ, PYREX, BORIC ACID COATING)

Oldenberg and Sommers[7] succeeded in obtaining fairly reproducible peak rates in uncoated silica and Pyrex vessels. It was necessary to age the silica vessels by a number of preliminary runs. Pyrex required little aging. The time required to reach the peak rate was extremely erratic. A plot of logarithm of peak rates *vs.* $1/T$ showed that the points were scattered more or less around straight lines, from which the authors inferred the absence of chain branching. However, Fig. 12 indicates that the curvature due to branching does not become pronounced until temperatures close to the theoretical isothermal explosion are reached. If thermal explosion occurs below this temperature range, only a slight curvature is expected which is likely to escape notice particularly if the data are scattered, as is the case in uncoated vessels. This is illustrated further by the following tentative treatment based upon the discussion in Section II. In an uncoated vessel where $\epsilon \ll \lambda/d$,

$$K_{12}=3\epsilon\bar{v}_{HO_2}/2d; \quad (41)$$

ϵ decreases during the course of the reaction due to poisoning of the surface by H_2O and perhaps also to obscure changes in the surface structure. When the fraction r of the mixture (assumed

stoichiometric) has reacted

$$b_r/b=(\epsilon/\epsilon_r)(1-r), \tag{42}$$

and

$$I_r/I=(\epsilon_r/\epsilon)(k_{i,r}/k_i)((M)_r/(M))$$
$$=(\epsilon_r/\epsilon)(k_{i,r}/k_i)[(1-r/3)], \tag{43}$$

where the symbols without subscript refer to the mixture at the beginning of the reaction. Developing $k_{i,r}/k_i$ for (H_2O) analogous to Eq. (40),

$$k_{i,r}/k_i=(3-2r)/3-r). \tag{44}$$

Furthermore,

$$a_r/a=1/(1+11.2r). \tag{45}$$

For large reaction rate $x_r \backsimeq b_r \gg 1$, and Eq. (14) for the reaction rate is approximated by

$$R_r \backsimeq 4I_r b_r^2/1-2a_r b_r, \tag{46}$$

$$=4Ib^2\frac{(1-0.667r)(1-r)^2}{(\epsilon_r/\epsilon)-2ab(1-r)/(1+11.2r)}. \tag{47}$$

For reasonably constant surface structure, which presumably obtained in Oldenberg and Sommers' experiments, the dependence of ϵ_r/ϵ on temperature and H_2O may be formulated on the basis of a model of the adsorption and poisoning process. Assuming that the chain-breaking efficiency is proportional to the number of active spots not occupied by adsorbed H_2O,

$$\epsilon_r=(S_a-S_p)/S, \tag{48}$$

where S is the total surface, S_a the surface occupied by all active spots, and S_p the poisoned part of the surface S_a. Using Langmuir's equation,

$$S_p/S_a=\varphi r/(1+\varphi r), \tag{49}$$

and since $\epsilon=S_a/S$,

$$\epsilon_r/\epsilon=1/1+\varphi r.^{49} \tag{50}$$

φ is represented by a temperature function of the form

$$\varphi=\varphi_0 e^{E/RT}, \tag{51}$$

where E is the adsorption energy. Toward high temperatures the surface becomes less poisoned, which counteracts the increase in branching, that is, both ϵ_r/ϵ and the product ab increase with temperature. The rate R_r may therefore increase until thermal explosion occurs before the isothermal explosion condition is established, even though chain branching may contribute substantially to the peak rate at low as well as at high temperatures. Concerning the numerical evaluation of Eq. (47), the product Ib, which is independent of K_{12}, and a are obtained for any temperature and pressure from Eqs. (21), (22), and (24). In principle, therefore, it should be possible to determine b from the initial rate, but this procedure is uncertain both because it is generally difficult to obtain the true initial rate (values in Table I do not represent initial rates at the exact origin) and because at the beginning of the reaction the relation $\epsilon \ll \lambda/d$ may not be fulfilled. It is possible, however, to obtain pairs of values of b, ϵ_r/ϵ from any experimental R_r. Choosing such a pair for a medium temperature in a series of Oldenberg and Sommers' experiments, taking r for the peak rate equal to about 0.2, and introducing a suitable value of E, curves of log of peak rates *vs.* $1/T$ are obtained which have only moderate slopes similar to the lower part of the curves in Fig. 12, although the branching term contributes considerably to each rate.[50]

If nitrogen is added to the mixture, the functions I and a change according to equations in Section IVd. On adding 200 mm N_2 to 300 mm stoichiometric mixture, I increases by a factor of about 1.4 and a decreases by a factor of about 0.73. Under conditions where the branching term is not very important, the addition of nitrogen should increase the rate 40 percent or less; for conditions where the branching term

[49] After combining Eqs. (50) and (47), the expression for R_r becomes very similar to the equation of Chirkov (reference 6) $R_r=\text{const. } p^3 r(1-r)^2$, derived empirically from a series of experiments with stoichiometric mixtures.

[50] With the removal of this difficulty concerning branching, the comprehensive criticism of Oldenberg and Sommers (Cf. references 7, 8, 38 and J. Chem. Phys. 9, 573 (1941)) insofar as it concerns the mechanism developed in this paper is no longer valid, and there is no further basis for consideration of the Bonhoeffer-Haber chain to which these authors have been inclined as an alternative to branched chains. Further, concerning questions raised by these authors (p. 577): (a) examination of the theory of the photochemical reaction developed in a former paper (reference 51) will show that there is no conflict between the role ascribed to the H atom in the photochemical and thermal reactions; (b) the theory of the thermal reaction shows that up to 500°C the homogeneous reaction at pressures above the second explosion limit is practically nil, but that the explosion below the second limit is still governed essentially by gas-phase reactions 2 and 6.

is important, that is, when the denominator in Eq. (47) is close to zero in the absence of nitrogen, addition of nitrogen should decrease the rate. The experiments in Table I appear to conform to the first condition.

Refinements of the above tentative theory for uncoated vessels must await further experimental work. Methods for examining the surface are desired for correlation of rates with surface data. Moreover, the above concept of surface poisoning is probably oversimplified.

VI. ABSOLUTE VALUES OF RATE COEFFICIENTS OF THE INDIVIDUAL REACTIONS OF THE MECHANISM, AND CHAIN CARRIER CONCENTRATIONS

From the foregoing at 530°C and vessel diameter 7.4 cm,

$$a_{st}p=\frac{2k_2}{k_{6,st}}=57.0\text{ mm Hg}=6.89\times10^{17}\text{ cm}^{-3}, \quad (52)$$

$$b_{st}/p^2=\frac{k_{11}}{k_{12,st}}0.667(7.4)^2=3.88\times10^{-6}\text{ mm}^{-2}=2.66\times10^{-38}\text{ cm}^6, \quad (53)$$

$$c_{st}p=\frac{k_5}{k_7}\frac{k_{12,st}}{k_2}\frac{1}{(7.4)^2}=29.9\text{ mm}=3.61\times10^{17}\text{ cm}^{-3}, \quad (54)$$

$$I_{st}=\frac{k_{i,st}k_{12,st}}{k_7(7.4)^2}=0.0718\text{ mm min.}^{-1}=1.45\times10^{13}\text{ cm}^{-3}\text{ sec.}^{-1}, \quad (55)$$

$$u_{st}p\text{ (Eq. (25a))}=K_{13}/k_{i,st}=420\text{ mm}=5.08\times10^{18}\text{ cm}^{-3}, \quad (56)$$

$$s_{st}=K_{14}/I_{st}=0.116. \quad (57)$$

From a previous publication,[51]

$$k_{6,\,H_2}(24°C)=2.26\times10^{-35}\text{ cm}^6\text{ sec.}^{-1}.$$

Assuming that reaction 6 has no activation energy,

$$k_{6,st}=2.26\times10^{-35}\left(\frac{T}{301}\right)^{\frac{1}{2}}0.784=2.90\left(\frac{T}{803}\right)^{\frac{1}{2}}\times10^{-35}\text{ cm}^6\text{ sec.}^{-1}, \quad (58)$$

and from Eqs. (52) and (21a),

$$k_2=\left(\frac{T}{803}\right)^{\frac{1}{2}}\times10^{-17}\exp-\left[\frac{17000}{803R}\left(\frac{803}{T}-1\right)\right]\text{cm}^3\text{ sec.}^{-1}. \quad (59)$$

From Eq. (37) and $\bar{v}=14500(T/33)^{\frac{1}{2}}$[52]

$$k_{12,st}=5.8\left(\frac{T}{803}\right)^{\frac{1}{2}}\times10^{20}\text{cm}^{-1}\text{sec.}^{-1} \quad (60)$$

and from Eqs. (53) and (22a),

$$k_{11}=4.23\left(\frac{T}{803}\right)^{\frac{1}{2}}\times10^{-19}\times\exp-\left[\frac{24000}{803R}\left(\frac{803}{T}-1\right)\right]\text{cm}^3\text{ sec.}^{-1} \quad (61)$$

From Eqs. (54), (55), (59), and (60)

$$(k_5/k_7)_{(530°C)}=3.41\times10^{-19}\text{ cm}^3, \quad (62)$$

$$(k_{i,st}/k_7)_{(530°C)}=1.37\times10^{-6}. \quad (63)$$

At the temperatures and pressures of Pease's[33] experiments, $k_{11}(H_2)\backsimeq k_7(H_2O_2)$. At 540°C, one calculates from his results an average value of 520 for the ratio $(H_2)/(H_2O_2)$. Hence,

$$(k_7/k_{11})_{(540°C)}=520.$$

Assuming equal steric factors, the Arrhenius equation yields $E_{11}-E_7=10{,}000$ cal.; hence, $(k_7/k_{11})_{(530°C)}=480$, and

$$k_7=2.0\left(\frac{T}{803}\right)^{\frac{1}{2}}\times10^{-16}\times\exp-\left[\frac{14000}{803R}\left(\frac{803}{T}-1\right)\right]\text{cm}^3\text{ sec.}^{-1}, \quad (64)$$

whence

$$k_5=6.8\left(\frac{T}{803}\right)^{\frac{1}{2}}\times10^{-35}\text{cm}^6\text{sec.}^{-1}. \quad (65)$$

This value is of the correct order for ternary reactions, as is seen by comparison with k_6. E_5 is taken as zero (cf. exponent of Eqs. (23)

[51] G. von Elbe and B. Lewis, J. Chem. Phys. **7**, 710 (1939).

[52] Cf. Tolman, reference 27, p. 63.

TABLE VIII. Absolute concentrations of HO_2 and H. $d=7.4$ cm, $2H_2+O_2$.

		$T=530°C$			
		p_{HO_2}	p_H	(HO_2)	(H)
p(total), mm Hg	x	mm Hg $\times 10^4$		molecules per cm^3 $\times 10^{-12}$	
100	0.044	0.31	0.21	0.37	0.25
200	.086	.73	.071	.88	.086
400	.482	7.5	.122	9.0	.147
600	1.39	36	.397	43.5	.48
772	2.37	120	1.28	145	1.55
		$T=560°C$			
170	0.540	37.7	9.7	44	11.4
200	.518	22.9	4.2	27	4.9
300	.790	38.2	2.5	45	2.9
500	1.88	208	5.4	242	6.3
700	3.43	1540	24.5	1800	28.6

and (23a); Further,

$$k_{i,st}=2.73\left(\frac{T}{803}\right)^{\frac{1}{2}}\times 10^{-22}$$

$$\times\exp-\left[\frac{45500}{803R}\left(\frac{803}{T}-1\right)\right]\text{cm}^3\text{ sec.}^{-1}, \quad (66)$$

where $E_i=45{,}500$ cal., is obtained from $E_i-E_7=31{,}500$ cal. (Eq. (24a)) and $E_7=14{,}000$ cal. It is noted that the dissociation of H_2O_2 to 2OH requires $51{,}000\pm 2000$ cal.[53] The difference between these values lies within the allowable variation of the various constants.

The collision-frequency factor Z_0 in the expression $Z=Z_0N_1N_2$ for the number of collisions per second per cm^3 between H_2 and HO_2 is, at 530°C, equal to 2.4×10^{-10} cm^3 sec^{-1}. If k_{11} is written as $fZ_0\exp[-E_{11}/RT]$, where f is the steric factor, this leads to a value of $f=0.6\times 10^{-2}$. Similarly, for reaction 2 the steric factor is found to be 10^{-3} and for reaction i about unity.

Further,

$$K_{13(530°C)}=1.4\times 10^{-3}\text{ sec.}^{-1}. \quad (67)$$

This value is about 1/1000 of the value of $4\pi^2D_{H_2O_2}/d^2$. Hence, ϵ' must be $\ll\lambda/d$, as mentioned in Section IVc. From $K_{13}=3\epsilon'\bar{v}_{H_2O_2}/2d$ one obtains $\epsilon'=4\times 10^{-8}$.

Finally, from Eq. (57) the rate of spontaneous formation of H_2O_2 by reaction 14 under the above conditions is found to be 1.7×10^{12} molecules per cm^3 per sec.

[53] Reference 13, p. 385, and value of $H+OH=H_2O+117.6$ (Dwyer, reference 40).

From Eqs. (11) and (12) and the above data, the absolute concentrations (HO_2) and (H) have been calculated (Table VIII). Values of x (Eq. (15)) are also included in the table. The concentrations (OH) and (O) cannot be calculated for lack of knowledge of k_1 and k_3. It is believed, however, that reactions 1 and 3 are very rapid, and hence (OH) and (O) are much smaller than (H). This seems to make remote the possibility of spectroscopic detection.[54] The difficulty of detecting HO_2 in the reacting mixture spectroscopically is apparent, although the method of the mass spectrograph may be feasible.

The average lifetime of an HO_2 molecule is $1/K_{12}$, which under the above conditions and pressures comparable to atmospheric is of the order of 1 second. Taking the extreme conditions of $P=700$ mm, $T=560°C$, an HO_2 molecule undergoes about 5×10^5 collisions with other HO_2 molecules and 6×10^3 collisions with H atoms. This would seem to afford a chance for second-order chain-breaking reactions such as $HO_2+HO_2=H_2O_2+O_2$, or second-order chain-branching reactions such as $HO_2+HO_2=2OH+O_2$ and $H+HO_2=2OH$. If these breaking and branching reactions occurred to a considerable extent they would profoundly alter the kinetics of the reaction, the former tending to obliterate the effect of vessel factors on the rate and the latter tending to narrow the region of steady-state reaction. However, inasmuch as the present development describes the experimental data over the entire region of small and large chain-carrier concentrations it would appear that they contribute only to a negligible extent. This means that reactions between HO_2 and HO_2 should not occur more than once in about 10^7 collisions and between H and HO_2 not more than once in about 10^4 collisions. It is possible that second-order branching reactions play a role in lowering the third limit (Fig. 7), but the present mechanism already adequately accounts for the lowering on the basis of the enormously large rates and accompanying thermal effect (Section IVa). The above reactions, though involving free radicals, nevertheless are metatheses where

[54] Oldenberg, Schneider, and Sommers (Phys. Rev. 58, 1121 (1940)), did not observe OH absorption bands in a rapidly reacting mixture of H_2 and O_2 with an arrangement permitting detection of 1 OH in 300,000 molecules.

activation energies and steric factors are to be expected. For example, the reaction $HO_2+HO_2=H_2O_2+O_2$ should have a much larger steric factor than reaction 11, possibly of the order of 10^{-6}.[55]

VII. THE ROLE OF INHIBITORS OF THE REACTION

The powerful inhibiting effect of iodine[56] is readily interpreted by the reaction $H+I_2=HI+I$, possibly followed by $H+HI=H_2+I$ and the reaction $HI+HO_2=H_2O_2+I$ studied by Bates and co-workers.[57]

The suppression of the low pressure explosion in a silver vessel[58] is explained by the destruction of H atoms at the silver surface with high efficiency as is readily shown by calculations using the value of k_2 and the diffusion equation for H. In a silver vessel the reaction at high pressures is also suppressed.[58] This cannot be accounted for by the destruction of H atoms at the surface because even for high efficiency the rate of the competing reaction 6 is far larger (at 500 mm about 50 times). The removal of H atoms by silver in the gas phase, probably in the form of oxide,[59] could be responsible for the inhibition at high pressures. However, it is known that H_2O_2 is rapidly decomposed at a silver surface[60] and according to the mechanism developed in this paper this may also account for the inhibition at high pressures, for if H_2O_2 is destroyed efficiently at the surface K_{13} and u become some 10^3 times larger than in salt-coated vitreous vessels and the reaction falls below observable rates. The latter process no longer makes gas phase reactions of silver exclusively responsible for the inhibition at high pressures as it appeared from the earlier scheme.[61]

Water is an inhibitor in a restricted sense, as it inhibits branching through reaction 6. It also may accelerate the reaction as an inert gas impeding diffusion and by poisoning the surface for chain-carrier destruction.

There are possibly a great many other inhibiting substances[62] that merit further attention. Another source of inhibition is the increase of surface to volume ratio by packing or suspended dusts.*

[55] The reaction scheme developed by Jost (*Explosions- und Verbrennungsvorgänge in Gasen* (Berlin, 1939), p. 323) which assigns a high probability to this reaction is inconsistent with experimental rates.

[56] Garstang and Hinshelwood, reference 23.

[57] Bates and Lavin, J. Am. Chem. Soc. **55**, 81 (1933); Cook and Bates, *ibid.* **57**, 1775 (1935).

[58] Hinshelwood, Moelwyn-Hughes, and Rolfe, Proc. Roy. Soc. **A139**, 521 (1933).

[59] Heiple and Lewis, J. Chem. Phys. **9**, 120 (1941).

[60] Cf. Mellor, *Inorganic Chemistry*, Volume 1, p. 942.

[61] Reference 13, p. 68.

[62] Cf. extensive work of Jorissen and co-workers, Rec. trav. chim. (1925), *et. seq.*

* *Note added to proof:* Concerning the recent discussion between Dainton (J. Chem. Phys. **9**, 826 (1941)) and Oldenberg and Sommers (*ibid.*, **10**, 193 (1942)) on the question of chain branching in the hydrogen-oxygen reaction, the authors wish to draw attention to Section V of this paper in which the problem of branched chains in uncoated vitreous vessels is outlined.

The Radial Distribution Function in Liquids

JOHN G. KIRKWOOD AND ELIZABETH MONROE BOGGS
Baker Laboratory, Cornell University, Ithaca, New York

(Received February 18, 1942)

In accordance with the general methods of an earlier paper (reference 1) an integral equation is evolved for the radial distribution function for pairs in a liquid, and an approximate solution is effected for a system of "hard spheres." The form of the function depends on a single parameter λ which can be related to certain observed physical properties of the liquid and to the diameter of closest approach. The theoretical function has been calculated for a value of λ appropriate to liquid argon at 90°K, and compared to experimental radial distribution functions derived from x-ray scattering data.

IN an earlier article, a general method[1] of study of molecular distribution functions in liquids has been proposed by one of us. In a later article,[2] the formulation of an integral equation for the radial distribution function in liquids was given, and an attempt at the solution of the equation was presented. In the present article, we shall employ the methods earlier developed to obtain a more complete solution to the problem of the radial distribution function in a system of spherical molecules with no attractive forces, subject to certain well-defined approximations. Comparison of the theoretical radial distribution function with recently determined experimental distribution curves for argon indicates that attractive forces probably play a secondary role in determining the radial distribution. This is physically plausible, since the fluctuations in the potential of intermolecular attraction at liquid densities are doubtless small.

Recently other methods of calculation of the radial distribution function have been proposed by Wall,[3] Rushbrooke and Coulson,[4,5] and Corner and Lennard-Jones.[6] Although intermolecular attractive forces are taken into account in the latter two papers, the distribution function is referred to an assumed lattice, and the positions of the maxima are not predicted by the theory. While these methods may be regarded as useful alternatives to our own, we believe that liquid structure cannot be adequately described in terms of a lattice blurred by thermal motion, but that the local order in liquids manifested in the radial distribution function is of an essentially different nature from the long range order in crystals.

Before proceeding to the details of the theory, we shall state certain of the fundamental properties of the radial distribution function, which we shall denote by $g(R)$. The function $g(R)$ is so defined that $(N/v)g(R)$ specifies the local molecular density at a distance R from any specified molecule in a system of N molecules occupying a volume v. At large distances $g(R)$ tends to unity and at small intermolecular distances tends to zero, due to intermolecular repulsive forces opposing interpenetration.

$$\lim_{R\to\infty} g(R)=1+0(1/N), \qquad \lim_{R\to 0} g(R)=0. \tag{1}$$

The normalization condition is

$$\frac{1}{v}\int^{v} g(R)dv=1. \tag{2}$$

In the development of the theory to follow, it is convenient to define a function $\varphi(R)/R$, vanishing at infinity, by the relation

$$g(R)=1+\varphi(R)/R+\epsilon, \tag{3}$$

where ϵ is of the order $1/N$. Because the volume is proportional to N, the integral $\rho_0\int\varphi(R)/dvR$ fails to vanish even in the infinite fluid. It has

[1] J. G. Kirkwood, J. Chem. Phys. **3**, 300 (1935), hereafter referred to as SMF, Statistical Mechanics of Fluid Mixtures.
[2] J. G. Kirkwood, J. Chem. Phys. **7**, 919 (1939).
[3] C. N. Wall, Phys. Rev. **58**, 307 (1940).
[4] G. S. Rushbrooke, Proc. Roy. Soc. Edinburgh **60**, 182 (1940).
[5] G. S. Rushbrooke and C. A. Coulson, Phys. Rev. **56**, 1216 (1939).
[6] J. Corner and J. E. Lennard-Jones, Proc. Roy. Soc. London **A178**, 401 (1941).

previously been shown[7] that

$$\rho_0 \int^v \frac{\varphi(R)}{R} dv = kT\kappa\rho_0 - 1, \tag{3a}$$

where ρ_0 is average density (N/v), κ the compressibility, and k Boltzmann's constant. The term $kT\kappa\rho_0$ is the relative density fluctuation of the fluid, which is of importance in the theory of light scattering.[7]

The radial distribution function, although only one of many types of molecular distribution which characterize liquid structure, is of particular interest since it determines the angular distribution of x-ray scattering and can be calculated by a Fourier integral transformation from the experimentally determined x-ray scattering curve.[8]

THE INTEGRAL EQUATION FOR THE RADIAL DISTRIBUTION FUNCTION

The distribution functions for sets of molecules in a fluid may be expressed in terms of local free energies $W_n(\mathbf{R}_1, \cdots \mathbf{R}_n)$, defined in the following manner,

$$\exp(-W_n(\mathbf{R}_1, \cdots \mathbf{R}_n)/kT) = v^n \int^v \cdots \int^v \exp(-V_N/kT) dv_1 \cdots dv_{N-n}, \tag{4}$$

where V_N is the potential of intermolecular force and the integration extends over the coordinates of all N molecules of the fluid in the volume v, except a fixed set n situated at positions $\mathbf{R}_1, \cdots \mathbf{R}_n$. We shall be concerned here only with distribution functions for sets of one, two, and three molecules;

$$\begin{aligned} \rho_1(\mathbf{R}_1) &= \exp\{-[W_1(\mathbf{R}_1) - W_0]/kT\}, \\ \rho_2(\mathbf{R}_1, \mathbf{R}_2) &= \exp\{-[W_2(\mathbf{R}_1, \mathbf{R}_2) - W_0]/kT\}, \\ {}^1\rho_2(\mathbf{R}_1, \mathbf{R}_2) &= \exp\{-[W_2(\mathbf{R}_1, \mathbf{R}_2) - \mathbf{W}_1(\mathbf{R}_1)]/kT\}, \\ {}^{12}\rho_3(\mathbf{R}_1, \mathbf{R}_2, \mathbf{R}_3) &= \exp\{-[W_3(\mathbf{R}_1, \mathbf{R}_2, \mathbf{R}_3) - W_2(\mathbf{R}_1, \mathbf{R}_2)]/kT\}, \end{aligned} \tag{5}$$

where $(N/v)\rho_1(\mathbf{R}_1)$ is the local density of molecules at the point $\mathbf{R}_1$, $(N/v)^2\rho_2(\mathbf{R}_1, \mathbf{R}_2)$ the density of molecules in the six-dimensional space of pairs, $(N/v)\,{}^1\rho_2(\mathbf{R}_1, \mathbf{R}_2)$ the local density of molecules at a point $\mathbf{R}_2$ in the neighborhood of a molecule fixed at a point $\mathbf{R}_1$, and $(N/v)\,{}^{12}\rho_3(\mathbf{R}_1, \mathbf{R}_2, \mathbf{R}_3)$ the density of molecules at a point $\mathbf{R}_3$ in the neighborhood of a fixed pair of molecules situated at the point $\mathbf{R}_1$ and $\mathbf{R}_2$. In a fluid system,[9] the distribution function $\rho_1(\mathbf{R})$ has the constant value unity, and the distribution functions $\rho_2(\mathbf{R}_1, \mathbf{R}_2)$ and ${}^1\rho_2(\mathbf{R}_1, \mathbf{R}_2)$ become identical and depend only on R_{12}, the distance between the points $\mathbf{R}_1$ and $\mathbf{R}_2$.

$$\rho_2(\mathbf{R}_1, \mathbf{R}_2) = {}^1\rho_2(\mathbf{R}_1, \mathbf{R}_2) = g(R_{12}), \tag{6}$$

where $g(R)$ is the radial distribution function, which we wish to investigate here. In studying the radial distribution function, we shall need to consider the distribution function ${}^{12}\rho_3(\mathbf{R}_1, \mathbf{R}_2, \mathbf{R}_3)$ related to the radial distribution function itself in the following manner,

$$\begin{aligned} {}^{12}\rho_3(\mathbf{R}_1, \mathbf{R}_2, \mathbf{R}_3) &= g(R_{13})g(R_{23}) \exp(-w_3/kT), \\ w_3 &= W_3(\mathbf{R}_1, \mathbf{R}_2, \mathbf{R}_3) - W_2(\mathbf{R}_1, \mathbf{R}_2) \\ &\quad - W_2(\mathbf{R}_1, \mathbf{R}_3) - W_2(\mathbf{R}_2, \mathbf{R}_3) + 2W_0, \end{aligned} \tag{7}$$

where the local free energy w_3 determines the correlation in the statistical density distributions around two fixed molecules at the points $\mathbf{R}_1$ and $\mathbf{R}_2$. In the approximation of vanishing w_3, the average force acting on a molecule at point $\mathbf{R}_3$ in the vicinity two molecules at points $\mathbf{R}_1$ and $\mathbf{R}_2$ is the sum of the forces which would act on the molecule at $\mathbf{R}_3$ if each of the fixed molecules at points $\mathbf{R}_1$ and $\mathbf{R}_2$ was present alone. This we shall call the superposition approximation.

We now proceed to set up an integral equation for the radial distribution function according to the methods of SMF. We suppose the potential of intermolecular force to have the form

$$V_N = \sum_{k<l} V(R_{kl}), \tag{8}$$

where $V(R_{kl})$ is the potential of the force between the molecular pair k, l situated a distance R_{kl} from each other. We introduce a coupling parameter ξ for an arbitrarily selected molecule and write

$$\begin{aligned} V_N(\xi) &= V_{N-1} + \xi V_1, \\ V_1 &= \sum_{k=2}^{N} V(R_{1k}). \end{aligned} \tag{9}$$

By allowing ξ to assume values in the interval

[7] L. S. Ornstein and F. Zernicke, Physik. Zeits. **27**, 261 (1926); J. Yvon, Thesis (Paris, 1937).

[8] F. Zernicke and J. A. Prins, Zeits. f. Physik **41**, 184 (1927); P. Debye and H. Mencke, Physik. Zeits. **31**, 797 (1930); B. E. Warren, J. App. Phys. **8**, 645 (1937).

[9] J. G. Kirkwood and E. Monroe, J. Chem. Phys. **9**, 514 (1941).

zero to unity, we can continuously vary the force acting between molecule 1 and the other molecules of the system from zero to its full value in the actual fluid. If we differentiate the distribution function ${}^1\rho_2(\mathbf{R}_1, \mathbf{R}_2, \xi)$ with respect to ξ, we obtain from Eqs. (4), (5), and (9),

$$\frac{\partial \log {}^1\rho_2(\mathbf{R}_1, \mathbf{R}_2, \xi)}{\partial \xi} = -\frac{1}{kT}[{}^{12}\langle V_1\rangle_{Av} - {}^1\langle V_1\rangle_{Av}], \quad (10)$$

where ${}^{12}\langle V_1\rangle_{Av}$ is the mean potential energy of molecule 1 fixed at point $\mathbf{R}_1$ in the neighborhood of a second molecule fixed at point $\mathbf{R}_2$, and ${}^1\langle V_1\rangle_{Av}$ is the mean potential energy of molecule 1, averaged over the configurations of all molecules. The mean potential energies ${}^{12}\langle V_1\rangle_{Av}$ and ${}^1\langle V_1\rangle_{Av}$ may be expressed in terms of the distribution functions in following manner,

$$\begin{aligned} {}^{12}\langle V_1\rangle_{Av} &= V(R_{12}) + \frac{N}{v} \\ &\quad \times \int^v V(R_{13})\,{}^{12}\rho_3(\mathbf{R}_1, \mathbf{R}_2, \mathbf{R}_3, \xi)\,dv_3, \quad (11) \\ {}^1\langle V_1\rangle_{Av} &= (N/v)\int^v V(R_{13})\,{}^1\rho_2(\mathbf{R}_1, \mathbf{R}_3, \xi)\,dv_3. \end{aligned}$$

If we restrict ourselves to a fluid system, for which Eq. (6) is valid, we obtain from Eqs. (10) and (11) after integration with respect to the coupling parameter ξ, and use of the fact that ${}^1\rho_2(\mathbf{R}_1, \mathbf{R}_2, 0)$ is equal to unity,

$$\begin{aligned} \log g(R) &= \chi(R) \\ &\quad - \int^v \psi(R, r, r')[g(r) - 1]\,dv, \\ \chi(R) &= -\frac{1}{kT}\Big\{ V(R) + \frac{N}{v} \\ &\quad \times \int^v \int_0^1 V(r')\,g(r', \xi) \\ &\quad \times [\exp(-w_3/kT) - 1]\,d\xi\,dv \Big\}, \quad (12) \\ \psi(R, r', r) &= \frac{N}{vkT} V(r') \\ &\quad \times \int_0^1 g(r', \xi)\exp(-w_3/kT)\,d\xi, \end{aligned}$$

where for convenience in notation the symbols R, r, r', replace R_{12}, R_{23}, R_{13}, respectively. We shall now introduce the approximation of superposition of average force between pairs. In this approximation Eq. (12) becomes

$$\begin{aligned} \log g(R) &= \chi_0(R) - \int^v \psi_0(r')[g(r) - 1]\,dv, \\ \chi_0(R) &= -V(R)/kT, \quad (13) \\ \psi_0(r') &= \frac{N}{vkT} V(r') \int_0^1 g(r', \xi)\,d\xi. \end{aligned}$$

Solution of the non-linear integral Eq. (13) with an appropriate potential of intermolecular force, for example one of the Lennard-Jones type, should yield an approximation to the radial distribution function consistent with the superposition assumption, which has been discussed in SMF.

SOLUTION OF THE INTEGRAL EQUATION FOR RIGID SPHERICAL MOLECULES WITH NO ATTRACTIVE FORCES

In a liquid composed of rigid spherical molecules of diameter a_0, the potential of intermolecular force $V(R)$ has the form,

$$\begin{aligned} V(R) &= 0, \quad R > a_0, \\ V(R) &= \infty, \quad R < a_0, \end{aligned} \quad (14)$$

and the radial distribution function has the property,

$$\begin{aligned} & g(R, \xi) = 0; \quad \xi > 0; \quad R < a_0 \\ & \frac{NV(R)}{kT} g(R, \xi) = \psi_0(R)\,\delta(\xi); \quad R < a_0 \end{aligned} \quad (15)$$

where $\delta(\xi)$ is the Dirac delta function. We shall denote by $\langle\psi_0\rangle_{Av}$ the integral,

$$\begin{aligned} \langle\psi_0\rangle_{Av} &= \frac{4\pi}{\omega_0}\int_0^{a_0} r^2\psi_0(r)\,dr, \\ \lambda &= 3\langle\psi_0\rangle_{Av}\omega_0, \quad (16) \\ \omega_0 &= \frac{4\pi a_0^3}{3}, \end{aligned}$$

where λ is a constant we shall presently use.

We desire to determine the radial distribution function $g(R)$ for intermolecular distances greater

than a_0 by means of Eq. (13). Since $V(r')$ vanishes for values of r' greater than a_0, $\psi_0(r')$ also vanishes for $r'>a_0$. Denoting by x the reduced intermolecular distance R/a_0 and carrying out the integration over r' in Eq. (13), we finally obtain the equation

$$\begin{aligned} &x \log (1+\varphi(x)/x) \\ &\quad=\frac{\lambda}{4}\int_{-\infty}^{+\infty} K(x-s)\varphi(s)ds; \quad 1<x<\infty \\ &K(t)=0; \quad |t|>1; \\ &K(t)=\frac{2}{\langle\psi_0\rangle_{Av}}\int_1^{|t|} x'\psi_0(x')dx'; \quad |t|\leqslant 1 \\ &g(R)=1+\varphi(x)/x; \\ &\varphi(x)=-x; \quad 0\leqslant x\leqslant 1, \end{aligned} \tag{17}$$

where the term of order $1/N$ in the expression (3) can be neglected. Before attempting to solve Eq. (17) we introduce the following two approximations,

$$\begin{aligned} \log (1+\varphi(x)/x)=\varphi(x)/x; \quad 1\leqslant x<\infty; \\ \psi_0(x)=\langle\psi_0\rangle_{Av}; \quad 0\leqslant x\leqslant 1. \end{aligned} \tag{18}$$

With the use of these approximations, Eq. (14) is reduced to the linear equation,

$$\begin{aligned} &\varphi(x)=\frac{\lambda}{4}\int_{-\infty}^{+\infty} K(x-s)\varphi(s)ds; \quad 1<x<\infty; \\ &K(t)=t^2-1; \quad |t|\leqslant 1 \\ &\quad=0; \quad |t|>1; \\ &\varphi(x)=-x; \quad 0<x<1. \end{aligned} \tag{19}$$

It is convenient to state the Eq. (19) valid for $x>1$ and the auxiliary condition $\varphi(x)=-x$ on the interval $0<x<1$ in a single integral equation. This may be done by extending the definition of $\varphi(x)$ to the entire real axis by the requirement $\varphi(-x)=\varphi(x)$ and introducing an inhomogeneous term $f(x)$, vanishing for $|x|>1$, and permitting the solution $\varphi(x)=-x$ on the interval $|x|\leqslant 1$:

$$\begin{aligned} &\varphi(x)=f(x)+\frac{\lambda}{4}\int_{-\infty}^{+\infty} K(x-s)\varphi(s)ds, \\ &f(-x)=f(x). \end{aligned} \tag{20}$$

$f(x)$ is to be determined so that

$$\varphi(x)=-|x|; \quad |x|<1.$$

Equation (17) is of known type, and the resolvent $k(x-s)$ of the kernel $(\lambda/4)K(x-s)$ may be constructed with the aid of Fourier transforms.[10,2] Using the method of Fourier transforms we obtain

$$\begin{aligned} &\varphi(x)=f(x)-\int_{-1}^{+1} k(x-s)f(s)ds, && \text{(a)} \\ &k(t)=\frac{-\lambda}{2\pi}\int_{-\infty}^{+\infty}\frac{G(-iu)}{1+\lambda G(-iu)}e^{-iut}du, && \text{(b)} \\ &G(z)=\frac{1}{z^3}[z\cosh z-\sinh z], && \text{(c)} \\ &F(z)=1+\lambda G(z). && \text{(d)} \end{aligned} \tag{21}$$

Equation (21) must first be used to determine $f(x)$. Using (21) on the interval $(x)<1$ and the known form $\varphi(x)=-|x|$, Eq. (21) becomes an inhomogeneous integral equation on the finite interval for $f(x)$;

$$f(x)=-|x|+\int_{-1}^{+1} k(x-s)f(s)ds; \quad |x|<1. \tag{22}$$

After determining $f(x)$ by means of Eq. (22), $\varphi(x)$ outside the interval $|x|<1$ may be calculated as

$$\varphi(x)=-\int_{-1}^{+1} k(x-s)f(s)ds \tag{23}$$

by virtue of the fact that $f(x)$ vanishes for $x>1$. By means of the theory of residues, two different expansions of the kernel of Eq. (21) may be obtained.

$$\begin{aligned} k(t)=&\frac{3\lambda}{4(\lambda+3)}\left[\frac{15+6\lambda}{15+5\lambda}-t^2\right] \\ &-\lambda\sum_{n=1}^{\infty}\frac{1+z_n\cosh z_n t}{z_n{}^3F'(z_n)}; \quad |t|<2; \quad \text{(a)} \end{aligned} \tag{24}$$

$$k(t)=\sum_{n=1}^{\infty}\frac{1}{F'(z_n)}\exp(-z_n t); \quad 0<t<\infty; \quad \text{(b)}$$

$$F'(z_n)=(dF/dz)_{z_n}.$$

[10] E. C. Titchmarsh, *Introduction to the Theory of Fourier Integrals* (Oxford, 1937).

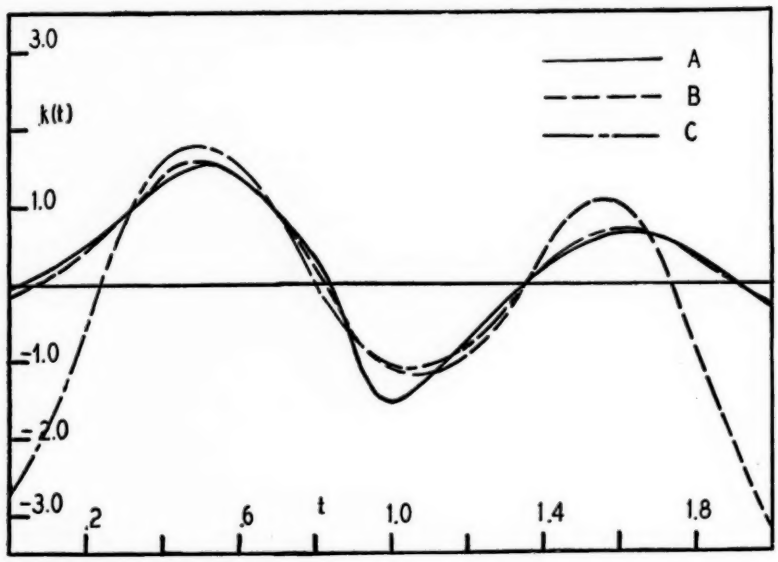

FIG. 1. Exact and approximate forms of $k(t)$, $\lambda=25$. Curve A: exact (numerical integration of Eq. (21)). Curve B: approximation (23a). Curve C: approximation (23b).

The expansion (24a) is appropriate for use in the integral Eq. (22), while the expansion (24b) is appropriate for the evaluation of the integral of Eq. (23). The sums in the Cauchy series of Eqs. (24) extend over all zeros $z_n=\alpha_n+i\beta_n$ with the real part,[11] α_n, positive, of the function $F(z)$ defined in Eq. (21). Introducing the expansion (21b) into the integral of Eq. (23), we obtain

$$\varphi(x)=\sum_{n=1}^{\infty} A_n \exp(-z_n x);\quad 1<x<\infty;$$
$$A_n=-M(z_n)/F'(z_n); \tag{25}$$
$$M(z)=\int_{-1}^{+1} f(x)e^{zx}dx.$$

The kernel $k(t)$ may be evaluated directly by numerical integration of Eq. (21) for each value of λ and t. Use of the tabulated function so found in conjunction with standard numerical methods would lead to a solution of Eq. (22), since such a solution may be assumed, in general, to exist. This leads in turn to the evaluation of $\varphi(x)$ from Eq. (23). Such a procedure is, however, laborious; for practical purposes an approximate expression in closed form for $k(t)$ should suffice. In this connection the use of the expansions (24a) and (24b), with higher order terms neglected, suggests itself. To ascertain how good an approximation is obtained by ignoring all but the first pair of conjugate terms, an accurate numerical integration to obtain $k(t)$ according to Eq. (21b) was carried out for $\lambda=25$, $t=2$. The result is plotted as curve A in Fig. 1 where it is compared with the expressions:

$$k_1(t)=\frac{3\lambda}{4(\lambda+3)}\left[\frac{15+6\lambda}{15+5\lambda}-t^2\right]$$
$$-\lambda\sum_{n=1}^{2}\frac{1+z_n}{z_n{}^3F'(z_n)}\cosh z_n t, \tag{26a}$$

$$k_2(t)=\sum_{n=1}^{2}\frac{\exp(-z_n t)}{F'(z_n)}, \tag{26b}$$

plotted B and C, respectively.

In order to carry out the computations of the last paragraph, as well as others, it is necessary to find explicitly some of the zeros of $F(z)$. The real and imaginary parts of the first two pairs are tabulated as functions of λ in Table I. It may be remarked that β_{n+2} is larger than β_n by approximately 2π in each case and that this together with the increasing real part assures the

[11] The zeros are ordered according to increasing real part $\alpha_{n+1}>\alpha_n$, n even. Since they occur in conjugate pairs, we let $\alpha_{n+1}=\alpha_n$, $\beta_{n+1}=-\beta_n$, n odd.

convergence of the series 23 in the regions indicated, as also of the expansion of φ with reasonable assumptions with regard to the behavior of the transforms $M(z_n)$.

We note, furthermore, that to find $\varphi(x)$ as in Eq. (25) it is unnecessary to evaluate $f(x)$ explicitly; only the transforms $M(z_n)$ need be determined. Using the expansion (24a), appropriate in this interval, for $k(t)$ we have rigorously:

$$f(x)=-|x|+\frac{3\lambda}{4(\lambda+3)}\times\left[\frac{15+6\lambda}{15+5\lambda}-t^2\right]M_{-1}-\frac{3\lambda}{4(\lambda+3)}M_0+-\lambda\sum_{n=1}^{\infty}\frac{1+z_n}{z_n{}^3F'(z_n)}M_n\cosh z_nx, \quad (27)$$

where

$$M_{-1}=\int_{-1}^{+1}f(s)ds;\quad M_0=\int_{-1}^{+1}s^2f(s)ds;\quad M_n=M(z_n),\quad n\geqslant 1.$$

This expression, when used to form the required definite integrals M_n, leads to an infinite set of simultaneous equations in which the unknowns are the M_n, $n=-1, 0, 1, 2, \cdots$ thus:

$$1=\sum_{n=-1}^{\infty}\gamma_{-1n}M_n,$$

$$\tfrac{1}{2}=\sum_{n=-1}^{\infty}\gamma_{0n}M_n, \quad (28)$$

$$P(z_m)=\sum_{n=-1}^{\infty}\gamma_{mn}M_n,\quad m=1, 2, \cdots,$$

where the γ's and $P(z_m)$ are known, if somewhat unwieldy, functions of λ and z_m, and hence implicitly of λ alone.

TABLE I. Zeros of $F(z)$. $F(z_n)=0$; $z_1=\alpha_1+i\beta_1$; $z_2=\alpha_1-i\beta_1$; $z_3=\alpha_3+i\beta_3$; $z_4=\alpha_3-i\beta_3$.

λ	α_1	β_1	α_3	β_3
10	1.90	5.45	3.45	11.91
15	1.46	5.52	3.03	11.99
20	1.12	5.61	2.73	12.04
25	.87	5.68	2.50	12.07
30	.56	5.73	2.31	12.10
34.8	0	5.76		
40	—	—	2.02	12.14
158.6	—	—	0	12.32

TABLE II. Approximate solution of Eq. (28). $y_1+iy_2=M_1[(z_1+1)/z_1{}^3][\exp(-z_1)]/F'(z_1)$.

λ	M_{-1}	M_0	$y_1\times10^2$	$y_2\times10^2$	A	δ
13.3			1.27	0.92	0.96	−0.48
20	−3.51	−1.20$_5$	1.48	.23	1.70	+ .10
25	−4.27	−1.40	1.28	.28	1.97	+ .40
34.8	−5.76	−1.38	.87	.24	1.65	+ .87

Now if we consider only the approximate kernel (26a), these sums become finite and the set (28) reduced to one of four equations in four unknowns. To the same degree of approximation as that afforded by (26a), the function $\varphi(x)$ may be represented by

$$\sum_{n=1}^{2}A_n\exp(-z_nx),\quad x>1,$$

the coefficients in which may be calculated from Eq. (25) using the roots of the finite set of simultaneous equations. More explicitly we have, in real form:

$$\varphi(x)=Ae^{-\alpha_1(x-1)}\cos(\beta_1x-\delta),$$
$$A=e^{\alpha}|M_1/F'(z_1)|, \quad (29)$$
$$\tan\delta=\Im_m(M_1/F'(z_1))/\Re(M_1/F'(z_1)).$$

The finite set of linear equations corresponding to (28) has been solved for several values of λ and the results are set out in Table II together with the corresponding values of A and δ. Little importance can be attached to the limiting case $\lambda=34.8$ for which α_1 vanishes, as it is apparent that modifications must be introduced into the two-term approximation in this immediate vicinity.

It is now possible to proceed with calculations provided a value can be assigned to the single parameter λ, which is characteristic of the physical system to which the calculated radial distribution function applies. By Eq. (18) of SMF, the chemical potential of the liquid is given by

$$\frac{\mu}{kT}=\log\frac{N}{v}+\frac{N}{vkT}\times\int^{v}\int_{0}^{1}V(r)g(r,\xi)d\xi dv+\mu^*(T)/kT, \quad (30)$$

where $\mu^*(T)$ is a function of temperature alone.

From Eqs. (13) and (16), we observe that

$$\frac{N}{vkT}\int^{v}\int_{0}^{1} V(r)g(r,\xi)d\xi = \frac{\lambda}{3} + \frac{N}{vkT}\int_{\omega_0}^{v}\int_{0}^{1} V(r)g(r,\xi)d\xi dv, \quad (31)$$

where the second integral extends over the region exterior to ω_0 and is confined to the region of intermolecular attraction. If, as we have supposed in the present treatment, $g(r,\xi)$ is determined by repulsive forces alone, we may write

$$g(r,\xi)=g(r); \quad \xi>0, \quad r>0;$$
$$\int_{0}^{1} g(r,\xi)d\xi = g(r); \quad r>a_0, \quad (32)$$

where $g(r)$ denotes the radial distribution function $g(r,1)$ for full intermolecular coupling. Thus

$$\frac{N}{vkT}\int_{\omega_0}^{v}\int_{0}^{1} V(r)g(r,\xi)d\xi dv = \frac{N}{vkT}\int_{\omega_0}^{v} V(r)g(r)dv = N\langle V\rangle_{Av}/vkT, \quad (33)$$

where $\langle V\rangle_{Av}$ is the mean potential energy of a molecular pair. The energy of vaporization of the liquid to vapor at zero density is

$$\Delta E_v = N^2\langle V\rangle_{Av}/2,$$
$$N\langle V\rangle_{Av}/vkT = 2\Delta E_v/NkT. \quad (34)$$

Thus in the approximation that the radial distribution is determined by repulsive forces exclusively, we have

$$\mu/kT = \log(N/v_l) + \frac{\lambda}{3} - \frac{2\Delta E_v}{NkT} + \mu^*(T)/kT,$$

where $\lambda/3$ may also be interpreted as the work of formation of a cavity of volume ω_0 in the liquid. Let us consider equilibrium between the liquid and its own vapor. At low vapor pressures, the chemical potential in the vapor is

$$\mu_g/kT = \log(N/v_g) + \mu^*(T)/kT, \quad (35)$$

where v_g is the molal volume of the vapor. Equating μ and μ_g and solving for λ, we obtain

$$\lambda = 3\left\{\frac{2\Delta E_v}{NkT} - \log v_g/v_l\right\}, \quad (36)$$

a formula which may be used for the determination of λ from the energy of vaporization, the volume of the liquid and the volume of the vapor in equilibrium with the liquid at the vapor pressure.

Another relation between λ and certain experimental quantities can be obtained through the normalization condition mentioned earlier. From Eq. (3) we find:

$$\int_{1}^{\infty} x\varphi(x)dx \equiv \Phi(\lambda) = \frac{1}{3}\left[1 - \frac{1}{\rho_0\omega_0}(kT\kappa\rho_0 - 1)\right]. \quad (37)$$

The left-hand side can be evaluated analytically, as has been done for φ in the approximate form (26), yielding the results listed in Table III(a). Table III(b) shows the values computed for the right-hand side of Eq. (37) using known values for the density and compressibility of liquid argon[12] and various assumed values for the diameter of closest approach a_0. It may be remarked that the term involving the compressibility is negligible for condensed liquids and that in effect $\Phi(\lambda)$ depends only on the "expansion," i.e., the ratio of the total to the excluded volume, which indeed must be the only intensive property affecting the radial distribution function for a system of hard spheres. Nevertheless, the method of the preceding section is probably the more reliable in the assignation of λ, and that has been used in the application which follows.

TABLE III.

(a) Theoretical		(b) Experimental		
λ	$\Phi(\lambda)$	a_0	$\Phi(T=83.4°)$	$\Phi(T=90°)$
13.3	0.074	3.35	0.240	0.238
20	.225	3.6	.258	.257
25	.298	3.72	.265	.264
34.8	.272	3.8	.269	.268

Application to Liquid Argon

As already suggested, the indications are that the attractive van der Waals forces in a system of neutral molecules of spherical symmetry play a role subordinate to that of the repulsive forces

[12] For physical data on argon see reference 9.

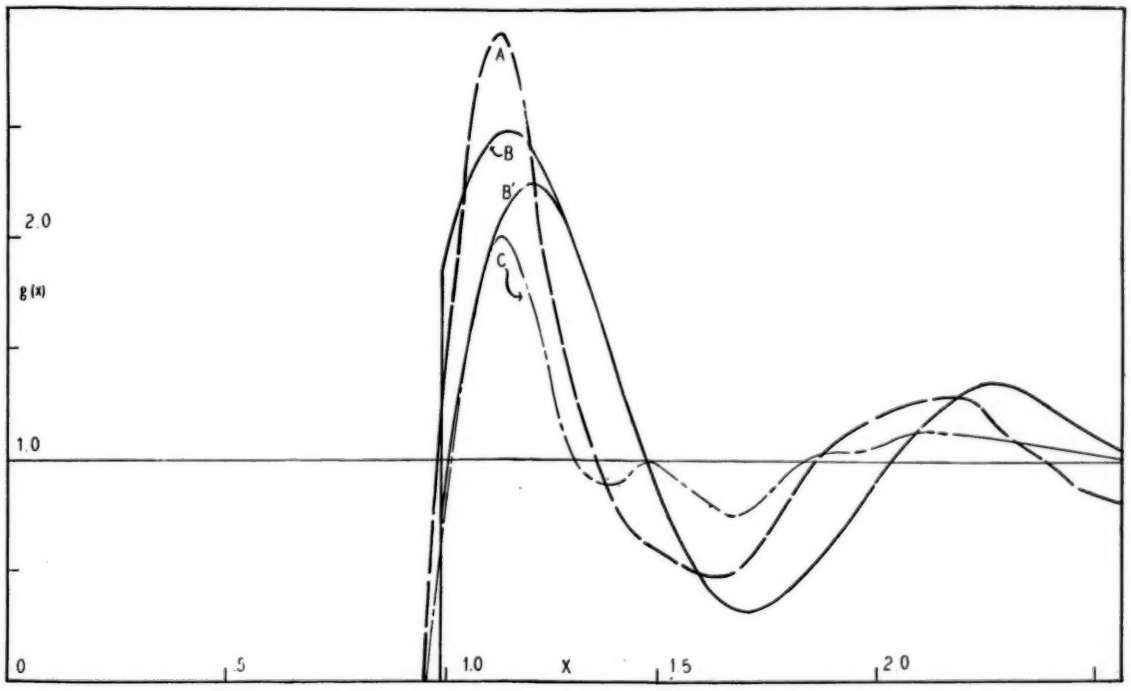

FIG. 2. Theoretical and experimental radial distribution functions for liquid argon at 90°K. Curve A from Lark-Horovitz and Miller. Curves B, B' theoretical. Curve C from Eisenstein and Gingrich. $g(x)$ gives ratio of local to average density. x in diameters, r/a_0.

in determining the radial distribution function. We may therefore anticipate that the results of the foregoing theory will be applicable to the rare gases in the liquid state. Among these argon has been most studied experimentally, and recent determinations[13,14] of its radial distribution function at 90°K from x-ray scattering data invite comparison.

The expression (36), appropriately evaluated,[12] gives us $\lambda=27.4$. Calculation of the corresponding $\varphi(x)$ to the approximation (29) yields the function $g(x)$ shown as curve B in Fig. 2.

In examining the integral (23), however, we observe that whereas in the first part of this range the approximation (23a) to $k(x-s)$ is satisfactory, that given by (26b) is better in the latter part of the range. If $f(s)$ is assumed known from Eq. (27) in terms of the M_n, a correction to $\varphi(x)$ can be calculated in the range $1<x<1.3$, say, by using the better approximation to $k(x-s)$. The result of such a calculation is shown as curve B' in Fig. 2. It should be observed, however, that the same error in $k(x-s)$ plays a part in the evaluation of $f(x)$ in Eq. (19). Examination of the effect of the consequent deviation in $f(s)$ on the evaluation of $\varphi(x)$ by Eq. (23) leads us to conclude that the correct curve for $g(x)$ lies intermediate between B and B'.

This observation is in accord with computations of $\Phi(\lambda)$. Using the analytic expression (29) for $\varphi(x)$, corresponding to curve B in Fig. 2, we find $\Phi(\lambda)=0.31$, whereas, using the $\varphi(x)$ corresponding to the over-corrected curve B', we obtain $\Phi(\lambda)=0.17$. The value for $\Phi(\lambda)$ given by the observed physical properties of liquid argon at 90°K (assuming a_0 to have the value found below) according to formula (37) is 0.24, intermediate between the two.

In order to compare the theoretical with the experimental results it is necessary to assign a value to a_0; this may be taken as the solution $r=a_0$, of the equation $V(r)=kT/2$ where $V(r)$ is the usual intermolecular potential function for

[13] A. Einsenstein and N. S. Gingrich, Phys. Rev. **58**, 307 (1940).

[14] K. Lark-Horovitz and E. P. Miller, Nature **146**, 459 (1940) and unpublished data. We are indebted to Professors Gingrich and Lark-Horovitz for private communications concerning these data.

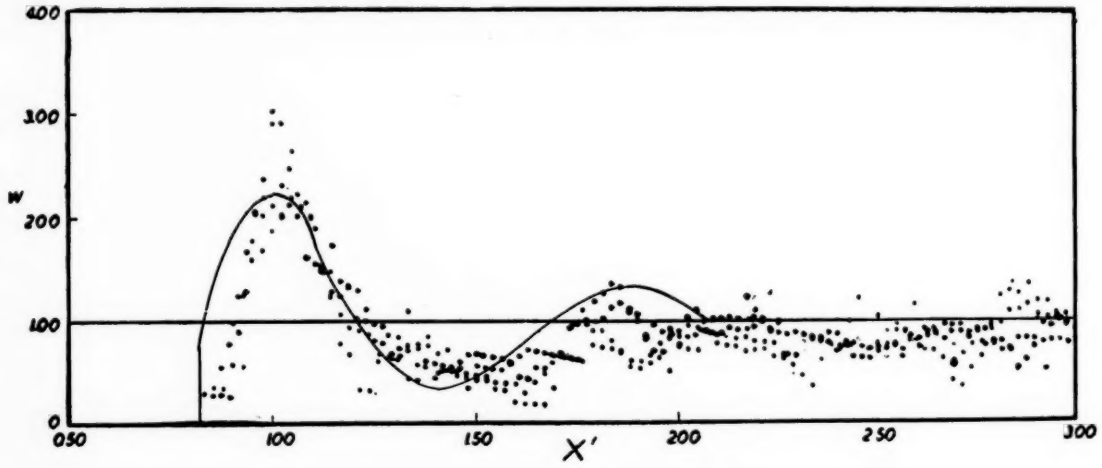

FIG. 3. Theoretical radial distribution function for expansion 1.81 (argon) compared with distribution in macroscopic systems of expansions 1.86, 1.92 (superimposed) from Morrell and Hildebrand. Abscissa x' in units of the first maximum. Scale of theoretical curve chosen to give coincidence of first maximum.

argon, which, for this purpose, we assume to have the analytic form due to Buckingham.[15] We thus obtain the value $a_0=3.35$A. Curves A[14] and C[13] represent experimentally determined radial distribution functions reduced to the scale $x=r/a_0$. The former is from recent (1941) unpublished data. It may be remarked that the deviations of the theoretical curve from A are in the direction that one would anticipate as a result of the neglect of attractive forces. The interatomic potential for argon shows a minimum in the neighborhood of $x=1.15$, and we would expect a sharpening of the first peak about this point and with it a shift to the left of the second peak, when these additional forces are introduced. Nevertheless, our contention that the principal characteristics of the radial distribution function are determined by repulsive forces seems to be borne out.

The observations of Morrell and Hildebrand[16] offer another opportunity for comparison, this time with a macroscopic model of a system of hard spheres. The parameter here is the expansion, expressed as the ratio of the molar volume to that of a mole of close packed spheres. This ratio for argon is 1.81 which is comparable with expansions used by Morrell and Hildebrand in two sets of their observations. In Fig. 3 we compare the theoretical curve B' for $\lambda=27.4$ with the macroscopic distribution (dots) for expansions of 1.86 and 1.92 (superimposed). We note that, *ceteris paribus*, λ is inversely proportional to the expansion, and from Tables I and II we see that increasing expansion is therefore associated with smaller amplitude A, greater damping and a longer period, as would be anticipated, and as is indicated by the observations of Hildebrand and Morrell.

[15] R. A. Buckingham, Proc. Roy. Soc. **A168**, 264 (1938).

[16] W. E. Morrell and J. Hildebrand, J. Chem. Phys. **4**, 224 (1936).

Letters to the Editor

The Detection of Free Radicals by Means of a Mass Spectrometer

G. C. ELTENTON
Shell Development Company, Emeryville, California
May 8, 1942

THE feasibility of detecting free radicals and other intermediate products of chemical reactions by means of a mass spectrometer has been under investigation for some considerable time in these laboratories.

Briefly the method consists in conducting a thermal reaction in a vessel adjacent to the ionization chamber of a mass spectrometer. A fraction of the products is allowed to effuse through a small orifice in a thin diaphragm, and a low pressure is maintained in the ionization chamber by fast pumping. By making use of the fact that the ionization potentials of the free radicals are lower than the appearance potentials of the same ions produced by electron dissociation of the parent molecule, it is possible to select a value of the electron voltage such that when no chemical reaction is taking place no ions of the given mass are formed, whereas any radicals produced at higher temperatures will be ionized and detected. In this way the growth and decay of radical concentration can be followed as a function of reactor temperature with great rapidity.

In the case of methane, methyl radicals appear to be the only intermediates produced in a quartz reactor. When a grid of short carbon filaments was used as a cracking surface at low pressures (<0.1 mm) no methylene could be detected, in contrast to the results of Belchetz and Rideal.[1] Methylene radicals, however, were readily detectable when a dilute mixture of diazomethane in helium was passed through the furnace.

By admixing 0.1 percent of lead tetramethyl in different carrier gases both the production and removal of methyl radicals can be followed at low pressures (10^{-2} to 10 mm). Typical results obtained with the carrier gases C_2H_4, C_2H_6, and C_3H_6 are reproduced in Fig. 1. The curves characterize the relative rates of production and removal, by interaction with the carrier gas, of the methyl radicals. With a contact time of about 0.001 second the lead tetramethyl is completely decomposed at about 730°C and the rate of removal of CH_3 thereafter overtakes the rate of production until the temperature is raised sufficiently to decompose the carrier gas. Reaction between the latter and the methyl radicals is evidently greatest in the case of propylene and least in that of ethylene. The results, therefore, tend to confirm those of, *inter alia*, Taylor and Smith[2] and Beeck and Rust[3] who also found evidence of greater reactivity of the hydrogen atoms attached to the single-bonded carbon, the reactivity being greatest in the case of propylene.

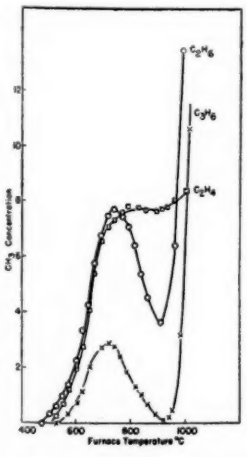

FIG. 1. Production and removal of methyl radicals in C_2H_4, C_2H_6, and C_3H_6 containing 0.1 percent tetramethyl-lead.

All efforts to detect the vinyl radical, which must be produced simultaneously with the methyl radical when propylene is decomposed, were unsuccessful. This can best be explained on the assumption that vinyl is so reactive that its equilibrium concentration is below the sensitivity limit of the instrument. Confirmation of this was obtained by following the formation of C_2H_4 which was found to increase in a manner paralleling the high temperature development of CH_3 and bearing no apparent relation to the development of the allyl radical which was detectable at lower temperatures and which was clearly identified with the reaction between the methyl radicals and propylene.

One further advantage of the method consists in its adaptability to the study of radicals at higher pressures than those so far used with the mirror method (upper limit *ca.* 5 mm). By using a specially designed furnace which eliminates the high pressure cool zone between the zones of formation and detection, methyl and ethyl radicals have been detected from ethane up to pressures of 120 mm and there is every reason to believe that this present limit can be very considerably increased.

More stable intermediates such as formaldehyde from dimethyl ether and from hydrocarbon flames have also been detected.

[1] L. Belchetz and E. K. Rideal, J. Am. Chem. Soc. **57**, 1168 (1935).
[2] H. S. Taylor and J. O. Smith, Jr., J. Chem. Phys. **8**, 543 (1940).
[3] O. Beeck and F. F. Rust, J. Chem. Phys. **9**, 480 (1941).

The Beta-Anomaly of Ruhemann and Simon in Rubber

LAWRENCE A. WOOD
National Bureau of Standards, Washington, D. C.
April 24, 1942

RUHEMANN and Simon[1] have reported that the specific heat of rubber shows three anomalies, which they name α, β, and γ. The α-anomaly, which occurs near -70°C, is a transition of the second order involving no latent heat. Its existence has been confirmed by the other investigations[2-4] in this field. The γ-anomaly, found at temperatures from 15° to 30°C, was present only in rubber which could be shown by other means to be at least partially crystallized, and was ascribed to the heat of fusion of the crystals. There has been no question as to the correctness of this explanation.

There has, however, been no satisfactory explanation of the β-anomaly which Ruhemann and Simon observed near 0°C. Other investigators[2-4] have not been able to find an anomaly in this region. Consequently, its existence and nature have remained a matter of doubt. This communication points out that the results of Ruhemann and Simon can now be explained as a phenomenon of crystallization under the particular conditions of their experiments,

without the assumption of an anomaly characteristic of rubber in general.

A recent communication[5] has presented data which show that the melting range of crystalline rubber is very much dependent on the temperature at which the crystallization takes place. More complete data not yet published show that when crystallization occurs between −40°C and +10°C, melting begins at a temperature of from 4° to 7° above that at which the crystals were formed, and the melting continues over a range of from 10° to 30° more. Crystallization is most rapid in the neighborhood of −20°C and occurs to a considerable extent within a few hours. At higher and lower temperatures the times involved are of the order of days.

Ruhemann and Simon unfortunately give little information about rates of heating or cooling during their measurements, but it may be presumed that it required several hours to take the observations in the range in which crystallization is sufficiently rapid to influence their results. This is ample time for appreciable crystallization, which would then take place for the most part between −20°C and −10°C. The corresponding melting would then be expected to occur in the region around 0°C.

In some cases observations were begun at about −100°C, but in others, especially where the β-anomaly was under particular investigation, the observations were started at −20°C. In the latter cases there was probably even more opportunity for crystallization at temperatures of −20°C and somewhat above.

In two experiments to study the β-anomaly, Ruhemann and Simon held rubber for 5 hours and 12 hours at a "low temperature" (presumably −20°C). The specimen held the longer time showed a much larger heat of transition. The anomaly extended in both cases from about −10° to about +10°C. Furthermore, the authors state: "In contrast to the α-anomaly, the β-anomaly was not strictly reproducible. Depending on the speed of heating as well as the previous cooling the curve is steeper or flatter. Also the energy, that is the area under the curve, was different in different measurements. The mean value for smoked sheet amounted to about 2 cal. per gram of rubber."

Ruhemann and Simon found no β-anomaly in a specimen of vulcanized rubber. This is in accordance with the observation[6] that only certain types of vulcanized rubber crystallize, when unstretched, and that even in these the rate of crystallization is much less than in unvulcanized rubber. Consequently, the amount of crystallization during the experiment was negligible.

In another part of their paper Ruhemann and Simon present a graph of volume against temperature. The graph clearly shows the effect of crystallization and subsequent melting. From about −20° to −5°C the observations fall farther and farther below the straight line representing the normal thermal expansion. From −5°C to +8°C the observations approach the straight line, and above 8°C fall on the line.

The conclusion may then be drawn that the β-anomaly represented merely the melting of crystals formed under the particular experimental conditions of Ruhemann and Simon. It was usually found near 0°C because the crystals were formed between about −20°C and −10°C. Below this range and above it crystallization was so slow as to be inappreciable during the time of an experiment.

[1] M. Ruhemann and F. Simon, "A contribution to the knowledge of the physical properties of rubber," Zeits. f. physik. Chemie **A138**, 1 (1928).
[2] N. Bekkedahl, "Forms of rubber as indicated by temperature-volume relationship," J. Research Nat. Bur. Stand. **13**, 411 (1934) RP 717. Reprinted in Rubber Chem. Tech. **8**, 5 (1935).
[3] N. Bekkedahl and H. Matheson, "Heat capacity, entropy, and free energy of rubber hydrocarbon," J. Research Nat. Bur. Stand. **15**, 503 (1935) RP 844. Reprinted in Rubber Chem. Tech. **9**, 264 (1936).
[4] L. A. Wood, N. Bekkedahl, and C. G. Peters, "Application of the interferometer to the measurement of dimensional changes in rubber," J. Research Nat. Bur. Stand. **23**, 571 (1939) RP 1253. Reprinted in Rubber Chem. Tech. **13**, 290 (1940).
[5] N. Bekkedahl and L. A. Wood, "Influence of the temperature of crystallization on the melting of crystalline rubber," J. Chem. Phys. **9**, 193 (1941). Reprinted in Rubber Chem. Tech. **14**, 544 (1941).
[6] N. Bekkedahl and L. A. Wood, "Crystallization of vulcanized rubber," Ind. Eng. Chem. **33**, 381 (1941). Reprinted in Rubber Chem. Tech. **14**, 347 (1941).

Polarization Measurements of Raman Lines

GEORGE GLOCKLER AND H. T. BAKER
Department of Chemistry, University of Iowa, Iowa City, Iowa
May 9, 1942

WE have lately studied the measurements of the depolarization factor of Raman lines. Our experimental arrangement seems to involve some advantages not considered by other investigators. We use the fixed polaroid located between the Raman tube and the spectrograph as employed by Cleveland and Murray.[1] The marked arrow of the polaroid disk is at an angle of 45° to the vertical direction.

The two arcs, the two filters, and one Raman tube are rigidly fastened so that all are parallel and lie in one plane. The first exposure is taken after rotating this plane by an angle of 45° from the horizontal position. The axis of the spectrograph which is also the axis of the Raman tube is the axis of rotation. The second exposure is taken after rotating the apparatus through a 45° angle in the opposite direction from the original horizontal position. The two exposures are therefore taken in positions which differ by a 90° angle. This change in angular position can be carried out with great ease. Moreover arcs, filters, and Raman tube are always in the same relative position, so that the light leaves the arcs and enters the Raman tube in exactly the same place.

For the calibration spectra we employed the continuum obtained from a gas-oxygen flame which could be controlled and varied easily. A rotating sector allowed different intensities to be photographed on the plate. Again ease of manipulation seems to be an important advantage. The use of continuous calibration spectra allows density comparisons at the exact wave-length of a given Raman line. Preliminary results on the depolarization factor for carbon tetrachloride are as follows: 218 cm^{-1} (0.79, 0.80, 0.82); 314 cm^{-1} (0.80, 0.78, 0.86); 459 cm^{-1} (0.24, 0.24, 0.38); 762 and 790 cm^{-1} (0.84, 0.83, 0.86). The results for the first, second, and fourth lines, which have a large depolarization factor check satisfactorily with other investigations.[1] Our values for the third line are high and we expect to investigate this matter further.

[1] F. F. Cleveland and J. M. Murray, Res. Publ. Illinois Inst. Tech. **2**, 1 (1941).